Single-component multilayered self-assembling protein nanoparticles displaying extracellular domains of matrix protein 2 as a pan-influenza A vaccine

Keegan Braz Gomes[1#], Yi-Nan Zhang[1#], Yi-Zong Lee[1], Mor Eldad[1], Alexander Lim[1], Garrett Ward[1], Sarah Auclair[1], Linling He[1], and Jiang Zhu[1,2]*

[1] Department of Integrative Structural and Computational Biology, The Scripps Research Institute, La Jolla, CA 92037, USA.

[2] Department of Immunology and Microbiology, The Scripps Research Institute, La Jolla, CA 92037, USA.

[#] These authors contributed equally to this work

* Correspondence and requests for materials should be addressed to:

JZ: Phone: (858) 784-8157; Email: jiang@scripps.edu

ABSTRACT (150 words)

The development of a cross-protective pan-influenza A vaccine remains a significant challenge. Here, we designed and characterized single-component, self-assembling protein nanoparticles (1c-SApNPs) presenting the conserved extracellular domain of matrix protein 2 (M2e) from influenza A viruses of human and other hosts. Vaccination with tandem repeats of M2e (M2ex3) displayed on 1c-SApNPs demonstrated higher survival and lower weight loss compared to the soluble M2ex3 antigen against lethal challenges of H1N1 and H3N2 in mice. The mechanism of vaccine-induced adaptive immunity was also investigated in mice. Compared with the soluble M2ex3 antigen, the M2ex3 I3-01v9a 1c-SApNP formulated with a squalene-based adjuvant showed 672 times longer follicular retention, 31 times greater exposure within follicular dendritic cell networks, and up to 2.5 times stronger germinal center reactions in lymph nodes. By inducing robust and durable M2e-specific functional antibody and T cell responses, the M2ex3-presenting I3-01v9a 1c-SApNP provides a promising pan-influenza A vaccine candidate.

ONE-SENTENCE SUMMARY (125 characters)

Protein nanoparticles displaying tandem M2e elicit robust and durable immunity that may protect against influenza A viruses of diverse origins.

35 **INTRODUCTION**

36 Influenza (flu) is a respiratory disease caused by influenza viruses of the Orthomyxoviridae family
37 (*1-5*). Influenza viruses are enveloped negative-sense, single-stranded RNA viruses (*6*) that can be
38 classified as type A, B, C, or D, with influenza A and B viruses (IAVs and IBVs) posing a major
39 threat to human health. The most abundant surface glycoprotein, hemagglutinin (HA), binds the
40 host cell receptors and facilitates cell entry (*7, 8*). Under the host's immune selection pressure, HA
41 can acquire amino acid substitutions that lead to escape mutants (*8*). Another surface glycoprotein,
42 neuraminidase (NA), aids in the release of viral particles through cleavage of residues on the host
43 cell's surface (*9, 10*). Matrix protein 1 (M1) is involved in virus budding, while matrix protein 2
44 (M2) functions as a proton channel to facilitate the maintenance of pH during viral entry and viral
45 replication in host cells (*11*). IAVs can be classified into subtypes based on the antigenic properties
46 of HA and NA (*4*), with H1N1 and H3N2 being responsible for most human infections (*8*). IBVs
47 have a single HA/NA subtype, which can be classified into two lineages, Victoria and Yamagata
48 (*1, 2*). IAVs can infect many hosts, whereas IBVs are restricted to humans (*12*).

49 Seasonal flu vaccines have been used as a cost-effective public health tool since the 1940s
50 (*13-15*). Current flu vaccines are typically quadrivalent, covering two IAV subtypes (H1N1 and
51 H3N2) and two IBV lineages (Victoria and Yamagata), and are produced in chicken eggs (*16*). As
52 a result, current flu vaccines mainly generate strain-specific neutralizing antibodies (NAbs) and
53 may not protect against mismatched seasonal strains or more distinct strains generated through
54 "antigenic drift", during which HA and NA accummulate small mutations over time. Occasionally,
55 IAVs have the potential to cause global pandemics through "antigenic shift", in which HAs and
56 NAs from different host species recombine to form novel IAV strains against which the human
57 population lacks pre-existing immunity (*17*). Viral reassortment resulting in highly pathogenic

58 avian influenza (HPAI) acquiring animal-to-human transmissibility has been on the rise in recent
59 years. As of 2021, there have been 863 cases of HPAI H5N1 and 66 cases of H5N6 in humans,
60 with a > 50% fatality rate (*18*). Therefore, there is an urgent need for cross-protective flu vaccines
61 (*16*), especially for potential pandemic strains originating from diverse animal reservoirs (*19*).

62 Various antigen and vaccine strategies have been explored to develop a universal influenza
63 vaccine (*20-27*). One strategy targets conserved internal proteins, such as nucleoprotein and M1,
64 to induce influenza-specific T cell responses (*28*). A second strategy aims to generate broadly
65 neutralizing antibodies (bNAbs) to the conserved regions of HA, such as the stem and parts within
66 the head domain (*29-32*), and of NA (*33*). Notably, the highly conserved ectodomain of the M2
67 protein (M2e) presents an attractive target for universal IAV vaccine development (*30, 34-37*)
68 because of the sequence conservation across IAVs and functional importance of the M2 proton
69 channel to virus fitness and replication. Although M2e is small (~23 aa) and poorly immunogenic,
70 it can be conjugated to large carriers to elicit antibody responses that effectively reduce viral
71 replication (*38*). Unlike HA and NA, M2e-specific antibodies protect via FcγR-dependent
72 mechanisms, such as antibody-dependent cellular cytotoxicity (ADCC) and phagocytosis (ADCP),
73 rather than direct neutralization (*37, 39-41*). Various carriers have been used to increase the
74 immunogenicity of M2e vaccines, including hepatitis B core protein (HBc) (*39*), tobacco mosaic
75 virus (TMV) coat protein (*42*), keyhole limpet hemocyanin (KLH) (*38*), rotavirus NSP4 (*43*),
76 GCN4 (*44*), bacterial flagellin (*45*), and liposomes (*46*). Early human trials confirmed the
77 immunogenicity and tolerance of M2e vaccines but also revealed several weaknesses. While an
78 adjuvanted M2e-HBc fusion protein (*39*) induced a short-lived anti-M2e antibody response, an
79 M2e-flagellin fusion vaccine (*45*) caused undesirable side effects at higher doses. A vaccine
80 combining M2e with cytotoxic T lymphocyte (CTL) epitopes (*47*) induced strong cellular

81 immunity, but the response was narrow and slow, making it unsuitable for effectively mitigating
82 a future influenza pandemic. These clinical trials highlight the challenges facing M2e-based
83 vaccine development (*35, 48*), as well as the importance of vaccine carriers, adjuvants, balanced
84 antibody and T cell responses, and durability.

85 In recent studies, we have demonstrated a rational vaccine strategy that combines antigen
86 optimization and nanoparticle (NP) display. This strategy was inspired by the success of virus-like
87 particles (VLPs), which can be used as vaccines against cognate viruses or as carriers to improve
88 the immunogenicity of subdominant antigens (*49-56*). Due to their inherent complexity, VLPs can
89 be challenging to produce with yield, purity, and quality acceptable for clinical use. However,
90 protein NPs can be constructed to mimic the size and antigen display of VLPs, with the capability
91 of displaying diverse antigens. We have previously designed multilayered single-component self-
92 assembling protein nanoparticles (1c-SApNP) based on bacterial proteins E2p and I3-01 that can
93 self-assemble into 60-mers of 22-25 nm (*57-62*). Genetic fusion of an antigen to the N-terminus
94 and a locking domain (LD) and pan-reactive T cell epitope (PADRE) to the C-terminus of an NP
95 subunit creates a "vaccine plasmid" encoding a single polypeptide, which will form a protein shell
96 with an array of antigens on the outside, a stabilizing inner LD layer, and a hydrophobic PADRE
97 core. These 1c-SApNPs can be expressed in Chinese hamster ovary (CHO) cells with high yield
98 and purity, and have been applied successfully to vaccines targeting HIV-1 (*57, 61, 62*), HCV (*60*),
99 Ebola virus (EBOV) (*58*), and SARS-CoV-1/2 (*59, 63*). Notably, these 1c-SApNPs can remain in
100 lymph nodes for weeks to interact with immune cells and generate robust germinal center (GC)
101 reactions, whereas individual soluble antigens are cleared within a few hours.

102 In this study, we rationally designed M2e-presenting 1c-SApNPs as cross-protective, pan-
103 influenza A vaccine candidates and characterized them both in vitro and in vivo. We first designed

104 I3-01v9a, a new version of the I3-01v9 1c-SApNP, for optimal presentation of monomeric antigens.
105 We then displayed human M2e (hM2e) on ferritin (FR), E2p, and I3-01v9a 1c-SApNPs, along
106 with a trimeric scaffold, for initial assessment. Following detailed in vitro characterization, these
107 hM2e immunogens were tested in mice, which were sequentially challenged with mouse-adapted
108 H1N1 and H3N2 after a two-dose vaccination. Based on the results, we next displayed tandem
109 copies of M2e (human, avian and swine), termed M2ex3, on the same carriers and characterized
110 these immunogens following a similar protocol. M2ex3 presented on 1c-SApNPs elicited
111 significantly higher M2e-specific antibody and T cell responses in immunized mice compared with
112 the soluble M2ex3 antigen. As a result, mice immunized with M2ex3-presenting 1c-SApNPs
113 showed higher survival against lethal heterosubtypic challenges. In the mechanistic analysis, the
114 M2ex3 1c-SApNPs exhibited prolonged retention (8 weeks) in lymph node follicles and generated
115 robust GC reactions, which may explain the vaccine-induced immunity and protection. Therefore,
116 the tandem M2e presented on an optimized I3-01v9a 1c-SApNP may provide an effective vaccine
117 candidate for durable cross-protection against seasonal and pandemic influenza A viruses.

118 **RESULTS**

119 **Rational design of an I3-01v9a NP scaffold for presenting monomeric antigens**

120 In our early studies, we utilized 24-mer ferritin (FR) and two 60-mers, E2p and I3-01, to display
121 HIV-1 and HCV antigens (*57, 60*). Locking domains (LDs) and a CD4 T-helper epitope (PADRE)
122 were later incorporated into E2p and I3-01 (and its variant I3-01v9) to generate "multilayered" NP
123 carriers, which were successfully used to display stabilized EBOV glycoprotein (GP) trimers (*58*),
124 SARS-CoV-1/2 spikes (*59, 63*), and HIV-1 envelope (Env) trimers (*57*) for vaccine development.
125 Notably, the I3-01 NP scaffold appeared to be particularly amendable to structural modification,
126 with multiple design variants tested in our previous studies (*57-61*). In this study, we rationally

127 optimized the I3-01v9 NP scaffold to improve the surface display of monomeric protein antigens
128 (**fig. S1**). The N-termini of I3-01v9 forms a wide triangle of 50.5 Å, making it more suitable than
129 E2p for displaying monomeric antigens. However, the first amino acid (the antigen anchoring site)
130 is below the NP surface, and as a result, a long flexible peptide linker must be used to connect the
131 antigen to the I3-01v9 N-terminus, leading to the increased structural instability of the antigen-NP
132 fusion constructs. Here, we hypothesized that extending the I3-01v9 N-terminal helix would allow
133 its first residue to reach the NP surface, and consequently, a short peptide linker between the
134 antigen and NP backbone would be sufficient. A computational procedure was devised to facilitate
135 rational design (**fig. S1**). Briefly, the backbone of a helix (residues 953-982) from a c-MYC
136 transcription factor protein (PDB ID: 6G6L) was grafted onto an I3-01v9 subunit by using residues
137 Glu2 and Glu3 of I3-01v9 for structural fitting. The extended N-terminal helix was then truncated
138 to 11 residues so that its first residue would be just above the NP surface. Then, a protein structure
139 sampling program, CONCOORD (*64*), was used to generate 1,000 slightly perturbed
140 conformations for the modified I3-01v9 subunit. Next, an ensemble-based protein design program
141 that was previously used to optimize HIV-1 Env trimers (*57*) and HCV E2 cores (*60*) was
142 employed to predict the sequence for the first 9 residues of the 11-residue segment using C_α and
143 C_β-based RAPDF scoring functions (*65*). The final design, termed I3-01v9a, was determined by
144 combining results from predictions using both scoring functions (**fig. S1**).

145 **Human M2e (hM2e) on multilayered 1c-SApNPs as human influenza A vaccines**

146 The M2 protein from IAVs is a highly conserved proton channel, with a small ectodomain of 24
147 amino acids in length (M2e) (*35*). Anti-human M2e (hM2e) antibodies have been shown to reduce
148 viral replication, thus decreasing clinical symptoms and severity of the disease. In the immunogen
149 design, M2e is hereafter defined as residues 2-24 excluding the first amino acid (M1).

150 Previously, we rationally redesigned viral antigens and engineered antigen-presenting
151 SApNPs for in vitro and in vivo characterization (*57-62*). Following a similar strategy, we
152 designed an hM2e scaffold and three SApNP constructs. The crystal structures of hM2e in complex
153 with antibodies mAb65 and mAb148 (*66, 67*) indicate that hM2e is flexible and can adopt different
154 conformations upon antibody binding. MAb65 recognizes a short turn of Pro10 to Asn13, whereas
155 mAb148 binds to an N-terminal epitope (Ser2-Glu8). We first utilized a capsid-stabilizing protein
156 of lambdoid phage 21, SHP (PDB ID: 1TD0), as a trimeric scaffold to present hM2e. With a 5GS
157 linker, two hM2e epitopes would span ~9.1 nm (measured at Pro10) when all three 1TD0-attached
158 hM2e segments were in a fully open conformation (**Fig. 1A**). We then displayed hM2e on FR 24-
159 mer and reengineered E2p and I3-01v9a 60-mers, all with a 5GS linker (**Fig. 1A**). Molecular
160 modeling revealed well-spaced hM2e peptides on the particle surface, with diameters of 20.9 nm,
161 29.1 nm, and 32.4 nm for FR, E2p, and I3-01v9, respectively (**Fig. 1A**). Following a similar
162 terminology, the "multilayered" E2p and I3-01v9a are named E2p-LD4-PADRE (or simply E2p-
163 L4P) and I3-01v9a-LD7-PADRE (or simply I3-01v9a-L7P), respectively. One hM2e scaffold and
164 three hM2e-presenting SApNPs were subjected to in vitro characterization.

165 All four hM2e constructs (**fig. S2A**) were transiently expressed in 25 ml ExpiCHO cells,
166 purified by immunoaffinity chromatography (*68*) using mAb65 or mAb148 columns, and analyzed
167 by size exclusion chromatography (SEC) (**Fig. 1B**). The SEC profiles indicated high yield for
168 hM2e-5GS-1TD0 and hM2e-5GS-FR and, in contrast, a notably lower yield for hM2e-5GS-I3-
169 01v9a-L7P, as shown by the ultraviolet absorbance at 280 nm (UV_{280}). Among the four constructs,
170 hM2e-5GS-E2p-L4P had the lowest yield. Of note, all three SApNPs showed two SEC peaks at 8-
171 9 ml and 13-14 ml, corresponding to different NP species. Sodium dodecyl sulfate-polyacrylamide
172 gel electrophoresis (SDS-PAGE) under reducing conditions showed bands for hM2e-5GS-1TD0

173 (13.9 kDa), FR (21.0 kDa), E2p-L4P (38.9 kDa) and I3-01v9a-L7P (33.3 kDa) that were consistent
174 with their calculated molecular weights (MW) (**Fig. 1C**, left). Blue native-polyacrylamide gel
175 electrophoresis (BN-PAGE) confirmed the high purity of SApNP samples after IAC using an
176 mAb148 column, displaying a single high-MW band for each SApNP with no sign of unassembled
177 species (**Fig. 1C**, right). The structural integrity of IAC-purified SApNPs was validated by
178 negative-stain electron microscopy (nsEM), which showed distinct morphologies for three hM2e-
179 presenting SApNPs (**Fig. 1D**). Notably, hM2e-presenting SApNPs appeared to form "clusters" in
180 solution, which likely correspond to the high-MW peak (8-9 ml) in their SEC profiles (**Fig. 1B**).
181 Analysis of mAb148-purified SApNPs by dynamic light scattering (DLS) revealed larger-than-
182 expected "particle" size for FR (57.2 nm), E2p-L4p (69.6 nm), and I3-01v9a-L7P (46.1 nm) (**Fig.**
183 **1E**), consistent with the nsEM results. Interestingly, DLS analysis of the SEC fraction (13-14 ml)
184 of an mAb148-purified hM2e-5GS-FR sample still showed three particle size populations,
185 suggesting that cluster formation is an intrinsic feature of hM2e-presenting SApNPs (**fig. S2B**).
186 Differential screening calorimetry (*39*) was used to quantify the thermostability of these hM2e
187 constructs. Thermograms were obtained for hM2e-5GS-1TD0 and hM2e-5GS-FR, which showed
188 a melting temperature (T_m) of 72.5-72.8°C and a similar T_{onset} of 57.9-58.7°C (Fig. 1F). For the
189 two large 60-mers, heating, enzyme-linked immunosorbent assay (ELISA), and nsEM were
190 combined to estimate thermostability. Briefly, SApNP samples were heated to 50°C, 60°C, and
191 70°C for 15 min prior to ELISA analysis against mAb148 and mAb65 (**Fig. 1G**, **fig. S2C**) and
192 nsEM (**fig. S2D**). While antibody binding, measured by half maximal effective concentration
193 (EC_{50}), largely remained comparable within the temperature range of 4-70°C, nsEM images
194 showed signs of irregular particle shapes at 70°C, suggesting that the melting points for hM2e-
195 5GS-E2p-L4P and I3-01v9a-L7P may be between 60 and 70°C. Lastly, we performed bio-layer

196 interferometry (BLI) to quantify antibody binding kinetics for the four hM2e immunogens.
197 Although the three SApNPs outperformed the trimeric hM2e scaffold regardless of the antibody
198 tested (**Fig. 1H**, **fig. S2E**), mAb148 and mAb65 showed different profiles with stronger binding
199 observed between mAb65 and the two large 60-meric SApNPs (**fig. S2E**).

200 In summary, hM2e can be successfully displayed on all three SApNPs, consistent with our
201 previous studies where stabilized HIV-1 (*57, 61, 62*), HCV (*60*), EBOV (*58*), and SARS-CoV-1/2
202 (*59, 63*) antigens were displayed on the NP surface. Extensive biochemical, biophysical, structural,
203 and antigenic characterizations provided detailed in vitro profiles of hM2e-presenting 1c-SApNPs,
204 thus allowing evaluation of these vaccine immunogens in vivo.

205 **In vivo evaluation of a scaffolded hM2e trimer and hM2e-presenting 1c-SApNPs in mice**

206 The immunogenicity and protective efficacy of hM2e trimer and hM2e-presenting SApNPs were
207 evaluated in BALB/c mice. First, mouse-adapted A/Puerto Rico/8/1934 (PR8) H1N1 and A/Hong
208 Kong/1/1968 (HK/68) H3N2 were grown in MDCK cells, and various dilutions of the propagated
209 viruses were used to challenge mice to establish a 50% lethal dose in mice (LD_{50}) (**Fig. 2A**).
210 Plaque-forming units (PFU) of the virus were measured via plaque assay. Using survival rates of
211 mice at various viral dilutions, the Reed-Muench and Spearman-Karber methods (*69, 70*) were
212 used to calculate the 50% endpoint titers for survival. For a stock of 3.8×10^5 PFU/ml PR8 (H1N1),
213 the LD_{50} was determined to be 12 PFU/ml, with the $LD_{50} \times 10$ calculated to be 120 PFU/ml. For a
214 stock of 5.5×10^4 PFU/mL of HK/68 (H3N2), the LD_{50} was determined to be 1.2×10^4 PFU/ml,
215 with the $LD_{50} \times 10$ determined to be 1.2×10^5 PFU/ml.

216 Groups of BALB/c mice were immunized at weeks 0 and 3 with hM2e vaccines adjuvanted
217 with aluminum phosphate (AP) and challenged at weeks 6 and 10 with mouse-adapted H1N1 and
218 H3N2, respectively (**Fig. 2B**). Survival and weight loss were measured after sequential challenges

219 with $LD_{50} \times 10$ of PR8 (H1N1) and HK/68 (H3N2) (**Fig. 2C**). For the PR8 H1N1 challenge, all
220 naïve mice succumbed to the challenge by day 8. In the hM2e-5GS-1TD0 (trimer) group, 80% of
221 mice died by day 9, with 20% of mice surviving the challenge. In contrast, 100% of mice survived
222 in the FR, E2p, and I3-01v9a SApNP groups. Similar trends were observed in the average peak
223 weight loss, with naïve mice losing the most weight (22.1 ± 1.3%). Similarly, 1TD0 mice lost 19.1
224 ± 3.3% of their total body weight on average. Among the hM2e SApNP groups, FR mice lost 12.1
225 ± 8.4% of their total body weight on average, E2p mice lost 16.4 ± 3.9%, and I3-01 lost the least
226 weight with an average of 10.6 ± 4.5%. In the positive control group, mice immunized with
227 inactivated PR8 H1N1 lost the least weight in the strain-matched challenge, with an average loss
228 of 6.5 ± 3.8%. For the second challenge with HK/68 H3N2, the lowest survival was observed for
229 the inactivated PR8 group, with only 56% of mice surviving the heterologous challenge. The two
230 surviving 1TD0 mice from the previous challenge and all SApNP mice survived the HK/68 H3N2
231 challenge. Following a similar trend, the highest body weight loss was observed for the inactivated
232 PR8 group with an average peak weight loss of 16.9 ± 4.9%. All hM2e vaccine groups showed
233 lower peak weight loss with 10.8 ± 2.4%, 4.4 ± 4.0%, 6.2 ± 3.4%, and 7.9 ± 2.8% for 1TD0, FR,
234 E2p, and I3-01v9a, respectively. The hM2e-binding antibody response in mouse serum was
235 assessed by ELISA using an hM2e-5GS-foldon trimer (**Fig. 2D**, **fig. S3A**). The hM2e SApNP
236 groups demonstrated superior serum binding, measured by EC_{50} titers, at all the time points tested,
237 with the greatest fold increase observed at week 5 for FR (31.2), E2p (52.3), and I3-01v9a (42.8)
238 compared to the 1TD0 group (**Fig. 2D**). The hM2e vaccine groups showed the highest antibody
239 EC_{50} titers 4 weeks after the H3N2 challenge at week 14.

240 In summary, hM2e SApNPs significantly outperformed the soluble hM2e trimer in the
241 vaccination/viral challenge experiment, showing higher survival and lower weight loss that were

242 well-correlated with the heightened M2e-specific serum antibody titers. These hM2e SApNPs also
243 demonstrated cross-protection against H1N1 and H3N2 challenges, whereas the inactivated PR8
244 H1N1 vaccine only protected against the strain-matched challenge.

245 **Tandem M2e (M2e×3) on multilayered 1c-SApNPs as pan-influenza A vaccines**

246 The effectiveness of seasonal influenza vaccines range between 10 and 60% as estimated by the
247 U.S. Flu Vaccine Effectiveness Network (*15*). In addition to antigenic drift in circulating human
248 influenza virus strains, the unanticipated emergence of novel strains from swine and avian hosts
249 often causes outbreaks with increased mortality and morbidity. Thus, a broadly protective M2e-
250 based influenza vaccine strategy must incorporate M2e from diverse species.

251 Following the same strategy for hM2e, we designed a trimeric scaffold and three SApNPs
252 to present tandem M2e repeats as vaccine immunogens. Briefly, the hM2e, avian/swine M2e, and
253 human/swine M2e sequences were linked in tandem with short G4 linkers. A structural model of
254 M2ex3 was generated from the crystal structure of hM2e in complex with mAb65 (PDB ID: 4N8C)
255 (**Fig. 3A**, left). Although this compact structural model may not represent M2ex3 conformations
256 in solution, it may facilitate rational design of the M2ex3 orientation on various carrier scaffolds.
257 For the M2ex3-5GS-1TD0 trimer, the two outmost hM2e epitopes would span ~9.4 nm (measured
258 at Pro10 of hM2e) when the scaffolded M2ex3 segments adopt an extended conformation (**Fig.
259 3A**, middle). For the three SApNPs, molecular modeling yielded diameters of 23.2 nm, 32.4 nm,
260 and 36.2 nm for M2ex3-5GS-FR, E2p-L4P, and I3-01v9a-L7P, respectively, measured at Pro10
261 of hM2e (**Fig. 3A**, right three). The display of tandem M2ex3 increased not only the particle size
262 but also the number of M2e epitopes, from 60 to 180, for enhanced immune recognition.

263 The four M2ex3 constructs (**fig. S4A**) were expressed and purified using the same strategy
264 as for their hM2e counterparts (**Fig. 3B**). Overall, M2ex3 immunogens showed a similar pattern

265 of expression yield in ExpiCHO cells, with the ranking of 1TD0 > FR > I3-01v9-L7P >> E2p-L4P.
266 Of note, the SEC profiles showed a less pronounced peak at 9 ml for FR and I3-01v9-L7P,
267 suggesting a reduced tendency to form NP clusters. Reducing SDS-PAGE showed bands on the
268 gel consistent with MW calculated for M2ex3-5GS-1TD0 (19.3 kDa), FR (26.3 kDa), E2p-L4P
269 (44.4 kDa), and I3-01v9a-L7P (38.7 kDa) (**Fig. 3C**, left). However, a second band was observed
270 on the gel for M2ex3-5GS-1TD0, FR, and E2p-L4P under reducing conditions. While the extra
271 bands for M2ex3-5GS-1TD0 and E2p-L4P may indicate higher-MW species that are resistant to
272 the reducing agents, the lower band noted for M2ex3-5GS-FR likely suggests degradation during
273 processing. Nonetheless, BN-PAGE confirmed particle assembly and purity for three M2ex3
274 SApNPs **(Fig. 3C**, right). Similarly, nsEM micrographs demonstrated well-formed, homogeneous
275 particles for all three M2ex3 SApNP samples following mAb148 purification (**Fig. 3D**). In the
276 DLS profiles (**Fig. 3E**), M2ex3-5GS-FR exhibited a two-peak distribution with the majority peak
277 showing single particles, indicated by an average size of 28.3 nm. Similarly, M2ex3-5GS-I3-
278 01v9a-L7P yielded a homogenous distribution consistent with single particles. In contrast, M2ex3-
279 5GS-E2p-L4P formed clusters, as seen in nsEM images and indicated by the DLS-derived particle
280 size distribution. The tandem design appeared to cause a reduction in thermostability for M2ex3-
281 5GS-FR, with lower T_m (60.9°C) and T_{onset} (45.7°C) values. The melting point was estimated for
282 the two 60-mer SApNPs using the alternative approach devised for hM2e SApNPs. Similar
283 antibody binding affinity, as indicated by the EC_{50} value, was observed for M2ex3 scaffolds and
284 SApNPs across the whole temperature range (4-70°C) (**Fig. 3G**, **fig. S4B**), although irregular
285 particle shapes were noted at 70°C in EM micrographs (**fig. S4C**). The interactions of M2ex3
286 immunogens with two human antibodies (mAb65 and mAb148) were assessed by BLI (**Fig. 3H**,
287 **fig. S4D**). The advantage of particulate display was exemplified by the higher binding signals,

288 similar to the case of hM2e SApNPs. Interestingly, the binding profiles (both on-rate and signals)
289 notably improved for M2ex3-5GS-I3-01v9a-L7P (**Fig. 3H**, rightmost), suggesting that antigenicity
290 may be affected by both the epitope number and spacing on a particular NP scaffold. In summary,
291 tandem M2ex3 SApNPs exhibit greater homogeneity and antigenicity than hM2e SApNPs, while
292 sharing similar yield, structure, and thermostability.

293 **Protection against influenza A virus challenge by tandem M2ex3 vaccines in mice**

294 BALB/c mice were immunized with tandem M2ex3 vaccines adjuvanted with AP or AddaVax (a
295 squalene-based nanoemulsion adjuvant; AV) at weeks 0 and 3 and thereafter challenged at weeks
296 6 and 10 with H1N1 and H3N2, respectively (**Fig. 4A**). Survival and weight loss were recorded
297 for both challenges (**Fig. 4B**). After an $LD_{50} \times 10$ challenge with PR8 (H1N1), all naïve mice died
298 by day 8. In mice immunized with AP-adjuvanted tandem M2ex3 vaccines, 50% of 1TD0 (trimer)
299 mice died by Day 9. Paired with the same AP adjuvant, M2ex3 SApNPs demonstrated higher
300 survival rates: 88% of FR, 100% of E2p, and 100% of I3-01v9a mice survived the H1N1 challenge.
301 In terms of peak weight loss, naïve mice lost the most weight with an average of 21.7 ± 2.9%, and
302 1TD0 (trimer) mice lost the second highest amount of weight (19.4 ± 7.3%), as expected for the
303 small soluble M2e antigen. In general, M2ex3 SApNP groups showed lower peak weight loss: FR
304 (15.5 ± 8.1%), E2P (11.2. ± 3.8%), and I3-01v9a (15.5 ± 5.3%). Several AddaVax-adjuvanted
305 M2ex3 vaccine groups outperformed their AP counterparts, demonstrating both higher survival
306 and lower peak weight loss. The AddaVax-adjuvanted M2ex3 trimer group showed a slightly
307 higher survival rate at 63% compared to its AP-adjuvanted counterpart (50%). All AddaVax-
308 adjuvanted M2ex3 SApNPs achieved 100% survival, with an improvement noted for the M2ex3
309 FR group (12% higher survival compared to its AP counterpart) and no difference in the E2p and
310 I3-01v9a groups between the two adjuvants (all 100% survival). For peak weight loss, amongst

311 AddaVax-adjuvanted groups, the M2ex3 trimer showed the highest weight loss with 18.9 ± 5.9%.
312 Most M2ex3 SApNPs adjuvanted with AddaVax showed lower peak weight loss compared with
313 their AP-adjuvanted counterparts: 13.1 ± 7.2% (FR), 12.5. ± 7.7% (E2p), and 10.0 ± 4.2% (I3-
314 01v9a). Inactivated PR8 mice lost the least weight against the strain-matched challenge, with an
315 average of 4.4 ± 5.3%. Next, protection against the second challenge with HK/68 H3N2 was
316 assessed (**Fig. 4B)**. While all mice in the naïve group died by day 5, inactivated PR8 showed
317 limited protection with a survival rate of 63% against the non-strain-matched challenge. All
318 M2ex3-immunized mice that survived the prior PR8 challenge, adjuvanted with AP or AddaVax,
319 survived the HK/68 challenge. Similar to the survival rates, the highest peak weight loss was seen
320 in the naïve group with 19.5 ± 2.9%, followed by the inactivated PR8 group with 15.7 ± 4.9%.
321 M2ex3 trimer and FR, E2p, and I3-01v9a SApNPs adjuvanted with AP showed lower weight loss
322 with 8.9 ± 5.2%, 4.7 ± 3.2%, 6.5 ± 1.9%, and 4.4 ± 3.0%, respectively. Similarly, M2ex3 trimer
323 and SApNP groups adjuvanted with AddaVax showed minimal weight loss: trimer with 4.3 ± 2.1,
324 FR with 4.3 ± 1.0%, E2p with 5.9 ± 3.4%, and I3-01v9a with 4.9 ± 3.3%. Amongst all M2ex3
325 vaccine formulations, M2ex3 I3-01v9a/AddaVax demonstrated the most effective protection
326 against sequential H1N1 and H3N2 challenges in a mouse model.

327 The viral load in lungs of mice at day 5 post-PR8 challenge was used as another metric to
328 evaluate the effectiveness of vaccine protection (**Fig. 4C**). Mice were immunized and challenged
329 as described above and sacrificed at day 5 post-infection. Lungs were collected, mechanically
330 disaggregated, and centrifuged to pellet cells. PFUs were measured in the supernatants via plaque
331 assay. Overall, naïve mice had the highest virus load, $6.0 \times 10^5 \pm 3.3 \times 10^5$ PFU/ml. The M2ex3
332 trimer, FR, E2p, and I3-01v9a groups showed significantly lower viral titers, with 2.9, 7.5, 24.3,
333 and 18.1-fold-lower virus load than the naïve group, respectively. Compared to M2ex3 trimer, FR,

334 E2p, and I3-01v9a showed 2.5, 8.3, and 6.3-fold-lower virus in lungs, although this difference was
335 not statistically significant. The mice immunized with inactivated PR8 adjuvanted with AddaVax
336 (positive control) did not show any detectable viral loads in lungs. Based on the criteria of survival,
337 weight loss, and viral load in lungs, M2ex3 I3-01v9a SApNP/AddaVax appeared to be the most
338 effective vaccine among all the NP/adjuvant formulations tested.

339 **Evaluation of M2e×3 vaccine-induced antibody responses**

340 Both E2p and I3-01v9a SApNP groups demonstrated superior serum binding to an M2ex3-5GS-
341 foldon probe at all time points compared to the trimer group **(Fig. 5A**, **fig. S5A**). The greatest fold
342 difference between SApNP and trimer groups was obtained at week 2, suggesting a rapid onset of
343 anti-M2ex3 antibody response elicited by SApNPs. When paired with AP, E2p and I3-01v9a
344 SApNPs yielded 31.6-fold and 83.8-fold higher EC_{50} titers than the 1TD0 trimer, whereas an even
345 greater fold difference, 47.6 and 102.4 respectively, was noted when these two SApNPs were
346 adjuvanted with AddaVax. The highest EC_{50} titers were observed for the SApNP groups at week
347 5, where E2p and I3-01v9a showed 6.7/5.7-fold and 4.9/4.7-fold higher EC_{50} values than the
348 M2ex3 trimer, respectively, when adjuvanted with AP/AddaVax. Interestingly, FR paired with
349 either adjuvant significantly underperformed E2p and I3-01v9a after the second dose, and trimer
350 at the later time points. Notably, AddaVax groups always outperformed AP groups with higher
351 EC_{50} titers, highlighting the importance of a potent adjuvant for eliciting M2e-specific antibody
352 responses. Importantly, we also confirmed that the incorporation of two non-human M2e epitopes
353 into the hM2e constructs does not reduce hM2e-specific EC_{50} titers in the M2ex3-immune sera
354 compared to the hM2e-immune sera, as indicated by the hM2e-5GS-foldon probe (**Fig. S5B)**. In
355 fact, mouse sera induced by the M2ex3 trimer and I3-01v9a SApNP formulated with AddaVax
356 showed similar or higher EC_{50} titers compared to their AP-adjuvanted hM2e counterparts.

357 The recognition of homotetrameric M2e, which represents the "native" M2e conformation
358 during IAV infection, by M2ex3-immune sera was assessed for the AddaVax-adjuvanted 1TD0,
359 FR, and I3-01v9 groups **(Fig. 5B**, **fig. S6**). In this experiment, ELISA was performed to test serum
360 binding to M2e presented on MDCK cells infected with pandemic or seasonal H1N1 and H3N2
361 strains. The I3-01v9a group demonstrated significantly higher serum binding to M2e expressed on
362 MDCK cells infected with challenge strain A/Puerto Rico/8/1934 (H1N1) and challenge/pandemic
363 strain A/Hong Kong/1/1968 (H3N2). Additionally, the I3-01v9a group also showed higher serum
364 binding to pandemic A/California/04/2009 (H1N1) and other H1N1 and H3N2 strains: A/Solomon
365 Islands/2/2006 (H1N1), A/Brisbane/10/2007 (H3N2), and A/Aichi/2/1968 (H3N2). As a negative
366 control, serum binding was also assessed against two IBV strains, which express an M2e that is
367 shorter than and antigenically distinct from IAV M2e. As expected, the 1TD0, FR, and I3-01v9a
368 groups showed minimal serum binding to IBV strains B/Brisbane/60/2008 (Victoria Lineage) and
369 B/Florida/4/2006 (Yamagata Lineage). A human M2e antibody in the immunoglobulin form (*71*),
370 termed mAb148 (*66*), was used as a positive control in serum ELISA against IAVs. Based on the
371 in vitro and in vivo evaluation, M2ex3 I3-01v9a SApNP adjuvanted with AddaVax was selected
372 as the lead M2ex3 vaccine candidate for further analysis.

373 **Distribution, trafficking, and retention of M2ex3 trimers and SApNPs in lymph nodes**

374 Following a similar protocol that was used to analyze HIV-1 and SARS-CoV-2 SApNP vaccines
375 (*57, 63*), we studied the in vivo behavior of the M2ex3 1TD0 trimer and two SApNPs (FR and I3-
376 01v9a) to achieve a better understanding of their interaction with immune cells in lymph nodes
377 and their ability to induce adaptive immune responses. To mount an effective humoral response,
378 these vaccines must be transported through lymphatics and accumulate in lymph node follicles.
379 The immunogens will then be presented to B cells to generate a robust antibody response through

380 crosslinking of B cell receptors (BCRs) (*72-75*). We first studied the transport and distribution of
381 M2ex3-presenting I3-01v9a SApNPs in lymph nodes. We injected a single dose of the immunogen
382 intradermally through the footpads (4 footpads, 10 μg/footpad) and isolated the sentinel brachial
383 and popliteal lymph nodes from both sides of the mouse's body at 48 h post-immunization.
384 Immunostaining of the excised lymph node sections was carried out using mAb148 and mAb65
385 (*66, 67*) to detect M2ex3 presented on I3-01v9a SApNPs (**Fig. 6A**). Immunohistological images
386 obtained after staining with both antibodies demonstrated a similar distribution of M2ex3 I3-01v9a
387 SApNPs in the center of lymph node follicles (**Fig. 6A**, images on the left; **Fig. 6B**, schematics on
388 the right). This intra-lymph node distribution pattern is consistent with the results obtained from
389 previous studies assessing SARS-CoV-2 spike SApNPs (*63*), HIV-1 Env SApNPs (*57*) and
390 ovalbumin-conjugated gold NPs (*76, 77*). Due to the better signal-to-noise ratio, mAb148 was used
391 hereafter to examine the trafficking of three M2ex3 immunogens in lymph nodes.

392 We next studied the trafficking and retention patterns of the M2ex3 trimer and two SApNPs
393 in lymph node follicles up to 8 weeks after a single-dose injection (4 footpads, 10 μg/footpad)
394 (**Fig. 6C**). The histological images showed that all M2ex3 immunogens were transported into
395 lymph nodes and accumulated in the subcapsular sinus within 2 h (**Fig. 6C**). The M2ex3 trimer
396 was trafficked into follicles within 2 h and completely cleared by 12 h. In contrast, the M2ex3 FR
397 SApNP began to be present in follicles at 12 h, reached peak accumulation at 1 week, and remained
398 detectable up to 5 weeks. The M2ex3 I3-01v9a SApNP demonstrated the most superior follicular
399 retention with a period of 8 weeks. The mAb148-stained area was quantified in a time-dependent
400 manner, showing a ~672-times longer retention for the I3-01v9 SApNP compared to the M2ex3
401 trimer (**Fig. 6C-D**). The area under the curve (*78*) suggested that the exposure of M2ex3 presented
402 on SApNPs in follicles would be 14-31 times higher than the soluble M2ex3 trimer (**Fig. 6E**).

403 Additionally, the FR and I3-01v9a SApNPs also showed 45-86 times greater accumulation
404 compared with the M2ex3 trimer at 1 week (**Fig. 6F**). These results are consistent with our previous
405 findings (*57, 63, 76*), in which small particles (< 15 nm) can be cleared from lymph node follicles
406 within 48 h, whereas large particles (30-100 nm) remain for weeks. Importantly, I3-01v9a SApNPs
407 displaying M2ex3 antigens or BG505 trimers showed significantly longer follicular retention than
408 those presenting SARS-CoV-2 spikes (~8 weeks vs. ~2 weeks), suggesting a correlation between
409 antigen retention and antigen thermostability (a T_m value of 65°C or greater for M2ex3 and BG505
410 Env vs. 48°C for SARS-CoV-2 spike). Surprisingly, the M2ex3 I3-01v9a SApNP with a low
411 glycan content exhibited identical trafficking and retention patterns to the highly glycosylated
412 BG505 Env SApNP (*57*), suggesting a minimal impact of glycan content on vaccine transport and
413 retention in lymph node follicles. Next, we studied the accumulation and retention patterns of these
414 three M2ex3 immunogens at 2 and 5 weeks using a prime-boost regimen (injected into 4 footpads
415 at weeks 0 and 3, 10 μg/footpad) (**Fig. 6G**). A similar pattern to the single-dose injection was
416 observed. Interestingly, M2ex3 trimers were detected in follicles at 5 weeks after the boost and
417 showed improved retention compared to the single dose, consistent with our previous SARS-CoV-
418 2 study (*63*). Improvement in accumulation and retention after boost were also observed for the
419 FR and I3-01v9a SApNPs. Overall, displaying tandem M2ex3 on the I3-01v9a SApNP showed 8-
420 fold greater accumulation in follicles compared to the soluble trimer 2 weeks after the boost (**Fig.
421 6H**). Prolonged retention of the M2ex3 I3-01v9a SApNP vaccine in lymph node follicles may
422 suggest improved longevity of vaccine-induced immunity.

423 Follicular dendritic cells (FDCs) located in the center of lymph node follicles are essential
424 for retention and presentation of the native-like antigens to stimulate B cell responses (*72, 74, 75*).
425 FDCs can collect and align soluble antigens, large particles such as immune complexes, viruses,

426 and bacteria on their surfaces or dendrites through a complement receptor-dependent mechanism
427 to generate and maintain GC reactions (*73-76, 79, 80*). Our previous studies of ovalbumin-
428 conjugated gold NPs (*76*), and SARS-CoV-2 and HIV-1 antigen-presenting SApNPs (*57, 63*)
429 suggest that FDC networks may be the key cellular component to retain M2ex3 SApNPs. To test
430 this possibility, we collected lymph nodes at the peak of SApNP accumulation (1 week) and other
431 timepoints (48 h to 8 weeks) following a single-dose injection (**Fig. 6I**, **fig. S7A-D**). Lymph node
432 tissue was stained with mAb148 (white) for M2ex3, anti-CD21 antibodies (green) for FDCs, and
433 anti-CD169 antibodies for subcapsular sinus macrophages. The signals from both M2ex3 FR and
434 I3-01v9 SApNPs (anti-M2e mAb148) showed colocalization with FDCs ($CD21^+$) at 1 week (**Fig.**
435 **6I**), confirming the retention of M2ex3 SApNPs in FDC networks.

436 **Characterization of GC reactions induced by M2ex3 trimers and SApNPs**

437 In GCs, B cells undergo somatic hypermutation, selection, affinity maturation, and class switching,
438 eventually becoming memory or antibody-secreting plasma cells (*73, 81-84*). FDC networks and
439 T follicular helper (T_{fh}) cells support GC formation and maintenance (*85, 86*). Here, we
440 hypothesized that M2ex3 SApNPs retained by FDC networks could induce more robust and long-
441 lived GC reactions in lymph node follicles compared to the soluble M2ex3 trimer. First, we
442 examined whether M2ex3 I3-01v9 SApNPs can induce strong GC reactions after single-dose
443 injections (4 footpads, 10 μg/footpad). Vaccine-induced GC B cells ($GL7^+$, red) and T_{fh} cells
444 ($CD4^+$ $Bcl6^+$, co-labeled with cyan and red) were characterized by immunohistology. We observed
445 large GCs attached to FDC networks ($CD21^+$, green) with organized dark zone (DZ) and light zone
446 (LZ) compartments in follicles ($B220^+$, blue) (**Fig. 7A**, left). In addition to antigen retention and
447 presentation by FDC networks, T_{fh} cells appear in the LZ of GCs to support B cell stimulation
448 (**Fig. 7A**, right). Next, we performed immunohistological analysis on the M2ex3 trimer and two

449 SApNPs at 2, 5, and 8 weeks after a single-dose injection (**Fig. 7B**, **fig. S8A-C**) and at 2 and 5
450 weeks after the boost (**Fig. 7C**, **fig. S8D-E**). Following a previously established protocol (*57, 63*),
451 we quantified GC reactions using two metrics: GC/FDC ratio (the frequency of GC formation
452 associated with FDC networks) and size of GCs. The M2ex3 trimer and both SApNPs induced
453 robust GCs, with the I3-01v9a SApNP showing the largest GCs at 2 weeks after a single-dose
454 injection (**Fig. 7B**, **fig. S8A**). As expected, the GC/FDC ratio and GC size declined over time in
455 all groups. Notably, while the GC/FDC ratio for the M2ex3 trimer group decreased to ~50%, the
456 I3-01v9a SApNP generated strong and durable GC reactions that lasted for 8 weeks (**Fig. 7B** and
457 **7D**, **fig. S8C**). GCs were restored for all vaccine groups after the boost, but the GC/FDC ratio for
458 the trimer group decreased again significantly at 5 weeks after the boost. Overall, the M2ex3 I3-
459 01v9a SApNP generated GCs 2.5 times the size after one dose (**Fig. 7B** and **7D**) and 1.7 times the
460 size after the boost (**Fig. 7C** and **7E**) of GCs elicited by the soluble trimer at 8 weeks.

461 The GCs were further analyzed by flow cytometry. We collected sentinel lymph nodes at
462 2, 5, and 8 weeks after a single-dose injection (**Fig. 7F**, and **fig. S9**), and at 2 and 5 weeks after the
463 boost (**Fig. 7G**) (4 footpads, 10 μg/injection) following the prime-boost regimen. The lymph node
464 tissues were disaggregated into a single cell suspension and stained with an antibody cocktail. The
465 percentage and number of GC B cells and T_{fh} cells were used to quantify the GC reactions, which
466 correlate with the immunohistological results (**Fig. 7A-E**). Flow cytometry indicated that M2ex3
467 I3-01v9 SApNP elicited the largest GC B cell and T_{fh} cell populations after a single-dose injection
468 (**Fig. 7F**). GC reactions peaked at 2 weeks for all tested groups and declined over time. While the
469 M2ex3 trimer failed to maintain the GC reactions, the M2ex3 I3-01v9a SApNP induced durable
470 GC reactions lasting for 8 weeks (**Fig. 7F**). Both the frequency and number of GC B cells and T_{fh}
471 cells could be improved by a boost injection (**Fig. 7G**). Interestingly, a significant expansion of

472 T_{fh} cells was noted for the FR and I3-01v9a SApNPs 2 weeks after the boost. Overall, the M2ex3
473 I3-01v9a SApNP elicited 5.7/1.1 times more GC B cells and 7.0/1.3 times more T_{fh} cells compared
474 with the soluble trimers at 8 weeks after the single-dose/prime-boost injections, respectively (**Fig.**
475 **7F** and **7G**). In summary, our immunological analysis suggests that M2ex3 I3-01v9a SApNPs can
476 generate long-lived GC reactions in lymph nodes more effectively than individual M2ex3 trimers,
477 resulting in potent and long-lasting M2ex3-specific humoral immunity.

478 **Antibody-dependent cell cytotoxicity and functional T cell responses**

479 The non-neutralizing M2e-specific antibody responses were evaluated for functional activity using
480 a surrogate antibody-dependent cell cytotoxicity (ADCC) assay (see Methods). The M2ex3 I3-
481 01v9a-immune sera elicited significantly higher relative light units (RLUs) in Jurkat effector cells
482 compared with the naïve, M2ex3 trimer, and M2ex3 FR groups, indicating detection of M2e
483 antibodies by mouse Fcγ receptor IV (mFcγRIV) expressed on Jurkat cells (**Fig. 8A**). The largest
484 difference in ADCC activity between the I3-01v9a SApNP and other groups was observed at the
485 lowest serum dilution tested, 20×, with I3-01v9a SApNP showing 7.2-fold, 5.9-fold, and 2.1-fold
486 higher RLU than naïve, trimer, and FR groups, respectively. Thus, this assay confirmed that
487 M2ex3 immune sera binding to homotetrameric M2e on influenza-infected cells has the potential
488 to activate ADCC pathways, which is an important mechanism for M2e-mediated protection.

489 While antibody-mediated neutralization plays a key role in blocking virus infection, T cell-
490 mediated cellular immunity effectively reduces disease severity, hospitalization, and death rate (*87,*
491 *88*). Enzyme-linked immunosorbent spot **(**ELISpot) analysis demonstrated that the M2ex3 I3-
492 01v9a SApNP group produced significantly higher spot formation in bulk IFN-γ-secreting
493 splenocytes stimulated with the M2ex3-5GS-foldon trimer probe compared to the naïve (> 28-
494 fold), M2ex3 trimer (7-fold), and M2ex3 FR (2.5-fold) groups per 8×10^5 splenocytes (**Fig. 8B**).

495 Similarly, the M2ex3 I3-01v9a group also produced, on average, more spots in IL-4-secreting
496 splenocytes compared to the naïve (21.8-fold), M2ex3 trimer (1.7-fold), and M2ex3 FR (1.7-fold)
497 groups, although the findings were not statistically significant.

498 For analysis of specific T cell subsets, T cells from splenic tissue were divided into several
499 subsets, including $CD4^+$ helper cells, which have multiple central roles in orchestrating adaptive
500 immune responses, and $CD8^+$ cytotoxic T cells, which control virus infection by killing virus-
501 infected cells and producing effector cytokines (*89-92*). Here, we designed a 13-color panel to
502 analyze functional T cell responses by measuring activation induced marker (AIM) and
503 intracellular cytokine staining (ICS) using flow cytometry. We compared various M2ex3 vaccine
504 constructs for the induction of $CD4^+$ and $CD8^+$ responses specific to the vaccine antigen at 5 days
505 after the PR8 (H1N1) challenge following a two-dose immunization regimen (**Fig. 4A**). Mouse
506 splenocytes from the M2ex3 trimer, FR, and I3-01v9a SApNP groups were stimulated with the
507 M2ex3-5GS-foldon trimer probe prior to analysis. All three M2ex3 constructs generated balanced
508 Th1 and Th2 responses and relatively lower Th17 responses (**Fig. 8C**, **fig. S10**). Among the three
509 vaccines, M2ex3 I3-01v9a SApNP was most effective in terms of the frequency and number of
510 intracellular cytokine (IFN-γ, TNF-α, IL-2, IL-17 and IL4)-producing $CD4^+$ T cells, $CD40L^+CD4^+$
511 T cells, and $CD40L^+CD4^+$ T cells that produce intracellular cytokines, as well as T_{fh} cells.
512 Importantly, M2ex3 I3-01v9a SApNP induced significantly more IFN-γ-producing functional
513 $CD4^+$ T cells, which contained 2.7 times more activated ($CD40L^+$) T cells compared with the
514 M2ex3 trimer, resulting in a Th1-skewed response. Similarly, M2ex3 I3-01v9a SApNP elicited
515 more intracellular cytokine (IFN-γ, TNF-α, IL-2)-producing $CD8^+$ T cells, $CD69^+CD8^+$ T cells,
516 and $CD69^+CD8^+$ T cells that produce IFN-γ than naïve, M2ex3 trimer, and M2ex3 FR groups (**Fig.
517 8D**). Overall, M2ex3 I3-01v9a SApNP induced stronger functional $CD4^+$ and $CD8^+$ T cell

518 responses than M2ex3 trimer and FR SApNP, consistent with the higher survival, lower weight
519 loss and viral loads (**Fig. 4**), and greater M2e-specific antibody responses (**Fig. 5**).

520 **DISCUSSION**

521 Since the 1918 Spanish flu, influenza has caused millions of deaths and hospitalizations worldwide
522 and remains a serious public health threat. From 2010 to 2017, seasonal flu caused 9.2 to 35.6
523 million reported cases of influenza and 140,000 to 710,000 hospitalizations. Each year, seasonal
524 flu causes an estimated 3-5 million cases of severe illness worldwide (*1*). Conventional influenza
525 vaccines, such as inactivated viruses produced in eggs, have been shown to significantly reduce
526 disease burden. However, these vaccines mainly induce NAbs to viral epitopes that are prone to
527 antigenic drift, allowing viruses to evade vaccine-induced immune responses (*17*). As a result,
528 annual updates are necessary for seasonal flu vaccines, yet they still may not offer sufficient
529 protection. Additionally, recent evidence has revealed the negative impact of repeated antigen
530 exposure on vaccine efficacy (*93*). Therefore, it is important to develop a vaccine that can provide
531 broad and durable protection against diverse influenza viruses.

532 An effective M2e vaccine covering all IAVs and eliciting durable M2e antibody responses
533 may address these two goals for developing a universal pan-influenza A vaccine. M2e antibodies
534 are non-neutralizing but can engage alveolar macrophages and natural killer cells to promote viral
535 clearance via ADCC (*94, 95*). In principle, a successful M2e vaccine could act as a standalone
536 pan-influenza A vaccine, reducing the severity of disease caused by pandemic strains originating
537 from various animal reservoirs that contain novel HA subtypes against which the majority of the
538 human population lacks pre-existing immunity (*17*). Alternatively, M2e can be used to
539 complement seasonal influenza vaccines, significantly boosting the breadth of these strain-specific
540 inactivated virus vaccines (*96*). However, to date, an approved M2e vaccine remains elusive. Here,

541 we approached M2e vaccine development with a rational strategy, in which newly developed 1c-
542 SApNPs were used as multivalent carriers to display 60 copies of an M2e antigen to overcome the
543 intrinsically poor immunogenicity associated with soluble M2e and increase durability of M2e-
544 specific immunity. Notably, we have previously developed vaccine candidates for HIV-1 (*57, 62*),
545 HCV (*60*), SARS-Cov-1/2 (*59*), and EBOV (*58*) based on the 1c-SApNP platform. In this study,
546 we first tested this strategy using hM2e and, based on the results, presented a tandem M2e antigen,
547 derived from human, avian, and swine IAVs, on FR and two multilayered 1c-SApNPs, E2p and
548 I3-01v9a. All the M2e vaccine constructs were evaluated in vitro and in vivo.

549 Our approach addresses the two limitations of previous M2e-based vaccine candidates in
550 clinical trials: 1) poor immunogenicity and 2) poor durability. First, the presentation of M2e on
551 the surface of 60-meric 1c-SApNPs significantly improves the immunogenicity of M2e. The large
552 size and high thermostability of the M2ex3-presenting I3-01v9a SApNP allows for long retention
553 in the lymph nodes follicles (8 weeks or longer), resulting in robust and prolonged GC reactions
554 compared to those elicited by the scaffolded M2e trimer. Combining the M2ex3 I3-01v9a SApNP
555 with commonly used adjuvants such as AP or AddaVax resulted in potent M2e-specific antibody
556 and functional T cell responses that likely conferred protection against sequential H1N1 and H3N2
557 challenges. In contrast, the inactivated PR8 (H1N1) virus vaccine and a strain-matched challenge
558 offered minimal protection against a follow-up heterologous challenge from a different subtype
559 (H3N2). Overall, our result suggest that the adjuvanted M2ex3 I3-01v9 SApNP can be developed
560 into a potent, durable, and cross-protective influenza vaccine that may overcome the limitations of
561 current marketed influenza vaccines, including the lack of protection against antigenically drifted
562 seasonal or novel pandemic strains (*97*). Additionally, this vaccine may have advantages over
563 previous M2e vaccine candidates in terms of effectiveness and durability.

564 Future studies will focus on several fronts. First, the lead candidate identified in this study,
565 M2ex3 I3-01v9a SApNP, may be formulated with more potent adjuvants to improve vaccine
566 efficacy. In a recent study, we tested the effect of various adjuvants on a SARS-CoV-2 spike 1c-
567 SApNP vaccine and found that toll-like receptor 9 (TLR9) and stimulator of interferon genes
568 (STING) agonists significantly increased NAb titers compared to other adjuvants, including AP
569 and AddaVax (*63*). Second, an M2e/inactivated virus combination vaccine concept may warrant
570 further evaluation. While M2ex3 1c-SApNP can be used as a standalone vaccine, it may also be
571 combined with a seasonal flu vaccine to boost protection against non-vaccine-matched circulating
572 strains and potential pandemic strains. Third, an M2ex3 1c-SApNP vaccine may protect against
573 highly pathogenic H5N1 and H7N9 influenza strains. Lastly, less commonly explored influenza B
574 M2e (in tandem) can be incorporated onto influenza A M2ex3 1c-SApNP to potentially yield a
575 truly universal, single component influenza vaccine against both influenza A and B viruses. Given
576 the sequence conservation of M2e across HA subtypes, the M2e vaccines developed in this study
577 may protect against diverse IAVs, which account for ~70% of all influenza cases annually, thereby
578 significantly reducing the deaths and hospitalizations associated with influenza worldwide.

579 **METHODS**

580 **Computational design of I3-01v9a for optimal nanoparticle display of monomeric antigens**

581 We redesigned the N-terminus of I3-01v9 for optimal surface display of monomeric antigens, such
582 as M2e, without using long linkers. Because I3-01v9 and I3-01 share nearly identical NP structures
583 (*57*), the I3-01 structure (PDB ID: 5KP9) was used here for all modeling purposes. We manually
584 extended the I3-01 N-terminal helix as an initial model. Briefly, an α-helix (residues 953-982) of
585 the transcription factor protein c-MYC (PDB ID: 6G6L) was grafted onto an I3-01 subunit by
586 using Glu2 and Glu3 of I3-01 for fitting. The grafted N-terminal helix was truncated to 11 residues

587 so that the first residue would be just above the surface after particle assembly. The CONCOORD
588 suite (*64*) was used to sample 1000 structures for the modified I3-01 subunit to facilitate ensemble-
589 based protein design. Using default OPLS-UA parameters and a *damp* parameter of 0.1, geometric
590 constraints were generated by the program dist as input for the program disco to generate slightly
591 perturbed conformations (*64*). An ensemble-based design method used in our previous studies (*57,*
592 *60*) was employed to predict the first 9 of the 11 residues in the extended N-terminal helix using
593 C_α and C_β-based RAPDF scoring functions (*65*). Given a scoring function, Monte Carlo simulated
594 annealing minimization (*57, 60*) was performed to predict the amino acid composition for each of
595 the 1000 CONCOORD-derived conformations. For each position of the 9-residue helical segment,
596 the frequency of each amino acid type was calculated from the entire ensemble. The final design,
597 I3-01v9a, was determined manually by combining results from both scoring functions.

598 **Expression and purification of various M2e immunogens**

599 Rationally designed hM2e and tandem M2ex3 scaffolds and SApNPs were characterized in vitro
600 and in vivo. Scaffolded trimers and SApNPs were transiently expressed in ExpiCHO™ cells
601 (Thermo Fisher) using a previously described protocol (*57, 58*). Briefly, ExpiCHO™ cells were
602 thawed and incubated with ExpiCHO™ Expression Medium (Thermo Fisher) in a shaker
603 incubator at 37°C, 135 rpm, and 8% CO_2. When cells reached a density of 10×10^6 cell/ml,
604 ExpiCHO™ Expression Medium was added to reduce cell density to 6×10^6 cell/ml for
605 transfection. ExpiFectamine™ CHO/plasmid DNA complexes were prepared for 100-ml
606 transfections in ExpiCHO cells following the manufacturer's instructions. For all constructs tested
607 in this study, 100 µg of antigen plasmid and 320 µl of ExpiFectamine™ CHO reagent were mixed
608 in 7.7 ml of cold OptiPRO™ medium (Thermo Fisher). After the first feed on day 1, ExpiCHO
609 cells were cultured in a shaker incubator at 32°C, 120 rpm, and 8% CO_2 following the Max Titer

610 protocol with an additional feed on day 5 (Thermo Fisher). Culture supernatants were harvested
611 13-14 days after transfection, clarified by centrifugation at 4000 rpm for 20 min, and filtered using
612 a 0.45 μm filter (Thermo Fisher). For all constructs, the M2e trimer or SApNP was extracted from
613 the culture supernatants by using mAb148 or mAb65 antibody columns. The bound protein was
614 eluted three times by 5 ml of glycine buffer (0.2M glycine, pH2.2) and neutralized by adding 0.375
615 ml Tris-base Buffer (2M Tris, pH9.0). Elutions were pooled and buffer exchanged via ultra-
616 centrifugal filtration to phosphate buffer saline (PBS). The size of trimers and SApNPs was
617 analyzed by size exclusion chromatography using AKTA pure 25 (Cytiva). Trimer was purified
618 on a Superdex 75 Increase 10/300 GL column (GE Healthcare), whereas SApNPs were
619 characterized on a Superose 6 10/300 GL column. Protein concentration was determined using
620 UV_{280} absorbance with theoretical extinction coefficients.

621 **SDS-PAGE and BN-PAGE**

622 The trimer and SApNPs were analyzed by sodium dodecyl sulfate-polyacrylamide gel
623 electrophoresis (SDS-PAGE) and blue native-polyacrylamide gel electrophoresis (BN-PAGE).
624 The proteins were mixed with loading dye and added to either a 10% Tris-Glycine Gel (Bio-Rad)
625 or a 4-12% Bis-Tris NativePAGE™ gel (Life Technologies). For SDS-PAGE under reducing
626 conditions, the proteins were first treated with dithiothreitol (DTT, 25 mM) and boiled for 5 min
627 at 100°C. SDS-PAGE gels were loaded with 1 μg of the sample and BN-PAGE gels were loaded
628 with 4 μg of the sample. SDS-PAGE gels were run for 20 min at 250 V using SDS running buffer
629 (Bio-Rad), and BN-PAGE gels were run for 2-2.5 h at 150 V using NativePAGE™ running buffer
630 (Life Technologies) according to the manufacturer's instructions. SDS-PAGE gels were stained
631 using InstantBlue (Abcam) and BN-PAGE gels were stained using Coomassie Brilliant Blue R-
632 250 (Bio-Rad) and de-stained using a solution of 6% ethanol and 3% glacial acetic acid.

633 **Differential scanning calorimetry**

634 Thermal melting curves of trimer and SApNPs following mAb148 or mAb65 purification were
635 obtained from a MicroCal PEAQ-DSC Man instrument (Malvern). Briefly, the purified SApNP
636 protein was buffer exchanged into 1×PBS buffer and concentrated to 0.5-3 μM prior to the
637 analysis. Melting was probed at a scan rate of 60°C·h^{-1} from 20°C to 100°C. Data processing,
638 including buffer correction, normalization, and baseline subtraction, was conducted using
639 MicroCal PEAQ-DSC software. Gaussian fitting was performed using Origin 9.0 software.

640 **Dynamic light scattering (DLS)**

641 Particle size distributions of hM2e and M2ex3 based on three NP platforms (FR, E2p-L4P, and I3-
642 01v9a-L7P) were obtained from a Zetasizer Ultra instrument (Malvern). MAb148/SEC-purified
643 NPs from ExpiCHO cells were diluted to 0.2 mg/ml using 1×PBS buffer, and 30 μl of the prepared
644 NP sample was added to a quartz batch cuvette (Malvern, catalog no. ZEN2112). Particle size was
645 measured at 25 °C in back scattering mode. Data processing was performed on the Zetasizer, and
646 the particle size distribution was plotted using Origin 9.0 software.

647 **Negative stain EM analysis**

648 The initial evaluation of various SApNP samples was performed by the Core Microscopy Facility
649 at The Scripps Research Institute. All SApNPs samples were prepared at the concentration of
650 0.005-0.02 mg/ml. Carbon-coated copper grids (400 mesh) were glow-discharged and 8 μl of each
651 sample was adsorbed for 2 min. Excess sample was wicked away and grids were negatively stained
652 with 2% uranyl formate for 2 min. Excess stain was wicked away and the grids were allowed to
653 dry. Samples were analyzed at 120 kV with a Talos L120C transmission electron microscope

654 (Thermo Fisher) and images were acquired with a CETA 16M CMOS camera. All SApNP samples
655 purified by mAb148 were validated under 52,000 × magnification before further use.

656 **Bio-layer interferometry (BLI)**

657 The kinetics profiles of both hM2e and M2ex3 trimers and SApNPs were measured using an Octet
658 RED96 instrument (FortéBio, Pall Life Sciences) against mAb148 and mAb65 antibody. All
659 assays were performed with agitation set to 1000 rpm in FortéBio 1× kinetic buffer. The final
660 volume for all solutions was 200 µl per well. Assays were performed at 30°C in solid black 96-
661 well plates (Geiger Bio-One). For all trimers and SApNPs, 5 µg/ml antibody in 1× kinetic buffer
662 was loaded onto the surface of anti-human Fc Capture Biosensors (AHC) for 300 s. A 60 s
663 biosensor baseline step was applied prior to the analysis of the association of the antibody on the
664 biosensor to the antigen in solution for 200 s. A two-fold concentration gradient of antigen, starting
665 at 25 nM for the hM2e trimer/SApNPs and 22 nM for the M2ex3 trimer/SApNPs, was used in a
666 titration series of six. The dissociation of the interaction was followed for 300 s. The correction of
667 baseline drift was performed by subtracting the mean value of shifts recorded for a sensor loaded
668 with antibody but not incubated with antigen, and for a sensor without antibody but incubated with
669 antigen. Octet data were processed by FortéBio's data acquisition software v.8.1. Peak signals at
670 the highest antigen concentration were summarized in a matrix to facilitate comparisons between
671 different vaccine platforms.

672 **Propagation of influenza viruses**

673 For challenge in mice, the following reagents were obtained through BEI Resources, NIAID, NIH:
674 Influenza A Virus, A/Puerto Rico/8/1934-Mouse Adapted (H1N1), NR-28652 and Influenza A
675 Virus, A/Hong Kong/1/1968-1 Mouse-Adapted 12 (H3N2), NR-28621. In brief, 4.4×10^6 Madin-
676 Darby canine kidney (MDCK) cells (CCL-34™; ATCC®) were plated overnight in 100 mm cell

677 culture dishes. The next day, cells were washed with PBS and incubated with a multiplicity of
678 infection (MOI) of 1 for PR8 or HK/68 in serum free media for 1 hour. Next, cells were washed
679 and 10 ml of serum-free DMEM containing 0.2% bovine serum albumin (BSA; VWR
680 international) and 1 μg/ml L-1-tosylamido-2-phenylethyl chloromethyl ketone (TPCK)-trypsin
681 (Sigma Aldrich) was added to the dishes. Cells were incubated for 65 h after which the supernatant
682 was collected, centrifuged at 4000 RPM for 10 min, aliquoted, and frozen at -80°C until use.

683 **Immunoplaque assay to quantify influenza viruses**

684 Virus PFU/ml of grown viruses was quantified using an immunoplaque assay. In brief, MDCK
685 cells were plated in 96-well plates at 25,000 cells/well. The cells were then washed with PBS and
686 infected with 10-fold serially diluted virus stocks. The inoculum was then removed, and cells were
687 overlayed with 0.7% low-melt agarose (Axygen) in serum-free DMEM containing 0.2% w/v BSA
688 and 1 μg/ml TPCK-trypsin. Twenty hours later, cells were fixed with 100 μl of 3.7% wt
689 formaldehyde for 1 h. Cells were then permeabilized with 50 μl ice-cold methanol for 20 min.
690 Fixed cells were then washed with deionized water and incubated with 50 μl of FluA-20 (non-
691 pandemic H1N1 strains), 2D1 (CA 09 H1N1), or F045-092 (pandemic or seasonal H3N2 strains)
692 IgG (10 μg/ml) for 1 h. Plates were washed and 50 μl of 1:5000 diluted HRP-goat anti-human IgG
693 was added to the wells. Plates were then placed on a shaker at 225 rpm for 1 h. Cells were then
694 washed and 50 μl of TrueBlue™ Peroxidase Substrate (SeraCare) was added to wells and
695 incubated for 10-15 min for the development of plaques. Lastly, plates were washed with deionized
696 water and left to dry overnight. Plaques were quantified using a Bioreader® 7000 (BIOSYS
697 Scientific®).

698 **Mouse immunization and challenge**

699 Six-to-eight-week-old female BALB/c mice were purchased from The Jackson Laboratory and
700 housed in ventilated cages in environmentally controlled rooms at The Scripps Research Institute,
701 in compliance with an approved IACUC protocol and Association for Assessment and
702 Accreditation of Laboratory Animal Care (AAALAC) international guidelines. Institutional
703 Animal Care and Use Committee (IACUC) guidelines were followed for all mice studies. Mice
704 were immunized at weeks 0 and 3, with 80 µl of antigen/adjuvant mix containing 10 µg of hM2e
705 or M2ex3 antigen in 40 µl PBS and 40 µl of adjuvant: aluminum phosphate (alum phosphate) or
706 AddaVax (InvivoGen). For the hM2e study, alum phosphate was used. For the M2ex3 study, both
707 alum phosphate and AddaVax were evaluated. The following reagent was obtained through BEI
708 Resources, NIAID, NIH: Influenza A Virus, A/Puerto Rico/8/1934 (H1N1), BPL-Inactivated, NR-
709 19325, and used as a positive control for the first strain-matched challenge (3 µg/mouse without
710 adjuvant). Each immunization dose was split amongst 4 footpads (20 µl/each). To assess the
711 protectivity and efficacy of the hM2e and M2ex3 constructs, immunized mice were sequentially
712 challenged with $LD_{50} \times 10$ of mouse-adapted A/Puerto Rico/8/1934 (PR8) H1N1 and A/Hong
713 Kong/1/1968 (HK/68) H3N2 at weeks 6 and 10, respectively. To establish the lethal dose of 50%
714 (LD_{50}) in mice for PR8 H1N1 and HK/68 H3N2, various dilutions of grown virus stock were
715 administered to mice (25 µl/nostril) after light anesthetization with isoflurane. Survival, weight
716 loss, and morbidity were monitored for 14 days. Mice that exhibited > 25% weight loss or showed
717 visible signs of distress were euthanized. Next, Reed-Muench and Spearman-Karber methods were
718 used to determine the 50% endpoint titer for both PR8 H1N1 and HK/68 H3N2 in mice (*69, 70*).
719 For first challenge at week 6, mice immunized with hM2e or M2ex3 constructs were lightly
720 anesthetized with isoflurane and $LD_{50} \times 10$ of PR8 H1N1 (50 µl) was administered to each mouse
721 (25 µl/nostril). Five mice from M2ex3 + AddaVax groups were sacrificed at Day 5 to assess the

722 viral load in lungs. In brief, mice were euthanized, and lungs were isolated. The lung tissue in PBS
723 was then crushed and spun down at 1200 rpm for 10 min. The lung supernatant was then aliquoted
724 and frozen at -80°C for future analysis. Viral loads were evaluated in lung supernatant using the
725 immunoplaque assay mentioned previously. Remaining mice were monitored for survival and
726 weight loss for 14 days post-challenge. At week 10, surviving mice were lightly anesthetized and
727 challenged with $LD_{50} \times 10$ HK/68 H3N2. Mice that exhibited > 25% weight loss or showed visible
728 signs of distress were euthanized. Blood of immunized mice was collected 2 weeks after each
729 immunization or challenge (weeks 2, 5, 10, and 14). All bleeds were performed through the facial
730 vein. Blood was spun down at 14,000 rpm for 10 min to separate serum from the rest of the whole
731 blood. The serum was then heat-inactivated at 56°C for 30 min and spun down at 8,000 rpm for
732 10 min to remove precipitates.

733 **Enzyme-linked immunosorbent assay (ELISA)**

734 For assessing hM2e-specific binding of hM2e-immune sera, 50 µl hM2e-5GS-foldon trimer probe
735 was coated on the surface of half-well 96-well high-binding polystyrene plates at a concentration
736 of 0.1 µg/well. Plates were kept at 4°C overnight. The next day, plates were washed 5× with PBS
737 containing 0.05% v/v Tween 20® (PBST). Plates were then blocked with 150 µl of 4% w/v nonfat
738 milk (Bio-Rad) for 1 h. Plates were then washed and 50 µl of hM2e-immune sera was added to
739 each well for 1 h. Serum was diluted 20× in 4% nonfat milk followed by seven 10-fold dilutions.
740 M2e antibodies mAb148 and mAb65 were used as positive controls. Next, plates were washed and
741 50 µl of 1:3000 dilution horseradish peroxidase (HRP)-conjugated goat anti-mouse IgG in PBST
742 was added to the wells and incubated for 1 h. Plates were then washed and 50 ul of 1-Step™
743 3,3',5,5'-tetramethylbenzidine (TMB; Thermo Fisher) substrate was added to each well and
744 incubated for 3 min. Plates were washed 6× and 50 µl of 2.0 N sulfuric acid (Aqua Solutions, Inc.)

745 was added to each well. Plates were then immediately read on a plate reader (BioTek Synergy)
746 using a wavelength of 450 nm. An identical ELISA method was used for M2ex3-specific binding
747 of M2ex3-immune sera, except for the use of M2ex3-5GS-foldon trimer probe.

748 **Cell-based ELISA**

749 For cell-based ELISA, the following 8 reagents were obtained through BEI Resources, NAID,
750 NIH: 1) Influenza A Virus, A/Puerto Rico/8/1934 (H1N1; NR-348), 2) Influenza A Virus,
751 A/California/04/2009 (H1N1; NR-136583), 3) Influenza A Virus, A/Solomon Islands/3/2006
752 (H1N1; NR-41798), 4) Influenza A Virus, A/Hong Kong/1/1968 (H3N2) (mother clone), ,NR-
753 28620, 5) Influenza A virus, A/Brisbane/10/2007 (H3N2; NR-12283, 6) Influenza A virus,
754 A/Aichi/2/1968 (H3N2; NR-3177), 7) Influenza B Virus, B/Florida/4/2006 (Yamagata Lineage;
755 NR-41795), and 8) Influenza B Virus, B/Brisbane/60/2008 (Victoria Lineage; NR-42005). The
756 viruses were grown in MDCK cells using the same method mentioned previously for propagating
757 challenge strains. For cell-based ELISA, MDCK cells were plated overnight in 96-well cell culture
758 plates at a density of 18,000 cells/well. The next day the cells were washed and infected with 100
759 µl of 1 of the 8 viruses at a MOI of 1. Twenty hours later, the virus was removed, and cells were
760 washed before being fixed with 100 µl of 3.7% wt formaldehyde. Cells were then washed, and the
761 previous ELISA protocol was used except with an incubation step with TMB for 5 min.

762 **Histology, immunostaining, and imaging**

763 To study vaccine distribution, trafficking, retention, cellular interaction, and GC reactions in
764 lymph nodes, M2ex3 trimer and FR and I3-01v9a SApNP immunogens formulated with AddaVax
765 adjuvant were injected intradermally into four mouse footpads using 29-gauge insulin needles.
766 Mice were anesthetized with 3% isoflurane in oxygen during immunization. Similar protocols of
767 mouse injection, lymph node collection and tissue analysis were utilized from our previous study

768 (*57, 63*). The injection dose was 80 µl of antigen/adjuvant mix containing 40 µg of vaccine
769 immunogen per mouse or 10 µg per footpad. Mice were euthanized at 2 h to 8 weeks after a single-
770 dose injection or 2 and 5 weeks after the boost, which occurred at 3 weeks after the first dose.
771 Brachial and popliteal sentinel lymph nodes were collected for immunohistological study. Fresh
772 lymph nodes were isolated and merged into frozen section compound (VWR International, catalog
773 no. 95057-838) in a plastic cryomold (Tissue-Tek at VWR, catalog no. 4565). Tissue samples were
774 frozen in liquid nitrogen and stored at -80°C before shipping to The Centre for Phenogenomics in
775 Canada for tissue processing, immunostaining, and imaging. Lymph node tissue sections were
776 sliced 8 µm thick on a cryostat (Cryostar NX70) and placed on a charge slide. Next, tissue slides
777 were fixed in 10% neutral buffered formalin and permeabilized in PBS buffer that contained 0.5%
778 Triton X-100 before immunostaining. The slides were blocked with protein Block (Agilent) to
779 prevent nonspecific antibody binding. Primary antibodies were applied on tissue slides and
780 incubated overnight at 4°C. After washing with tris-buffered saline with 0.1% Tween-20 (TBST),
781 secondary antibodies that we conjugated with either biotin or a fluorophore were utilized and
782 incubated at 25°C for 1 hour. Lymph node tissues were stained with anti-human Ab148 or Ab65
783 (1:200), and biotinylated goat anti-human secondary antibody (Abcam, catalog no. ab7152, 1:300),
784 followed by streptavidin-horseradish peroxidase (HRP) reagent (Vectastain Elite ABC-HRP Kit,
785 Vector, catalog no. PK-6100) and diaminobenzidine (ImmPACT DAB, Vector, catalog no. SK-
786 4105).

787 To study cellular interactions between M2ex3 trimer immunogens and cell components in
788 lymph nodes, FDCs were labelled using anti-CD21 primary antibody (Abcam, catalog no.
789 ab75985, 1:1800), followed by anti-rabbit secondary antibody conjugated with Alexa Fluor 555
790 (Thermo Fisher, catalog no. A21428, 1:200). Subcapsular sinus macrophages were labeled using

791 anti-sialoadhesin (CD169) antibody (Abcam, catalog no. ab53443, 1:600), followed by anti-rat
792 secondary antibody conjugated with Alexa Fluor 488 (Abcam, catalog no. ab150165, 1:200). B
793 cells were labeled using anti-B220 antibody (eBioscience, catalog no. 14-0452-82, 1:100),
794 followed by anti-rat secondary antibody conjugated with Alexa Fluor 647 (Thermo Fisher, catalog
795 no. A21247, 1:200). GC reactions induced by M2ex3 trimers and SApNPs were studied by
796 immunostaining. GC B cells were labeled using rat anti-GL7 antibody (FITC; BioLegend, catalog
797 no. 144604, 1:250). T_{fh} cells were labeled using anti-CD4 antibody (BioLegend, catalog no.
798 100402, 1:100), followed by anti-rat secondary antibody conjugated with Alexa Fluor 488
799 (Abcam, catalog no. ab150165, 1:1000). GC forming cells were stained using Bcl6 antibody
800 (Abcam, catalog no. ab220092, 1:300), followed by anti-rabbit secondary antibody conjugated
801 with Alexa Fluor 555 (Thermo Fisher, catalog no. A21428, 1:1000). Nuclei were labeled using
802 4′,6-diamidino-2-phenylindole (DAPI) (Sigma-Aldrich, catalog no. D9542, 100 ng/ml). The
803 immunostained lymph node tissues were scanned using an Olympus VS-120 slide scanner with a
804 Hamamatsu ORCA-R2 C10600 digital camera. The vaccine transport and induced GC reactions
805 in lymph nodes were quantified through bright-field and fluorescent images using ImageJ
806 software.

807 **Lymph node disaggregation, cell staining, and flow cytometry**

808 GC reactions in terms of frequency and numbers of GC B cells ($GL7^+B220^+$) and T_{fh} cells
809 ($CD3^+CD4^+CXCR5^+PD\text{-}1^+$) were characterized using flow cytometry (**fig. S9**). Mice were
810 euthanized at 2, 5, and 8 weeks after a single-dose injection or 2 and 5 weeks after the boost,
811 occurring at 3 weeks after the first dose (4 footpads, 10 μg/footpad). Fresh axillary, brachial, and
812 popliteal sentinel lymph nodes were collected for GC study. Lymph node tissues were
813 disaggregated mechanically and merged in enzyme digestion solution in an Eppendorf tube with

814 958 μl of Hanks' balanced salt solution (HBSS) buffer (Thermo Fisher Scientific, catalog no.
815 14185052), 40 μl of 10 mg/ml collagenase IV (Sigma-Aldrich, catalog no. C5138), and 2 μl of 10
816 mg/ml DNase (Roche, catalog no. 10104159001) and incubated at 37°C for 30 min. The lymph
817 node tissue was then filtered through a 70 μm cell strainer to obtain a single cell suspension. Cell
818 samples were spun down at 400 × *g* for 10 min and the cell pellets were resuspended in HBSS
819 blocking buffer containing 0.5% (w/v) bovine serum albumin and 2 mM EDTA. Anti-CD16/32
820 antibody (BioLegend, catalog no. 101302) was added into the Eppendorf tube to block the
821 nonspecific binding on Fc receptors. Cells were kept on ice for 30 min and transferred to 96-well
822 V-shaped-bottom microplates with pre-prepared cocktail antibodies, including Zombie NIR
823 live/dead stain (BioLegend, catalog no. 423106), Brilliant Violet 510 anti-mouse/human
824 CD45R/B220 antibody (BioLegend, catalog no. 103247), FITC anti-mouse CD3 antibody
825 (BioLegend, catalog no. 100204), Alexa Fluor 700 anti-mouse CD4 antibody (BioLegend, catalog
826 no. 100536), PE anti-mouse/human GL7 antibody (BioLegend, catalog no. 144608), Brilliant
827 Violet 605 anti-mouse CD95 (Fas) antibody (BioLegend, catalog no. 152612), Brilliant Violet 421
828 anti-mouse CD185 (CXCR5) antibody (BioLegend, catalog no. 145511), and PE/Cyanine7 anti-
829 mouse CD279 (PD-1) antibody (BioLegend, catalog no. 135216). Cells were mixed with antibody
830 cocktail and placed on ice for 30 min. Cell samples were spun down at 400 × *g* for 10 min and the
831 cell pellets were resuspended in HBSS blocking solution for washing one more time. Cells were
832 then fixed with 1.6% paraformaldehyde (Thermo Fisher Scientific, catalog no. 28906) in HBSS
833 and placed on ice for 30 min. Cells were spun down at 400 × *g* for 10 min and placed in HBSS
834 blocking buffer at 4°C before test. Sample events were acquired using a 5-laser AZE5 flow
835 cytometer (Yeti, Bio-Rad) with Everest software at the Core Facility of The Scripps Research
836 Institute. The data were analyzed using FlowJo 10 software.

837 **ADCC (antibody-dependent cell cytotoxicity) surrogate assay**

838 The potential for M2e-specific antibodies to induce antibody-dependent cell cytotoxicity (ADCC)
839 was evaluated using a mouse FcγRIV ADCC Reporter kit (Promega). In brief, MDCK cells were
840 plated in white 96-well plates overnight at 18,000 cells/well. The next day, cells were washed with
841 PBS and infected with PR8 H1N1 at a MOI of 1. Twenty hours later, the cells were washed and
842 25 µl of M2ex3-immune sera was added to the wells for 1 h (sera was diluted 20× followed by 10-
843 fold dilutions). Next, as per the kit's instructions (Promega), 75,000 mouse FCγRIV Jurkat cells
844 were added to each well. The plates were incubated for 6 h at 37°C. Lastly, 75 µl of Bio-Glo™
845 Reagent were added to the well. Relative light units were measured using a plate reader after a 5-
846 min incubation of each plate.

847 **Splenocyte isolation**

848 At week 14, mice were anesthetized using isoflurane and euthanized using cervical dislocation.
849 Spleens were harvested from mice and kept in PBS on ice. Next, spleens were crushed with the
850 back of a syringe and resuspended in 20 ml of PBS. Cells were centrifuged at 1200 rpm for 10
851 min. Next, supernatant was discarded, and 3 ml of ACK lysis buffer (Lonza) was added to the cells
852 and incubated for 5 min. Next 12 ml of PBS was added to the tubes, which were then centrifuged
853 at 1200 rpm for 5 min. Supernatant was then discarded, and cells were resuspended in 1 ml PBS.
854 Cells were passed through a 70-µm cell strainer. Cells were then centrifuged for 5 min. Lastly,
855 cells were resuspended in 10% DMSO in FBS, transferred into a -80°C freezer overnight, and then
856 stored in the vapor phase of liquid nitrogen until analysis.

857 **Enzyme-linked immunosorbent spot (ELISpot) assay**

858 For analyzing IFN-γ and IL-4-secreting splenocytes of mice immunized with M2ex3, ELISpot was
859 used. First, Multiscreen® filter plates (Millipore Sigma) were coated with capture IFN-γ or IL-4

860 (BD Biosciences) at a 1:200 dilution. The plates were incubated at 4 °C overnight. The next day,
861 plates were washed and blocked with 200 µl of complete RPMI 1640 (10% FBS, 1% Penn-Strep,
862 1% L-glutamine; Gibco) medium. Next, the M2ex3-5GS-foldon trimer probe was prepared at 50
863 µg/ml in complete RPMI. Concanavalin A (10 µg/ml; BD Biosciences) was prepared as a positive
864 control. Next, spleen samples were thawed, resuspended in RPMI and centrifuged at 1200 RPM
865 for 10 min. Cells were then counted using an automated cell counter (Countess II; Thermo Fisher)
866 and suspended to reach a concentration of 1.6×10^7 cells/ml. Next, RPMI was discarded from the
867 filter plates and 50 µl of antigen was added to the well. Next, 50 µl of cell suspension was added
868 to each well, producing a final cell concentration of 8×10^5 splenocytes/well. After addition of
869 cells, the final concentrations of the M2ex3-5GS-foldon trimer probe and Concanavalin A were
870 2.5 µg/well and 0.5 µg/well, respectively. Cells without antigen were used as a negative control.
871 Plates were incubated for 48 h at 37°C. Next, cells were washed 2× with deionized water followed
872 by 3 washes with PBST. Next, 50 µl detection IFN-γ or IL-4 antibodies (BD Biosciences) diluted
873 1:250 in dilution buffer (10% FBS in PBS) were added to corresponding wells. Plates were then
874 incubated for 2 h at room temperature (RT). Next, plates were washed 3× with PBST and 50 µl
875 Streptavidin-HRP (BD Biosciences) diluted 1:100 in dilution buffer was added to the well and
876 incubated for 1 h. Plates were then washed 4× with PBST and 2× with PBS. AEC Final Substrate
877 (BD Biosciences) was then added to the wells for 15-20 min for the development of spots. Plates
878 were kept in the dark overnight and read using a Bioreader® 7000.

879 **T cell culture and stimulation**

880 Functional M2e-specific T cells responses were characterized by measuring activation induced
881 marker (AIM) and intracellular cytokine staining (ICS) using flow cytometry (**fig. S10**). Mouse
882 splenocytes were isolated from naïve or vaccinated mice at 5 days after prime-boost immunizations

883 and followed by a H1N1 virus challenge. Cryopreserved splenocytes were thawed by diluting cells
884 in 10 ml pre-warmed complete RPMI media with 10% deactivated fetal bovine serum (FBS) and
885 1% penicillin/streptomycin (P/S). Cells were spun down at 400 × *g* for 10 min and cell pellets were
886 resuspended in RPMI media. The numbers of splenocytes were counted and adjusted to 10 million
887 cells/ml. One million splenocytes for each mouse were placed into 96-well U-shaped-bottom
888 microplates. Cells were cultured in the presence of the M2ex3-5GS-foldon trimer probe (1 μg per
889 well) at 37°C for a total of 24 h. After 20 h, Brefeldin A Solution (BioLegend, catalog no. 420601)
890 was added in the culture to enhance intracellular cytokine staining signals by inhibiting the protein
891 transport processes in the rough endoplasmic reticulum and Golgi apparatus. After 4 h, cells were
892 then spun down at 400 × *g* for 10 min and cell pellets were resuspended in HBSS blocking buffer.
893 Anti-CD16/32 antibody (BioLegend, catalog no. 101302) was added for 30 min on ice to block
894 nonspecific binding to Fc receptors. Cells were then transferred to 96-well V-shaped-bottom
895 microplates with pre-prepared cocktail antibodies for surface marker staining, including
896 LIVE/DEAD Fixable Blue Dead Cell Stain Kit (Thermo Fisher Scientific, catalog no. L34962),
897 FITC anti-mouse CD3 antibody (BioLegend, catalog no. 100204), Alexa Fluor 700 anti-mouse
898 CD4 antibody (BioLegend, catalog no. 100536), BUV737 Anti-Mouse CD8a antibody (BD
899 Bioscience, catalog no. 612759), APC anti-mouse CD154 antibody (BioLegend, catalog no.
900 106510), Brilliant Violet 421 anti-mouse CD69 Antibody (BioLegend, catalog no. 104527),
901 APC/Fire 810 anti-mouse CD279 (PD-1) antibody (BioLegend, catalog no. 135251), and Brilliant
902 Violet 605 anti-mouse CD185 (CXCR5) Antibody (BioLegend, catalog no. 145513). Splenocytes
903 were mixed with antibody cocktail and placed on ice for 30 min. Cells were spun down at 400 × *g*
904 for 10 min and the cell pellets were resuspended in HBSS blocking solution, then washed once
905 more. Cells were fixed with 1.6% paraformaldehyde (Thermo Fisher Scientific, catalog no. 28906)

906 in HBSS and placed on ice for 30 min. Cell were then washed two times with intracellular staining
907 permeabilization wash buffer (BioLegend, catalog no. 421002) and stained with previously
908 prepared antibody cocktail for intracellular staining, including PE anti-mouse IFN-γ antibody
909 (BioLegend, catalog no. 505808), Brilliant Violet 785 anti-mouse TNF-α antibody (BioLegend,
910 catalog no. 506341), PE/Cyanine5 anti-mouse IL-2 antibody (BioLegend, catalog no. 503824),
911 PE/Cyanine7 anti-mouse IL-4 antibody (BioLegend, catalog no. 504118), and Brilliant Violet 711
912 anti-mouse IL-17A Antibody (BioLegend, catalog no. 506941). Cells were mixed with
913 intracellular antibodies and placed on ice for 30 min. Cells were then washed again with
914 intracellular staining permeabilization wash buffer. Cells were stored in HBSS blocking buffer at
915 4°C prior to analysis. Sample events were acquired using a Cytek Aurora spectral analytical flow
916 cytometer with SpectroFlo software at the Flow Cytometry Core Facility of The Scripps Research
917 Institute. The data were analyzed using FlowJo 10 software.

918 **Statistical analysis**

919 Data was collected from 8-13 mice per group in the immunization studies, challenge experiments,
920 and sera binding assays. For the vaccine transport and GC study in lymph nodes and T cells in
921 spleens, 5 mice per group with different vaccine constructs were compared using one-way
922 ANOVA, followed by Tukey's multiple comparison *post hoc* test. Statistical significance is
923 indicated as the following in the figures: ns (not significant), *$p < 0.05$, **$p < 0.01$, ***$p < 0.001$,
924 ****$p < 0.0001$. The graphs were generated using GraphPad Prism 9.3.1 software.

925 **SUPPLEMENTARY MATERIALS**

926 Supplementary material for this article is available at XXX.

927 Supplementary Figures 1-10.

928 **ACKNOWLEDGEMENTS**

929 Y.-N.Z. thanks support from the Natural Sciences and Engineering Research Council of Canada
930 (NSERC) for the postdoctoral fellowship. We acknowledge G. Ossetchkine, K. Duffin, M.
931 Ganguly, and V. Bradaschia at The Centre for Phenogenomics for their expertise and technical
932 support in immunohistology. We acknowledge A. Saluk, B. Seegers, and B. Monteverde of the
933 Flow Cytometry Core Facility at The Scripps Research Institute for their technical support in flow
934 cytometry. We thank V. Tong for proofreading the manuscript. **Funding:** This work was
935 supported by Ufovax/SFP-2018-1013 (J.Z.). **Author contributions:** Project design by K.B.G.,
936 Y.-N.Z., Y.-Z.L., L.H. and J.Z.; immunogen expression and purification by M.E., A.L., G.W.,
937 and L.H.; negative stain EM by Y.-Z.L. and L.H.; mouse immunization and sample collection by
938 K.B.G. and Y.-N.Z.; virus challenge and serum binding analysis by K.B.G.; lymph node
939 isolation, immunohistology, and flow cytometry by Y.-N.Z.; manuscript written by K.B.G., Y.-
940 N.Z., Y.-Z.L., S.A., L.H. and J.Z. All authors were asked to comment on the manuscript. The
941 Scripps Research Institute manuscript number is 30235. **Competing interests:** The authors declare
942 that they have no competing interests. **Data and material availability:** All data to understand and
943 assess the conclusions of this research are available in the main text and Supplementary Materials.

944 References
945

946 1. F. Krammer *et al.*, Influenza. *Nat. Rev. Dis. Primers* **4**, 3 (2018).
947 2. C. Paules, K. Subbarao, Influenza. *Lancet* **390**, 697-708 (2017).
948 3. N. M. Bouvier, P. Palese, The biology of influenza viruses. *Vaccine* **26**, D49-D53 (2008).
949 4. D. Dou, R. Revol, H. Ostbye, H. Wang, R. Daniels, Influenza A virus cell entry,
950 replication, virion assembly and movement. *Front. Immunol.* **9**, (2018).
951 5. D. A. Steinhauer, J. J. Skehel, Genetics of influenza viruses. *Annu. Rev. Genet.* **36**, 305-
952 332 (2002).
953 6. Y. Y. Chou *et al.*, One influenza virus particle packages eight unique viral RNAs as
954 shown by FISH analysis. *P Natl Acad Sci USA* **109**, 9101-9106 (2012).
955 7. C. J. Russell, M. Hu, F. A. Okda, Influenza hemagglutinin protein stability, activation,
956 and pandemic risk. *Trends Microbiol.* **26**, 841-853 (2018).
957 8. J. E. Hernandez-Davies *et al.*, Administration of multivalent influenza virus recombinant
958 hemagglutinin vaccine in combination-adjuvant elicits broad reactivity beyond the
959 vaccine components. *Front. Immunol.* **12**, (2021).

960 9. I. Kosik, J. W. Yewdell, Influenza hemagglutinin and neuraminidase: yin-yang proteins
961 coevolving to thwart immunity. *Viruses* **11**, (2019).
962 10. R. K. Du, Q. H. Cui, L. J. Rong, Competitive cooperation of hemagglutinin and
963 neuraminidase during influenza A virus entry. *Viruses* **11**, (2019).
964 11. J. To, J. Torres, Viroporins in the influenza virus. *Cells-Basel* **8**, (2019).
965 12. M. C. Zambon, The pathogenesis of influenza in humans. *Rev. Med. Virol.* **11**, 227-241
966 (2001).
967 13. F. Krammer, P. Palese, Advances in the development of influenza virus vaccines. *Nat.*
968 *Rev. Drug Discov.* **14**, (2015).
969 14. S. Yamayoshi, Y. Kawaoka, Current and future influenza vaccines. *Nat. Med.* **25**, 212-
970 220 (2019).
971 15. C. J. Wei *et al.*, Next-generation influenza vaccines: opportunities and challenges. *Nat.*
972 *Rev. Drug Discov.* **19**, 239-252 (2020).
973 16. F. B. Scorza, V. Tsyetnitsky, J. J. Donnelly, Universal influenza vaccines: shifting to
974 better vaccines. *Vaccine* **34**, 2926-2933 (2016).
975 17. H. Kim, R. G. Webster, R. J. Webby, Influenza virus: dealing with a drifting and shifting
976 pathogen. *Viral Immunol.* **31**, 174-183 (2018).
977 18. W. F. Zhu *et al.*, Epidemiologic, clinical, and genetic characteristics of human infections
978 with influenza A(H5N6) viruses, China. *Emerg. Infect. Dis.* **28**, 1332-1344 (2022).
979 19. W. N. Harrington, C. M. Kackos, R. J. Webby, The evolution and future of influenza
980 pandemic preparedness. *Exp. Mol. Med.* **53**, 737-749 (2021).
981 20. C. L. D. McMillan, P. R. Young, D. Watterson, K. J. Chappell, The next generation of
982 influenza vaccines: towards a universal solution. *Vaccines* **9**, (2021).
983 21. R. K. Du, Q. H. Cui, L. J. Rong, Flu universal vaccines: new tricks on an old virus. *Virol.*
984 *Sin.* **36**, 13-24 (2021).
985 22. L. D. Estrada, S. Schultz-Cherry, Development of a universal influenza vaccine. *J.*
986 *Immun.* **202**, 392-398 (2019).
987 23. G. A. Sautto, G. A. Kirchenbaum, T. M. Ross, Towards a universal influenza vaccine:
988 different approaches for one goal. *Virol. J.* **15**, (2018).
989 24. S. L. Epstein, Universal influenza vaccines: progress in achieving broad cross-protection
990 in vivo. *Am. J. Epidemiol.* **187**, 2603-2614 (2018).
991 25. L. Coughlan, P. Palese, Overcoming barriers in the path to a universal influenza virus
992 vaccine. *Cell Host Microbe* **24**, 18-24 (2018).
993 26. R. Nachbagauer, F. Krammer, Universal influenza virus vaccines and therapeutic
994 antibodies. *Clin. Microbiol. Infect.* **23**, 222-228 (2017).
995 27. F. Krammer, Novel universal influenza virus vaccine approaches. *Curr Opin Virol* **17**,
996 95-103 (2016).
997 28. S. Jegaskanda, P. C. Reading, S. J. Kent, Influenza-specific antibody-dependent cellular
998 cytotoxicity: toward a universal influenza vaccine. *J. Immun.* **193**, 469-475 (2014).
999 29. B. L. Bullard, E. A. Weaver, Strategies targeting hemagglutinin as a universal influenza
1000 vaccine. *Vaccines* **9**, (2021).
1001 30. F. Kostolansky, K. Tomcikova, K. Briestenska, M. Mikusova, E. Vareckova, Universal
1002 anti-influenza vaccines based on viral HA2 and M2e antigens. *Acta Virol.* **64**, 417-426
1003 (2020).

1004 31. S. C. Wang, H. Y. Liao, J. Y. Zhang, T. J. R. Cheng, C. H. Wong, Development of a
1005 universal influenza vaccine using hemagglutinin stem protein produced from Pichia
1006 pastoris. *Virology* **526**, 125-137 (2019).
1007 32. F. Krammer, P. Palese, Universal influenza virus vaccines that target the conserved
1008 hemagglutinin stalk and conserved sites in the head domain. *J. Infect. Dis.* **219**, S62-S67
1009 (2019).
1010 33. A. L. Skarlupka, A. G. Bebin-Blackwell, S. F. Sumner, T. M. Ross, Universal influenza
1011 virus neuraminidase vaccine elicits protective immune responses against human seasonal
1012 and pre-pandemic strains. *J. Virol.* **95**, (2021).
1013 34. L. Deng, K. Cho, W. Fiers, X. Saelens, M2e-based universal influenza A vaccines.
1014 *Vaccines* **3**, 105-136 (2015).
1015 35. D. Mezhenskaya, I. Isakova-Sivak, L. Rudenko, M2e-based universal influenza vaccines:
1016 a historical overview and new approaches to development. *J. Biomed. Sci.* **26**, (2019).
1017 36. X. Saelens, The role of matrix protein 2 ectodomain in the development of universal
1018 influenza vaccines. *J. Infect. Dis.* **219**, S68-S74 (2019).
1019 37. M. Schotsaert, M. De Filette, W. Fiers, X. Saelens, Universal M2 ectodomain-based
1020 influenza A vaccines: preclinical and clinical developments. *Expert Rev. Vaccines* **8**, 499-
1021 508 (2009).
1022 38. J. A. Fan *et al.*, Preclinical study of influenza virus A M2 peptide conjugate vaccines in
1023 mice, ferrets, and rhesus monkeys. *Vaccine* **22**, 2993-3003 (2004).
1024 39. S. Neirynck *et al.*, A universal influenza A vaccine based on the extracellular domain of
1025 the M2 protein. *Nat. Med.* **5**, 1157-1163 (1999).
1026 40. T. A. Von Holle, M. A. Moody, Influenza and antibody-dependent cellular cytotoxicity.
1027 *Front. Immunol.* **10**, (2019).
1028 41. B. Schepens, D. De Vlieger, X. Saelens, Vaccine options for influenza: thinking small.
1029 *Curr. Opin. Immunol.* **53**, 22-29 (2018).
1030 42. N. V. Petukhova *et al.*, Immunogenicity and protective efficacy of candidate universal
1031 influenza A nanovaccines produced in plants by tobacco mosaic virus-based vectors.
1032 *Curr. Pharm. Des.* **19**, 5587-5600 (2013).
1033 43. A. M. C. Andersson *et al.*, Increased immunogenicity and protective efficacy of influenza
1034 M2e fused to a tetramerizing protein. *PLoS One* **7**, (2012).
1035 44. M. De Filette *et al.*, An influenza A vaccine based on tetrameric ectodomain of matrix
1036 protein 2. *J. Biol. Chem* **283**, 11382-11387 (2008).
1037 45. J. W. Huleatt *et al.*, Potent immunogenicity and efficacy of a universal influenza vaccine
1038 candidate comprising a recombinant fusion protein linking influenza M2e to the TLR5
1039 ligand flagellin. *Vaccine* **26**, 201-214 (2008).
1040 46. J. P. Adler-Moore *et al.*, Monomeric M2e antigen in VesiVax® liposomes stimulates
1041 protection against type a strains of influenza comparable to liposomes with multimeric
1042 forms of M2e. *J. Liposome Res.* **27**, 210-220 (2017).
1043 47. G. A. Stoloff, W. Caparros-Wanderley, Synthetic multi-epitope peptides identified in
1044 silico induce protective immunity against multiple influenza serotypes. *Eur. J. Immunol.*
1045 **37**, 2441-2449 (2007).
1046 48. A. Kolpe, B. Schepens, W. Fiers, X. Saelens, M2-based influenza vaccines: recent
1047 advances and clinical potential. *Expert Rev Vaccines* **16**, 123-136 (2017).
1048 49. L. H. L. Lua *et al.*, Bioengineering virus-like particles as vaccines. *Biotechnol. Bioeng.*
1049 **111**, 425-440 (2014).

1050 50. Q. Zhao, S. Li, H. Yu, N. Xia, Y. Modis, Virus-like particle-based human vaccines:
1051 quality assessment based on structural and functional properties. *Trends Biotechnol.* **31**,
1052 654-663 (2013).
1053 51. W. A. Rodriguez-Limas, K. Sekar, K. E. J. Tyo, Virus-like particles: the future of
1054 microbial factories and cell-free systems as platforms for vaccine development. *Curr.*
1055 *Opin. Biotechnol.* **24**, 1089-1093 (2013).
1056 52. P. Pushko, P. Pumpens, E. Grens, Development of virus-like particle technology from
1057 small highly symmetric to large complex virus-like particle structures. *Intervirology* **56**,
1058 141-165 (2013).
1059 53. N. Kushnir, S. J. Streatfield, V. Yusibov, Virus-like particles as a highly efficient vaccine
1060 platform: diversity of targets and production systems and advances in clinical
1061 development. *Vaccine* **31**, 58-83 (2012).
1062 54. G. T. Jennings, M. F. Bachmann, Coming of age of virus-like particle vaccines. *J. Biol.*
1063 *Chem.* **389**, 521-536 (2008).
1064 55. C. Ludwig, R. Wagner, Virus-like particles - universal molecular toolboxes. *Curr. Opin.*
1065 *Biotechnol.* **18**, 537-545 (2007).
1066 56. E. V. L. Grgacic, D. A. Anderson, Virus-like particles: passport to immune recognition.
1067 *Methods* **40**, 60-65 (2006).
1068 57. Y.-N. Zhang *et al.*, Single-component multilayered self-assembling protein nanoparticles
1069 presenting glycan-trimmed uncleaved prefusion optimized envelope trimers as HIV-1
1070 vaccine candidates. *Nat. Commun.* **14**, 1985 (2023).
1071 58. L. He *et al.*, Single-component multilayered self-assembling nanoparticles presenting
1072 rationally designed glycoprotein trimers as Ebola virus vaccines. *Nat. Commun.* **12**,
1073 (2021).
1074 59. L. He *et al.*, Single-component, self-assembling, protein nanoparticles presenting the
1075 receptor binding domain and stabilized spike as SARS-CoV-2 vaccine candidates. *Sci.*
1076 *Adv.* **7**, eabf1591 (2021).
1077 60. L. He *et al.*, Proof of concept for rational design of hepatitis C virus E2 core nanoparticle
1078 vaccines. *Sci. Adv.* **6**, eaaz6225 (2020).
1079 61. L. He *et al.*, HIV-1 vaccine design through minimizing envelope metastability. *Sci. Adv.*
1080 **4**, aau6769 (2018).
1081 62. L. He *et al.*, Presenting native-like trimeric HIV-1 antigens with self-assembling
1082 nanoparticles. *Nat. Commun.* **7**, 12041 (2016).
1083 63. Y.-N. Zhang *et al.*, Mechanism of a COVID-19 nanoparticle vaccine candidate that elicits
1084 a broadly neutralizing antibody response to SARS-CoV-2 variants. *Sci. Adv.* **7**, eabj3107
1085 (2021).
1086 64. B. L. deGroot *et al.*, Prediction of protein conformational freedom from distance
1087 constraints. *Proteins: Struct. Funct. Genet.* **29**, 240-251 (1997).
1088 65. J. Zhu, H. Fan, X. Periole, B. Honig, A. E. Mark, Refining homology models by
1089 combining replica-exchange molecular dynamics and statistical potentials. *Proteins:*
1090 *Struct. Funct. Genet.* **72**, 1171-1188 (2008).
1091 66. K. J. Cho *et al.*, Crystal structure of the conserved amino terminus of the extracellular
1092 domain of matrix protein 2 of influenza A virus gripped by an antibody. *J. Virol.* **90**, 611-
1093 615 (2016).
1094 67. K. J. Cho *et al.*, Structure of the extracellular domain of matrix protein 2 of influenza A
1095 virus in complex with a protective monoclonal antibody. *J. Virol.* **89**, 3700-3711 (2015).

1096 68. S. Afkhami *et al.*, Respiratory mucosal delivery of next-generation COVID-19 vaccine
1097 provides robust protection against both ancestral and variant strains of SARS-CoV-2.
1098 *Cell* **185**, 896-915.e819 (2022).
1099 69. M. A. Ramakrishnan, Determination of 50% endpoint titer using a simple formula. *World*
1100 *J. Virol.* **5**, 85-86 (2016).
1101 70. C. Lei, J. Yang, J. Hu, X. Sun, On the calculation of TCID(50) for quantitation of virus
1102 infectivity. *Virol. Sin.* **36**, 141-144 (2021).
1103 71. C. D. Higgins, V. N. Malashkevich, S. C. Almo, J. R. Lai, Influence of a heptad repeat
1104 stutter on the pH-dependent conformational behavior of the central coiled-coil fro
1105 influenza he agglutinin HA2. *Proteins: Struct. Funct. Genet.* **82**, 2220-2228 (2014).
1106 72. R. Rappuoli, Glycoconjugate vaccines: principles and mechanisms. *Sci. Transl. Med.* **10**,
1107 (2018).
1108 73. G. D. Victora, M. C. Nussenzweig, Germinal centers. *Annu. Rev. Immunol.* **30**, 429-457
1109 (2012).
1110 74. J. G. Cyster, B cell follicles and antigen encounters of the third kind. *Nat. Immunol.* **11**,
1111 989-996 (2010).
1112 75. B. A. Heesters, R. C. Myers, M. C. Carroll, Follicular dendritic cells: dynamic antigen
1113 libraries. *Nat. Rev. Immunol.* **14**, 495-504 (2014).
1114 76. Y.-N. Zhang *et al.*, Nanoparticle size influences antigen retention and presentation in
1115 lymph node follicles for humoral immunity. *Nano Lett.* **19**, 7226-7235 (2019).
1116 77. Y.-N. Zhang, W. Poon, E. Sefton, W. C. W. Chan, Suppressing subcapsular sinus
1117 macrophages enhances transport of nanovaccines to lymph node follicles for robust
1118 humoral immunity. *ACS Nano* **14**, 9478-9490 (2020).
1119 78. E. J. Erbelding *et al.*, A universal influenza vaccine: the strategic plan for the national
1120 institute of allergy and infectious diseases. *J. Infect. Dis.* **218**, 347-354 (2018).
1121 79. T. Tokatlian *et al.*, Innate immune recognition of glycans targets HIV nanoparticle
1122 immunogens to germinal centers. *Science* **363**, 649-654 (2019).
1123 80. M. C. Carroll, The role of complement and complement receptors in induction and
1124 regulation of immunity. *Annu. Rev. Immunol.* **16**, 545-568 (1998).
1125 81. C. Viant *et al.*, Antibody affinity shapes the choice between memory and germinal center
1126 B cell fates. *Cell* **183**, 1298-1311.e1211 (2020).
1127 82. C. D. Allen, T. Okada, J. G. Cyster, Germinal-center organization and cellular dynamics.
1128 *Immunity* **27**, 190-202 (2007).
1129 83. J. G. Cyster, C. D. C. Allen, B cell responses: cell interaction dynamics and decisions.
1130 *Cell* **177**, 524-540 (2019).
1131 84. B. A. Heesters, C. E. van der Poel, A. Das, M. C. Carroll, Antigen presentation to B cells.
1132 *Trends Immunol.* **37**, 844-854 (2016).
1133 85. Z. Shulman *et al.*, T follicular helper cell dynamics in germinal centers. *Science* **341**,
1134 673-677 (2013).
1135 86. S. Crotty, T follicular helper cell differentiation, function, and roles in disease. *Immunity*
1136 **41**, 529-542 (2014).
1137 87. M. M. Hufford, T. S. Kim, J. Sun, T. J. Braciale, The effector T cell response to influenza
1138 infection. *Curr. Top. Microbiol. Immunol.* **386**, 423-455 (2015).
1139 88. Y. Janssens *et al.*, The role of cell-mediated immunity against influenza and its
1140 implications for vaccine evaluation. *Front. Immunol.* **13**, 959379 (2022).

1141 89. S. L. Swain, K. K. McKinstry, T. M. Strutt, Expanding roles for CD4+ T cells in
1142 immunity to viruses. *Nat. Rev. Immunol.* **12**, 136-148 (2012).
1143 90. A. J. Sant, A. T. DiPiazza, J. L. Nayak, A. Rattan, K. A. Richards, CD4 T cells in
1144 protection from influenza virus: viral antigen specificity and functional potential.
1145 *Immunol. Rev.* **284**, 91-105 (2018).
1146 91. M. Koutsakos *et al.*, Human CD8+ T cell cross-reactivity across influenza A, B and C
1147 viruses. *Nat. Immunol.* **20**, 613-625 (2019).
1148 92. E. A. Hemann, S. M. Kang, K. L. Legge, Protective CD8 T cell-mediated immunity
1149 against influenza A virus infection following influenza virus-like particle vaccination. *J.*
1150 *Immun.* **191**, 2486-2494 (2013).
1151 93. N. Saito *et al.*, Negative impact of prior influenza vaccination on current influenza
1152 vaccination among people infected and not infected in prior season: a test-negative case-
1153 control study in Japan. *Vaccine* **35**, 687-693 (2017).
1154 94. Y. N. Lee, M. C. Kim, Y. T. Lee, Y. J. Kim, S. M. Kang, Mechanisms of cross-protection
1155 by influenza virus M2-based vaccines. *Immune Netw.* **15**, 213-221 (2015).
1156 95. K. Frank, S. Paust, Dynamic natural killer cell and T cell responses to influenza infection.
1157 *Front Cell Infect Mi* **10**, 425 (2020).
1158 96. N. Pica, P. Palese, Toward a universal influenza virus vaccine: prospects and challenges.
1159 *Annu. Rev. Med.* **64**, 189-202 (2013).
1160 97. W. C. Wang, E. E. Sayedahmed, S. Sambhara, S. K. Mittal, Progress towards the
1161 development of a universal influenza vaccine. *Viruses* **14**, (2022).
1162 98. C. C. D. Lee *et al.*, A cross-neutralizing antibody between HIV-1 and influenza virus.
1163 *PLOS Pathog.* **17**, (2021).
1164

1165 **Figure Legends**

1166 **Figure 1. Design and in vitro characterization of hM2e immunogens.** (**A**) Structural models of
1167 human M2e (hM2e), hM2e-5GS-1TD0 trimer, and three hM2e-presenting nanoparticles (NPs).
1168 Left: Amino acid sequence and ribbons/surface model of hM2e (from PDB ID 4N8C). Middle:
1169 Ribbons/surface model of hM2e-5GS-1TD0 trimer, in which a trimeric viral capsid protein SHP
1170 (PDB ID: 1TD0) is used to display hM2e. Right: Surface models of hM2e on 24-meric ferritin
1171 (FR) and 60-meric E2p-L4P and I3-01-L7P 1c-SApNPs. The SApNP size is indicated by diameter
1172 (in nm). (**B**) SEC profiles of hM2e-5GS-1TD0 trimer and hM2e-presenting FR, E2p-L4P and I3-
1173 01-L7P SApNPs. The hM2e trimer was processed on a Superdex 75 10/300 increase GL column,
1174 while three SApNPs were processed on a Superose 6 increase 10/300 GL column. (**C**) SDS-PAGE
1175 under reducing conditions (left) and BN-PAGE (*98*) of hM2e-presenting FR, E2p-L4P and I3-

1176 01v9a-L7P SApNPs. Notably, hM2e-5GS-1TD0 is included on the SDS gel for comparison. (**D**)
1177 Negative-stain EM micrographs of mAb148-purified FR, E2p-L4P and I3-01v9a-L7P SApNPs.
1178 (**E**) DLS profiles of mAb148-purified FR, E2p-L4P and I3-01v9a-L7P SApNPs. Average particle
1179 size derived from DLS are labeled. (**F**) Thermostability of the hM2e-5GS-1TD0 trimer and hM2e-
1180 5GS-FR SApNP with Tm, $\Delta T_{1/2}$ and T_{on} measured by DSC. (**G**) ELISA analysis of the hM2e trimer
1181 and SApNPs (FR, E2p-L4P and I3-01v9a-L7P) binding to mAb65 (left) and mAb148 (*98*) after
1182 heating to 50 °C, 60 °C and 70 °C for 15 minutes. (**H**) Antigenic profiles of the hM2e trimer and
1183 SApNPs (FR, E2p-L4P and I3-01v9a-L7P) to mAb148 using BLI.

1184 **Figure 2. Assessment of hM2e scaffolds and nanoparticles in a mouse challenge model.**
1185 (**A**) Benchmark challenge studies assessing survival and weight loss to establish the 50% lethal
1186 intranasal challenge dose in mice for mouse-adapted A/Puerto Rico/8/1934 (PR8) H1N1 and
1187 A/Hong Kong/1/1968 (HK/68) H3N2; N = 10 mice/group. Mice were monitored for survival,
1188 weight loss, and morbidities for 14 days. (**B**) Schematic representation of mouse immunization
1189 regimen for hM2e constructs, sequential challenges of LD_{50} × 10 of PR8 and HK/68, blood
1190 collection, and sacrifice; N = 10 mice/group. (**C**) Survival and weight loss of mice challenged with
1191 LD_{50} × 10 of PR8 (H1N1) followed by an LD_{50} × 10 of HK/68 (H3N2). Mice were monitored for
1192 survival, weight loss, and morbidities for 14 days. (**D**) ELISA curves showing hM2e-immune sera
1193 binding to the hM2e-5GS-foldon trimer probe and calculated 50% effective concentration (EC_{50})
1194 values for weeks 2, 5, 10, and 14. The assay was performed in duplicate with a starting serum
1195 dilution of 20× followed by seven 10-fold titrations. Images of mouse immunization, virus
1196 challenge, and blood and organ collection created with BioRender.com.

1197 **Figure 3. Design and characterization of tandem M2ex3 immunogens.** (**A**) Structural models
1198 of tandem M2ex3, M2ex3-5GS-1TD0 trimer, and three M2ex3-presenting SApNPs. Left: Amino

1199 acid sequences of human, avian/swine, and human/swine M2e and ribbons/surface model of
1200 tandem M2ex3 (based on hM2e from PDB ID 4N8C). The G4 linker is shown as a dotted line.
1201 Middle: Ribbons/surface model of M2ex3-5GS-1TD0 trimer, in which 1TD0 is a trimeric viral
1202 capsid protein. Right: Surface models of M2ex3 on 24-meric ferritin (FR) and 60-meric E2p-L4P
1203 and I3-01-L7P 1c-SApNPs. The SApNP size is indicated by diameter (in nm). (**B**) SEC profiles of
1204 M2ex3-5GS-1TD0 trimer and M2ex3-presenting FR, E2p-L4P and I3-01-L7P SApNPs. The
1205 tandem M2ex3 trimer and three SApNPs were processed on a Superdex 75 10/300 increase GL
1206 column and a Superose 6 increase 10/300 GL column, respectively. (**C**) SDS-PAGE (left) under
1207 reducing conditions and BN-PAGE (*98*) of tandem M2ex3-presenting FR, E2p-L4P and I3-01v9a-
1208 L7P SApNPs. Notably, M2ex3-5GS-1TD0 is included on the SDS gel for comparison. (**D**)
1209 Negative-stain EM micrographs of mAb148-purified FR, E2p-L4P and I3-01v9a-L7P SApNPs.
1210 (**E**) DLS profiles of mAb148-purified FR, E2p-L4P and I3-01v9a-L7P SApNPs. Average particle
1211 size derived from DLS are labeled. (**F**) Thermostability of the M2ex3-5GS-1TD0 trimer and
1212 M2ex3-5GS-FR SApNP with Tm, $\Delta T_{1/2}$ and T_{on} measured by DSC. (**G**) ELISA analysis of the
1213 M2ex3 trimer and SApNPs (FR, E2p-L4P and I3-01v9a-L7P) binding to mAb65 (left) and
1214 mAb148 (*98*) after heating to 50 °C, 60 °C and 70 °C for 15 minutes. (**H**) Antigenic profiles of the
1215 M2ex3 trimer and SApNPs (FR, E2p-L4P and I3-01v9a-L7P) to mAb148 using BLI.

1216 **Figure 4. Survival and weight loss assessment of tandem M2ex3 scaffold and nanoparticles**
1217 **in a mouse challenge model.** (**A**) Schematic representation of mouse immunization regimen for
1218 M2ex3 constructs, sequential intranasal challenges of $LD_{50} \times 10$ of mouse-adapted PR8 (H1N1)
1219 and HK/68 (H3N2), blood collection, and sacrifice. Groups were as follows: M2ex3 groups
1220 adjuvanted with alum phosphate (n = 8), M2ex3 groups adjuvanted with AddaVax (n = 13), and
1221 Inactivated PR8 (n = 8). Inactivated PR8 + AddaVax (n = 13) was used as a positive control for

1222 lung viral titers for the PR8 challenge. (**B**) Survival and weight loss of mice challenged with LD_{50}
1223 × 10 of PR8 (H1N1) followed by an LD_{50} × 10 of HK/68 (H3N2). Mice were monitored for
1224 survival, weight loss, and morbidities for 14 days. (**C**) Lung viral titers in M2ex3-immunized mice
1225 at Day 5 post-PR8 H1N1 challenge (n = 5). Visual representation of plaques formed from the lung
1226 supernatants of various M2ex3-immunized mice. The highest countable plaques were observed in
1227 naïve mice. The lowest number of plaques were observed in the lung supernatants of E2p- and I3-
1228 01v9a NP-immunized mice. The assay was performed in duplicate starting at a lung supernatant
1229 dilution of 1x followed by 10-fold titrations. Statistical analysis shows significance between
1230 M2ex3 groups compared to naïve mice using One-way ANOVA. The error bars indicate
1231 mean ± standard deviation; $^{**}p < 0.01$, $^{***}p < 0.001$, and $^{****}p < 0.0001$. Images of mouse
1232 immunization, virus challenge, and blood and organ collection created with BioRender.com.

1233 **Figure 5. M2ex3-immune sera binding to scaffolded M2ex3 and homotetrameric M2e.** (**A**)
1234 ELISA curves showing M2ex3-immune sera (adjuvanted with alum phosphate or AddaVax)
1235 binding to the M2ex3-5GS-foldon trimer probe and calculated 50% effective concentration (EC_{50})
1236 values for weeks 2, 5, 10, and 14. N = 8 or 13 at weeks 2 and 5. N = variable based on surviving
1237 mice/group post-challenge for weeks 10 and 14. The assay was performed in duplicate with a
1238 starting serum dilution of 20× followed by seven 10-fold titrations. (**B)** Serum binding to M2e on
1239 the surface of MDCK cells infected with various influenza A strains. Strains: A/Puerto
1240 Rico/8/1934 (H1N1), A/California/04/2009 (H1N1)pdm09, A Solomon Islands/2/2006 (H1N1),
1241 A/Hong Kong/1/1968 (H3N2), A/Brisbane/10/2007 (H3N2), A/Aichi/2/1968 (H3N2),
1242 B/Brisbane/60/2008 (Flu B, Victoria Lineage B/Florida/4/2006), and (Flu B, Yamagata Lineage).
1243 MAb148 (M2e antibody) was used as a positive control. The assay was performed in duplicate
1244 with a starting serum dilution of 50x followed by five 10-fold titrations. Statistical analysis shows

1245 significance between trimer and NP groups and positive control using Two-way ANOVA. The
1246 error bars indicate mean ± standard deviation; *$p < 0.05$, **$p < 0.01$, ***$p < 0.001$, and
1247 ****$p < 0.0001$.

1248 **Fig. 6. Prolonged retention of M2ex3-presenting SApNPs in lymph node follicles.** (**A**)
1249 Distribution of I3-01v9a SApNPs displayed M2ex3 trimers in a lymph node at 48 h after a single-
1250 dose injection (10 μg/injection, 40 μg/mouse). Anti-M2e Ab148 and Ab65 were used to stain the
1251 lymph node tissues. (**B**) schematics of M2ex3 trimer presenting SApNP accumulation in lymph
1252 node tissues. (**C**) Trafficking and retention of the M3ex3 trimer and FR and I3-01v9a SApNPs in
1253 lymph node follicles at 2 h to 8 weeks after a single-dose injection. Scale bar = 50 μm for each
1254 image. (**D**) Time-dependent curve and (**E**) Area under the curve (*78*) of the Ab148-stained area in
1255 immunohistological images of M3ex3 immunogen retention in lymph node follicles up to 8 weeks.
1256 (**F**) Quantification of M3ex3 vaccine accumulation in lymph node follicles at 1 week after a single-
1257 dose injection. (**G**) Histological images of the M2ex3 trimer and two SApNP vaccine accumulation
1258 and retention in lymph node follicles at 2 weeks and 5 weeks after the boost, which occurred at 3
1259 weeks after the first dose. (**H**) Quantification of vaccine accumulation in lymph node follicles at 1
1260 week after the boost. In mouse injection, all vaccine immunogens were mixed with AddaVax
1261 adjuvant. Data were collected from more than 10 lymph node follicles (n = 3-5 mice/group). (I)
1262 Interaction of M2ex3 trimer presenting SApNPs with FDC networks in lymph nodes at 1 week
1263 after a single-dose injection. Both FR and I3-01v9a SApNP immunogens were colocalized with
1264 FDC networks. Immunofluorescent images are pseudo-color-coded ($CD21^+$, green; $CD169^+$, red;
1265 Ab148, white). Scale bars = 500 and 100 μm for a complete lymph node and enlarged image of a
1266 follicle, respectively. The data points are expressed as mean ± SEM for (D) and SD for (E, F and

1267 H). The data were analyzed using one-way ANOVA followed by Tukey's multiple comparison
1268 post hoc test. ***$p < 0.001$, ****$p < 0.0001$.

1269 **Fig. 7. Induction of robust and long-lived germinal center reactions by M2ex3-presenting**
1270 **SApNPs.** (**A**) Top image: Immunofluorescent images of M2ex3 trimer presenting I3-01v9a
1271 SApNP vaccine candidate induced germinal centers (GCs) at 2 weeks after a single-dose injection
1272 (10 μg/injection, 40 μg/mouse). Bottom image: robust GC reaction with organized light zone (LZ)
1273 and dark zone (DZ) compartments in lymph node follicles. GC B cells ($GL7^+$, red) attached to
1274 FDCs ($CD21^+$, green) and T_{fh} cells located in LZ of GCs. Scale bars = 500 and 100 μm for a
1275 complete lymph node and the enlarged image of a follicle, respectively. (**B**) and (**C**) quantification
1276 of GCs in terms of the GC/FDC ratio and the size of GCs induced by the M2ex3 trimer, and FR
1277 and I3-01v9a SApNP vaccines using immunohistological images at 2, 5, and 8 weeks after a
1278 single-dose injection or at 2 and 5 weeks after the boost, which occurred at 3 weeks after the first
1279 dose (n = 5 mice/group). (**D**) and (**E**) representative GC images induced by three M2ex3 vaccine
1280 constructs at 8 weeks using a single-dose or prime-boost regimen. Scale bar = 50 μm for the image
1281 of an enlarged lymph node follicle. (**F**) and (**G**) Quantification of GC reactions in terms of the
1282 percentage and number of GC B cells and T_{fh} cells using flow cytometry after a single-dose or
1283 prime-boost immunizations. In mouse immunization, all vaccine constructs were formulated with
1284 AddaVax adjuvant. The data points are shown as mean ± SD. The data were analyzed using one-
1285 way ANOVA followed by Tukey's multiple comparison post hoc test for each timepoint. *$p <$
1286 0.05, **$p < 0.01$, ***$p < 0.001$, ****$p < 0.0001$.

1287 **Figure 8. Innate and T cell responses of M2ex3 scaffolds and M2ex3-presenting SApNPs**
1288 (**A**) ADCC activity measured by RLU of FcγRIV-expressing Jurkat effector cells binding to

1289 M2ex3-immune sera bound to M2e on PR8 (H1N1)-infected MDCK cells. The data is presented
1290 as mean ± SEM (**B**) Spot formation of IFN-γ and IL-4-secreting splenoctyes from M2ex3-
1291 immunized mice at Day 5 post-PR8 H1N1 challenge. Mouse splenocytes were isolated from
1292 immunized mice with M2ex3 trimer and FR and I3-01v9a SApNP vaccine constructs at 5 days
1293 after prime-boost immunization followed by H1N1 virus challenge (n = 5 mice/group).
1294 Splenocytes of naïve mice without immunization but with a H1N1 virus challenge were included
1295 as control samples. Quantification of the percentage and number of vaccine-induced functional (**C**)
1296 $CD4^+$ and (**D**) $CD8^+$ T cell responses using flow cytometry. In mouse immunization, all vaccine
1297 immunogens were coupled with AddaVax adjuvant. The data points are shown as mean ± SD. The
1298 data were analyzed using one-way ANOVA followed by Tukey's multiple comparison post hoc
1299 test for each timepoint. *$p < 0.05$, **$p < 0.01$, ***$p < 0.001$, ****$p < 0.0001$.

1300 **SUPPLEMENTAL LEGENDS**

1301 **fig. S1.** Schematic of computational design for I3-01v9a.

1302 **fig. S2.** Construct and in vitro characterization of hM2e-presenting trimer and SApNPs.

1303 **fig. S3.** Serum binding of individual mice immunized with hM2e 1TD0 trimer and SApNPs.

1304 **fig. S4.** Construct and in vitro characterization of M2ex3-presenting trimer and SApNPs.

1305 **fig. S5.** Serum binding of individual mice immunized with M2ex3 1TD0 trimer and SApNPs.

1306 **fig. S6.** M2ex3 serum binding of individual mice to cell-surface homotetrameric M2e.

1307 **fig. S7.** Immunohistological images of M2ex3 1TD0 trimer and SApNPs in lymph nodes.

1308 **fig. S8.** Immunohistological analysis of M2ex3 1TD0 trimer and SApNP-induced GCs.

1309 **fig. S9.** Flow cytometry analysis of M2ex3 1TD0 trimer and SApNP-induced GCs.

1310 **fig. S10.** Flow cytometry analysis of M2ex3 1TD0 trimer and SApNP-induced T cell responses.

Fig. 1

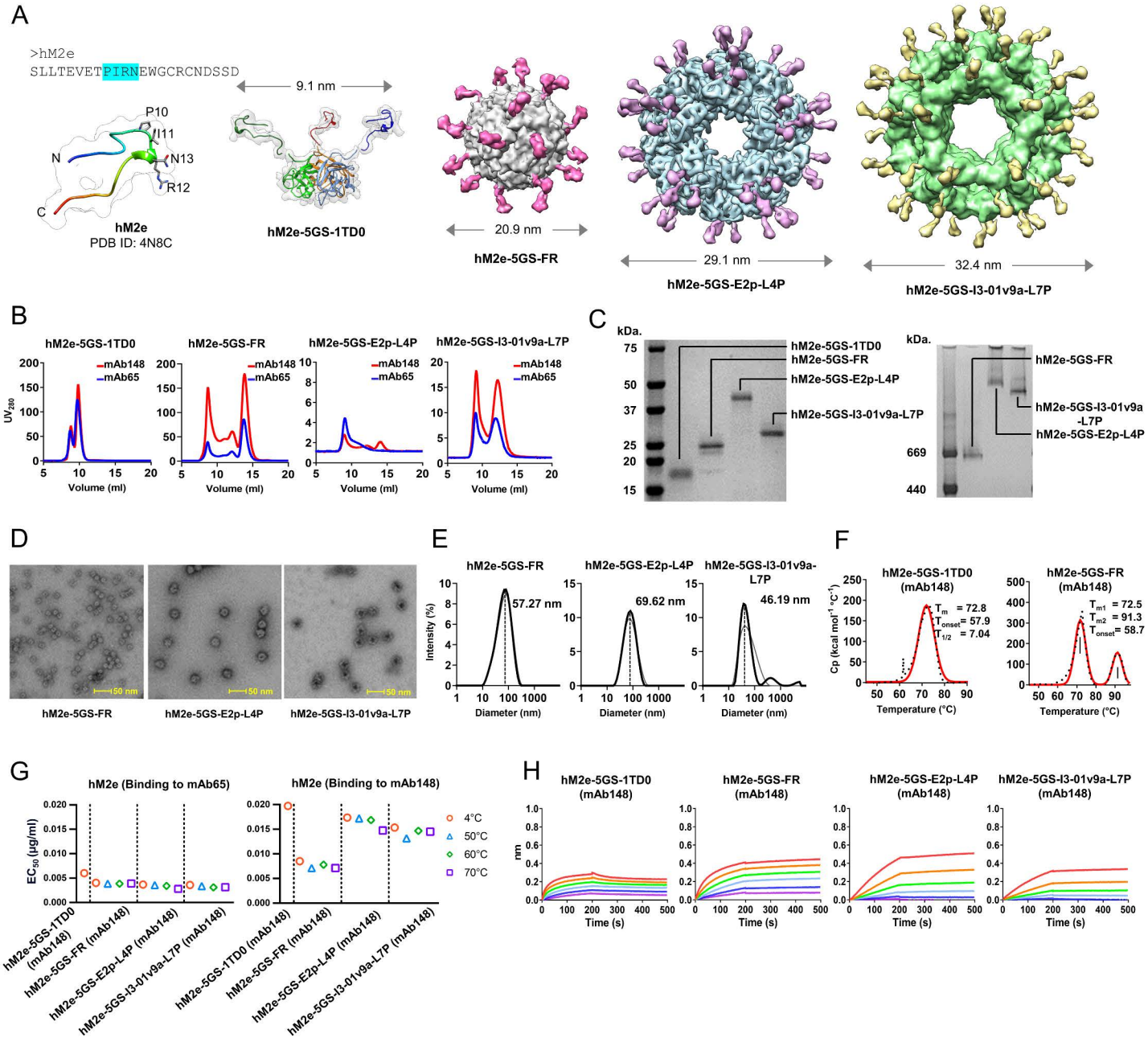
A
>hM2e
SLLTEVETPIRNEWGCRCNDSSD
9.1 nm
P10
I11
N
N13
R12
C
hM2e
PDB ID: 4N8C
hM2e-5GS-1TD0
20.9 nm
hM2e-5GS-FR
29.1 nm
hM2e-5GS-E2p-L4P
32.4 nm
hM2e-5GS-I3-01v9a-L7P
B
hM2e-5GS-1TD0
hM2e-5GS-FR
hM2e-5GS-E2p-L4P
hM2e-5GS-I3-01v9a-L7P
mAb148
mAb65
UV280
Volume (ml)
C
kDa.
75
50
37
25
20
15
hM2e-5GS-1TD0
hM2e-5GS-FR
hM2e-5GS-E2p-L4P
hM2e-5GS-I3-01v9a-L7P
669
440
hM2e-5GS-I3-01v9a -L7P
D
50 nm
hM2e-5GS-FR
hM2e-5GS-E2p-L4P
hM2e-5GS-I3-01v9a-L7P
E
57.27 nm
69.62 nm
46.19 nm
Intensity (%)
Diameter (nm)
F
hM2e-5GS-1TD0 (mAb148)
Tm = 72.8
Tonset = 57.9
T1/2 = 7.04
hM2e-5GS-FR (mAb148)
Tm1 = 72.5
Tm2 = 91.3
Tonset = 58.7
Cp (kcal mol-1 °C-1)
Temperature (°C)
G
hM2e (Binding to mAb65)
hM2e (Binding to mAb148)
EC50 (µg/ml)
4°C
50°C
60°C
70°C
hM2e-5GS-1TD0 (mAb148)
hM2e-5GS-FR (mAb148)
hM2e-5GS-E2p-L4P (mAb148)
hM2e-5GS-I3-01v9a-L7P (mAb148)
H
hM2e-5GS-1TD0 (mAb148)
hM2e-5GS-FR (mAb148)
hM2e-5GS-E2p-L4P (mAb148)
hM2e-5GS-I3-01v9a-L7P (mAb148)
nm
Time (s)

Fig. 2

A

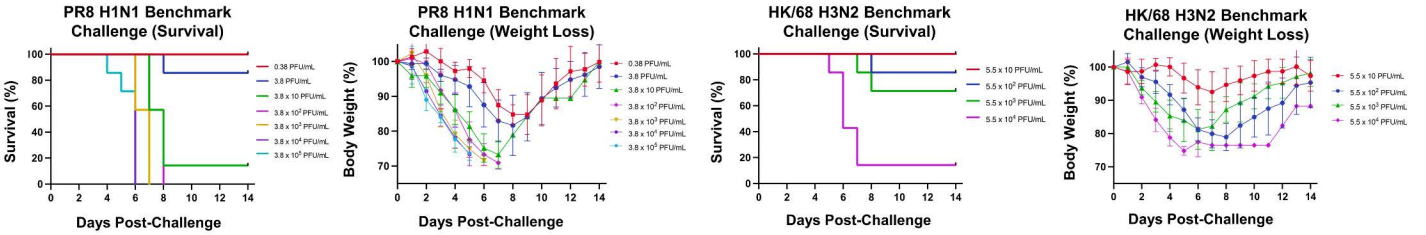

B

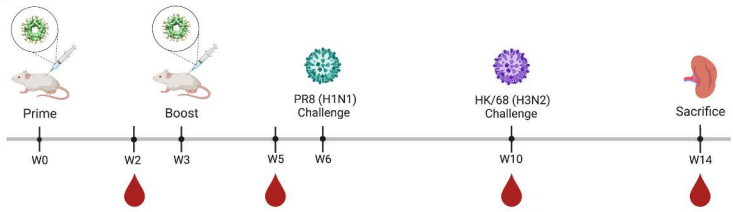

C

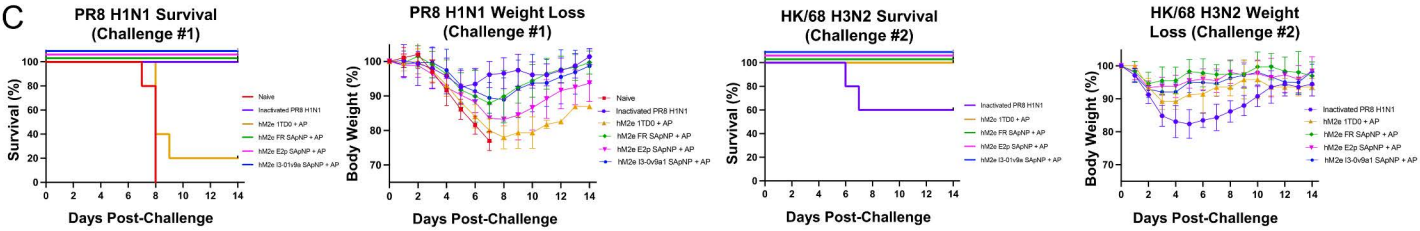

D

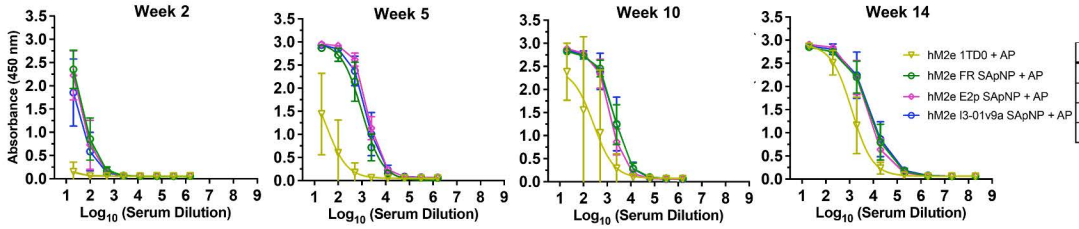

ID_{50} Serum Dilution

hM2e + AP	1TD0	FR	E2p	I3-01v9a
Week 2	N/A	21.82	15.72	13.04
Week 5	31.99	997.2	1678	1369
Week 10	263.4	1925	1249	1878
Week 14	1252	6940	5451	7510

Fig. 3

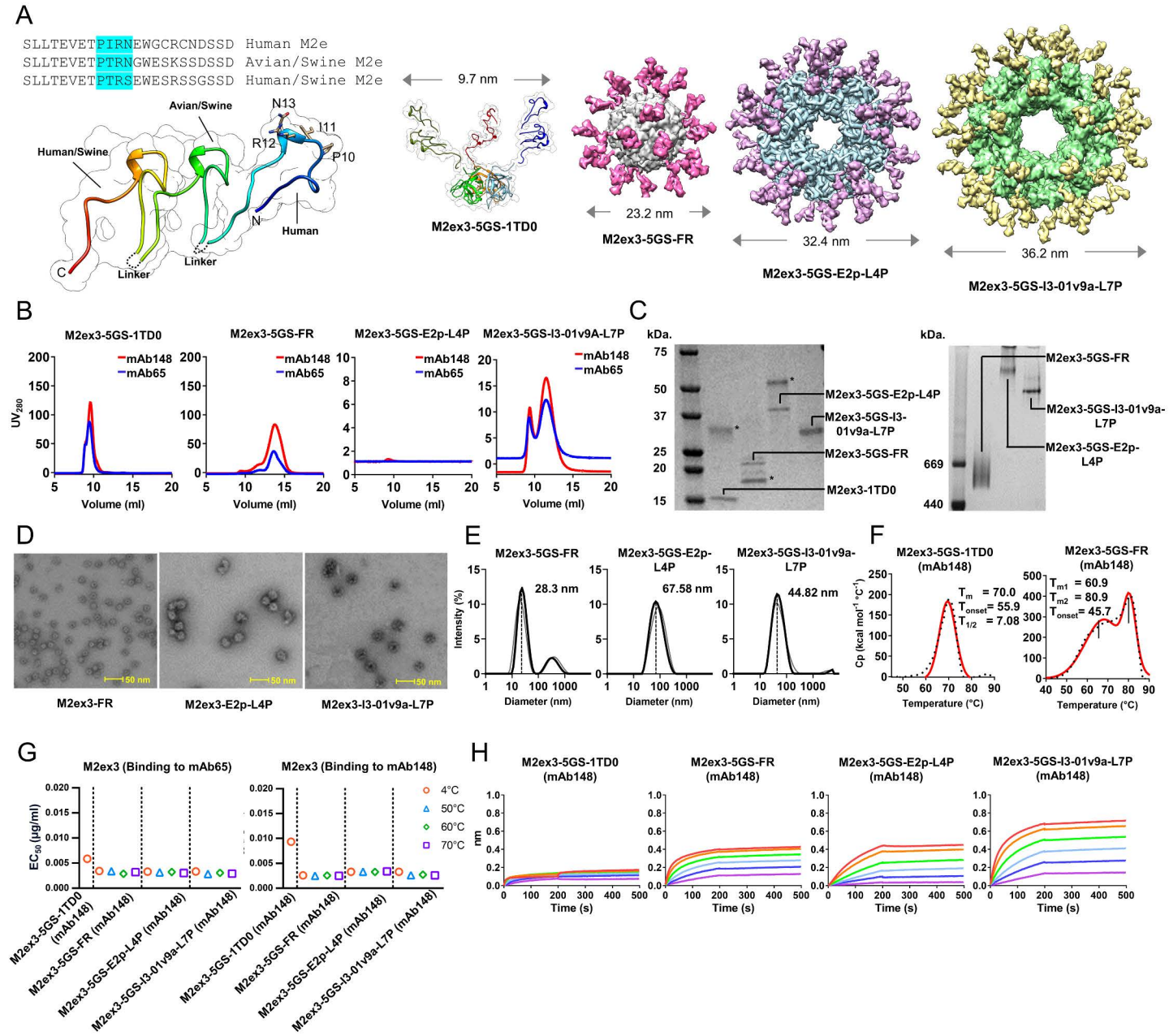
A
SLLTEVETPIRNEWGCRCNDSSD Human M2e
SLLTEVETPTRNGWESKSSDSSD Avian/Swine M2e
SLLTEVETPTRSEWESRSSGSSD Human/Swine M2e
Avian/Swine
N13
I11
R12
P10
Human/Swine
N
Human
C
Linker
Linker
9.7 nm
M2ex3-5GS-1TD0
23.2 nm
M2ex3-5GS-FR
32.4 nm
M2ex3-5GS-E2p-L4P
36.2 nm
M2ex3-5GS-I3-01v9a-L7P
B
M2ex3-5GS-1TD0
M2ex3-5GS-FR
M2ex3-5GS-E2p-L4P
M2ex3-5GS-I3-01v9A-L7P
mAb148
mAb65
UV280
Volume (ml)
C
kDa.
M2ex3-5GS-E2p-L4P
M2ex3-5GS-I3-01v9a-L7P
M2ex3-5GS-FR
M2ex3-1TD0
669
440
D
150 nm
M2ex3-FR
M2ex3-E2p-L4P
M2ex3-I3-01v9a-L7P
E
M2ex3-5GS-FR
28.3 nm
M2ex3-5GS-E2p-L4P
67.58 nm
M2ex3-5GS-I3-01v9a-L7P
44.82 nm
Intensity (%)
Diameter (nm)
F
M2ex3-5GS-1TD0 (mAb148)
Tm = 70.0
Tonset = 55.9
T1/2 = 7.08
M2ex3-5GS-FR (mAb148)
Tm1 = 60.9
Tm2 = 80.9
Tonset = 45.7
Cp (kcal mol-1 °C-1)
Temperature (°C)
G
M2ex3 (Binding to mAb65)
M2ex3 (Binding to mAb148)
EC50 (µg/ml)
4°C
50°C
60°C
70°C
M2ex3-5GS-1TD0 (mAb148)
M2ex3-5GS-FR (mAb148)
M2ex3-5GS-E2p-L4P (mAb148)
M2ex3-5GS-I3-01v9a-L7P (mAb148)
H
M2ex3-5GS-1TD0 (mAb148)
M2ex3-5GS-FR (mAb148)
M2ex3-5GS-E2p-L4P (mAb148)
M2ex3-5GS-I3-01v9a-L7P (mAb148)
nm
Time (s)

Fig. 4

A

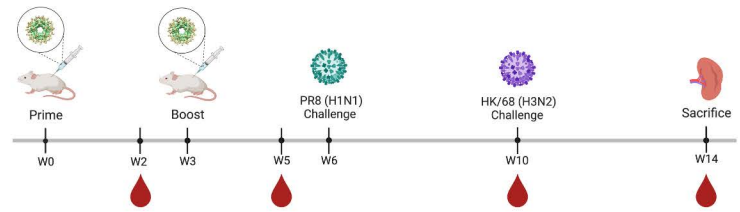

B

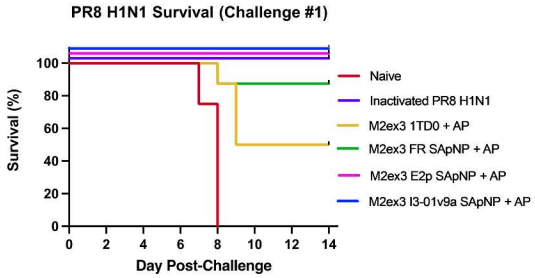

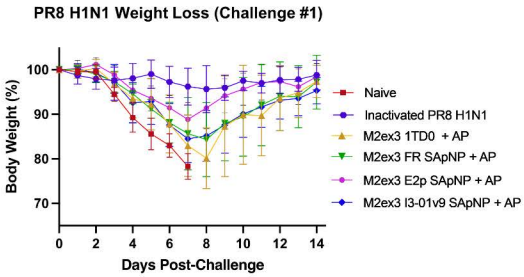

Group (n = 8)	Survival (%)	Peak Weight Loss (%)
Naive	0	21.7 ± 2.9
Inactivated PR8 H1N1	100	4.4 ± 5.3
M2ex3 iTD0	50	19.4 ± 7.3
M2ex3 FR SApNP	88	15.5 ± 8.1
M2ex3 E2p SApNP	100	11.2 ± 3.8
M2ex3 I3-01v9a SApNP	100	15.5 ± 5.3

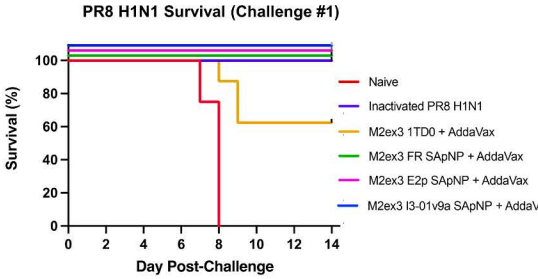

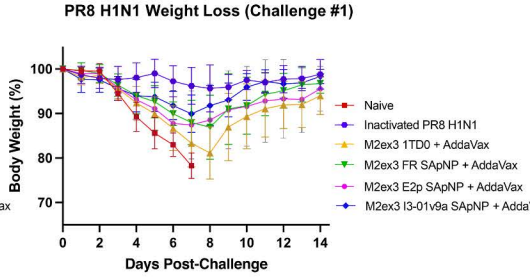

Group (n = 13 up to day 5; n = 8 up to Day 14)	Survival (%)	Peak Weight Loss (%)
Naive	0	21.7 ± 2.9
Inactivated PR8 H1N1	100	4.4 ± 5.3
M2ex3 iTD0	63	18.9 ± 5.9
M2ex3 FR SApNP	100	13.1 ± 7.2
M2ex3 E2p SApNP	100	12.5. ± 7.7
M2ex3 I3-01v9a SApNP	100	10.0 ± 4.2

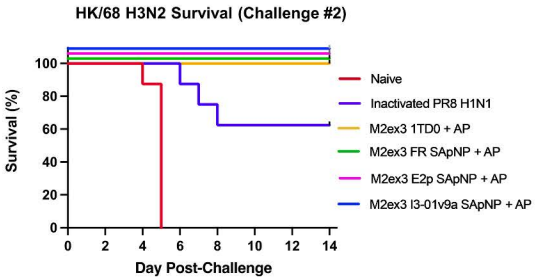

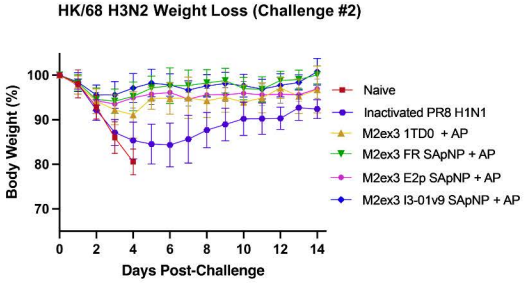

Group	Survival (%)	Peak Weight Loss (%)
Naïve (n = 8)	0	19.5 ± 2.9
Inactivated PR8 H1N1 (n = 8)	63	15.7 ± 4.9
M2e 1TD0 (n = 4)	100	8.9 ± 5.2
M2ex3 FR SApNP (n = 7)	100	4.7 ± 3.22
M2ex3 E2p SApNP (n = 8)	100	6.5 ± 1.9
M2ex3 I3-01v9a SApNP (n = 8)	100	4.4 ± 3.0

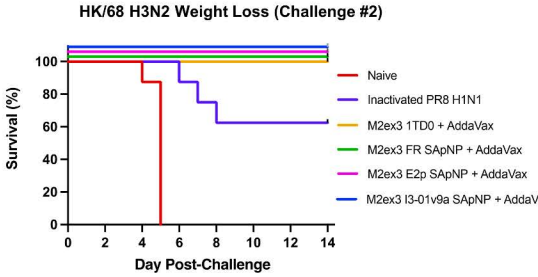

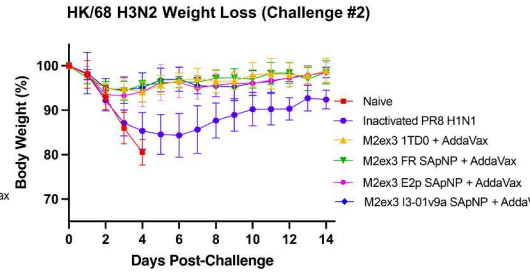

Group	Survival (%)	Peak Weight Loss (%)
Naïve (n = 8)	0	19.5 ± 2.9
Inactivated PR8 H1N1 (n = 8)	63	15.7 ± 4.9
M2ex3 1TD0 (n = 5)	100	4.3 ± 2.1
M2ex3 FR SApNP (n = 8)	100	4.3 ± 1.0
M2ex3 E2p SApNP (n = 8)	100	5.9 ± 3.4
M2ex3 I3-01v9a SApNP (n = 8)	100	4.9 ± 3.3

C

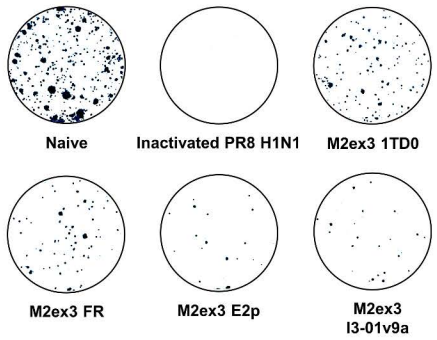

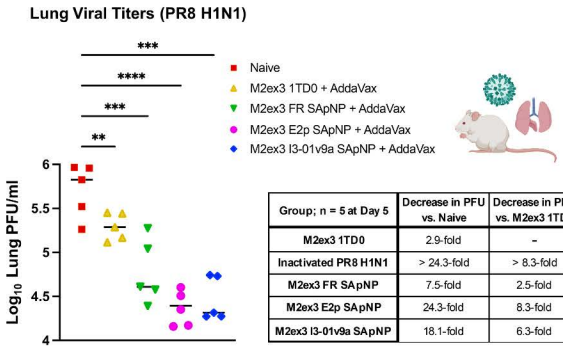

Group; n = 5 at Day 5	Decrease in PFU vs. Naive	Decrease in PFU vs. M2ex3 1TD0
M2ex3 1TD0	2.9-fold	-
Inactivated PR8 H1N1	> 24.3-fold	> 8.3-fold
M2ex3 FR SApNP	7.5-fold	2.5-fold
M2ex3 E2p SApNP	24.3-fold	8.3-fold
M2ex3 I3-01v9a SApNP	18.1-fold	6.3-fold

Fig. 5

A

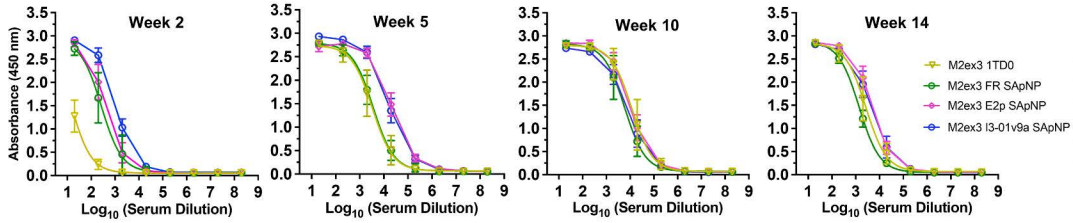

Aluminum Phosphate (AP)

M2ex3 + AP	1TD0	FR	E2p	I3-01v9a
Week 2	12.4	264.4	382.1	1039
Week 5	3340	3564	22383	16448
Week 10	11731	5876	10485	8511
Week 14	2702	1405	4944	4524

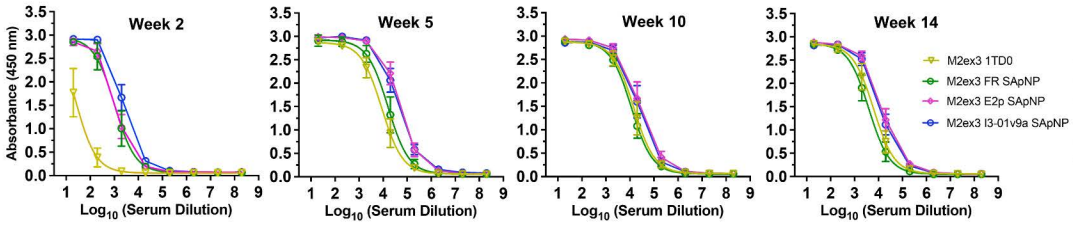

AddaVax (AV)

M2ex3 + AV	1TD0	FR	E2p	I3-01v9a
Week 2	23.19	1026	1104	2375
Week 5	8823	15989	50231	41779
Week 10	14463	11508	25419	23588
Week 14	6239	3947	14225	12500

B

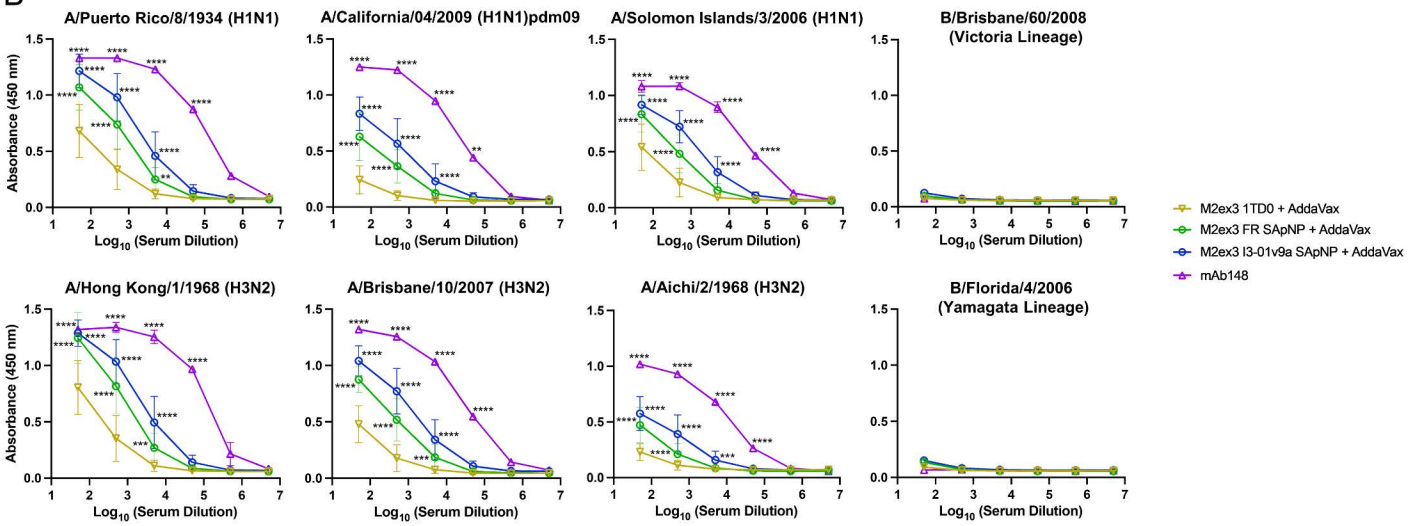

Fig. 6

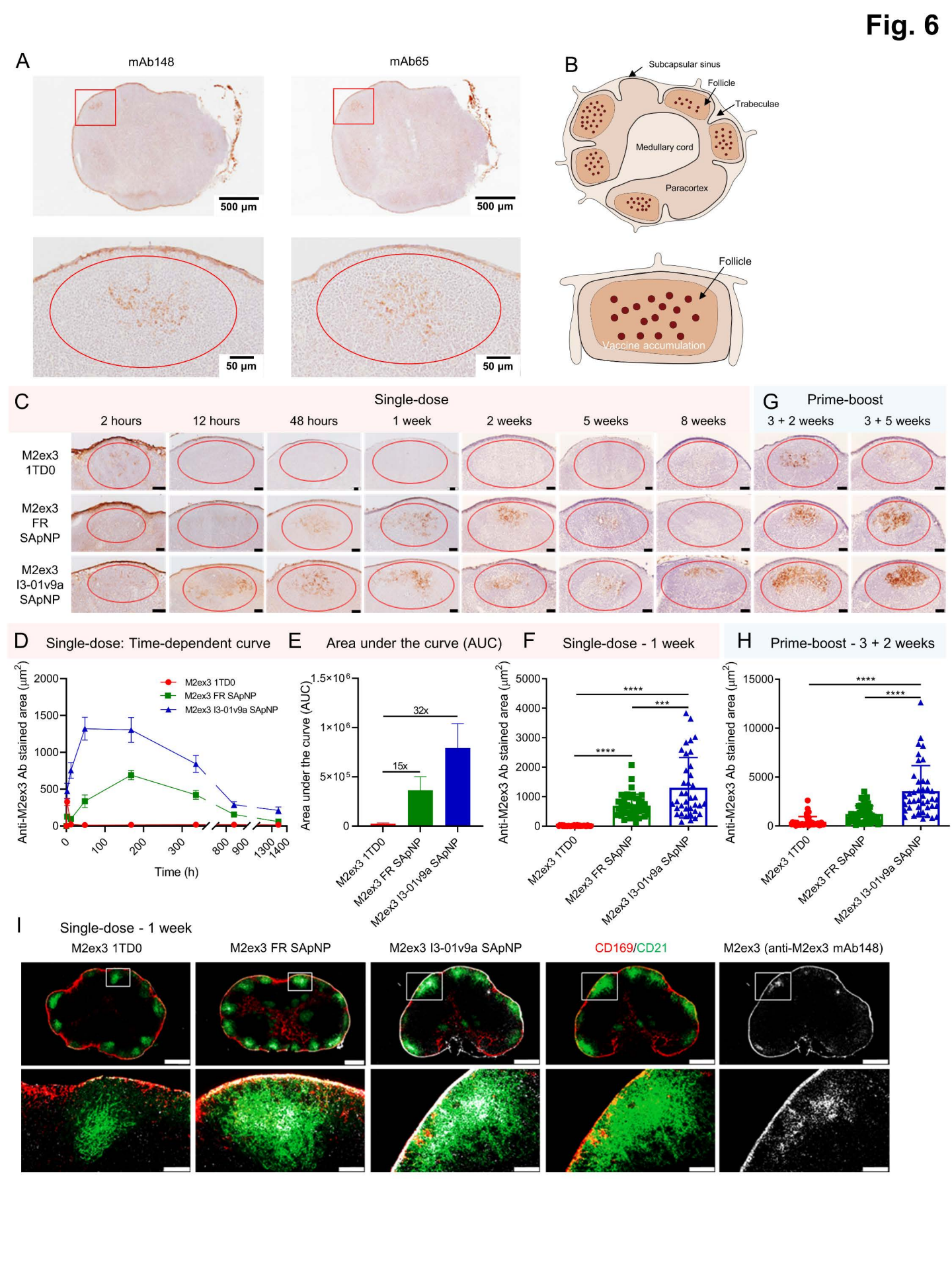
A
mAb148
mAb65
500 µm
500 µm
50 µm
50 µm
B
Subcapsular sinus
Follicle
Trabeculae
Medullary cord
Paracortex
Follicle
Vaccine accumulation
C
Single-dose
2 hours
12 hours
48 hours
1 week
2 weeks
5 weeks
8 weeks
G
Prime-boost
3 + 2 weeks
3 + 5 weeks
M2ex3 1TD0
M2ex3 FR SApNP
M2ex3 I3-01v9a SApNP
D
Single-dose: Time-dependent curve
Anti-M2ex3 Ab stained area (µm²)
Time (h)
M2ex3 1TD0
M2ex3 FR SApNP
M2ex3 I3-01v9a SApNP
E
Area under the curve (AUC)
Area under the curve (AUC)
32x
15x
F
Single-dose - 1 week
H
Prime-boost - 3 + 2 weeks
I
Single-dose - 1 week
M2ex3 1TD0
M2ex3 FR SApNP
M2ex3 I3-01v9a SApNP
CD169/CD21
M2ex3 (anti-M2ex3 mAb148)

Fig. 7

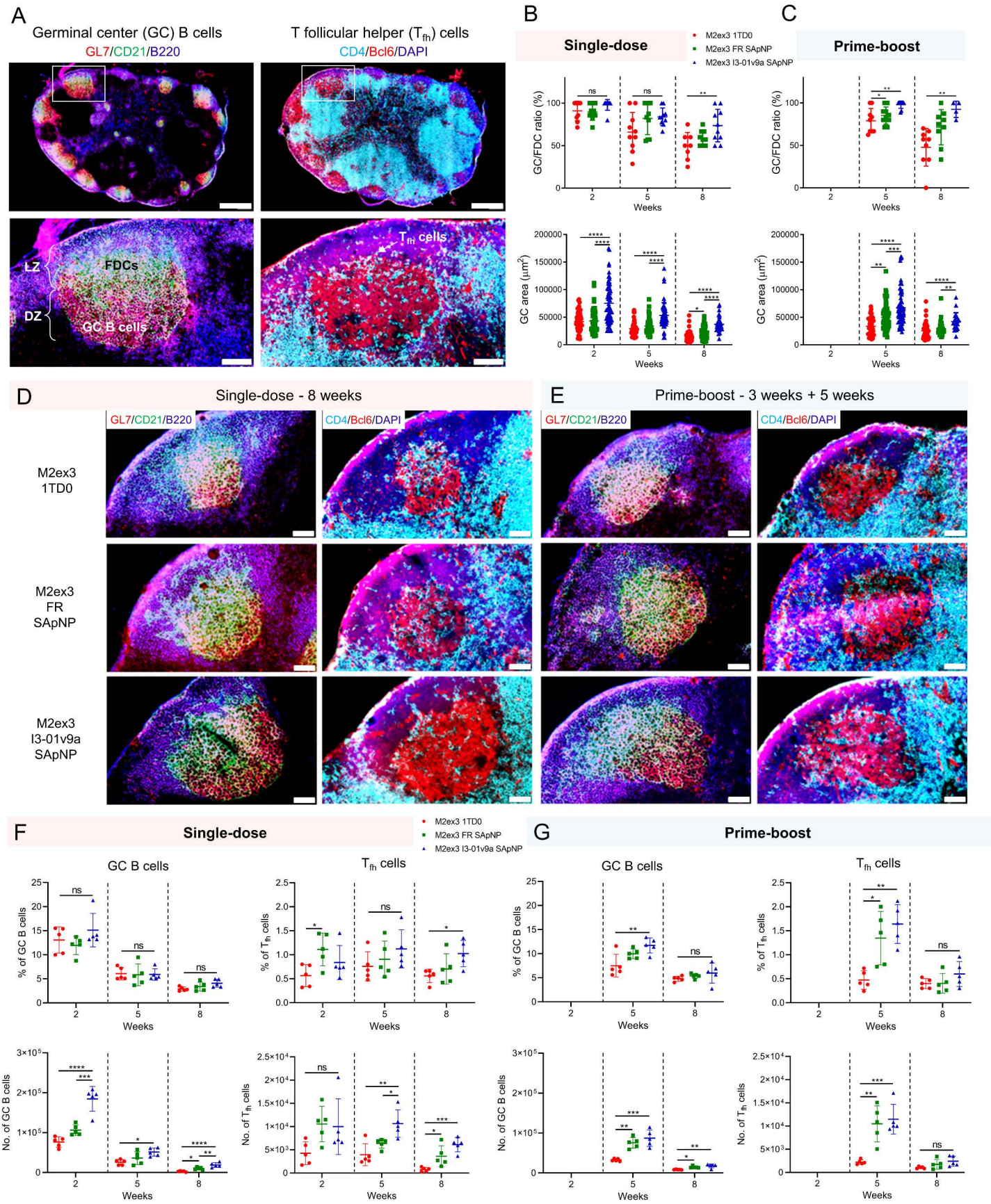
A
Germinal center (GC) B cells
GL7/CD21/B220
T follicular helper (T_{fh}) cells
CD4/Bcl6/DAPI
LZ
FDCs
DZ
GC B cells
T_{fh} cells
B
Single-dose
C
Prime-boost
M2ex3 1TD0
M2ex3 FR SApNP
M2ex3 I3-01v9a SApNP
GC/FDC ratio (%)
GC area (μm²)
Weeks
D
Single-dose - 8 weeks
E
Prime-boost - 3 weeks + 5 weeks
GL7/CD21/B220
CD4/Bcl6/DAPI
M2ex3 1TD0
M2ex3 FR SApNP
M2ex3 I3-01v9a SApNP
F
Single-dose
G
Prime-boost
GC B cells
T_{fh} cells
% of GC B cells
% of T_{fh} cells
No. of GC B cells
No. of T_{fh} cells
Weeks

Fig. 8

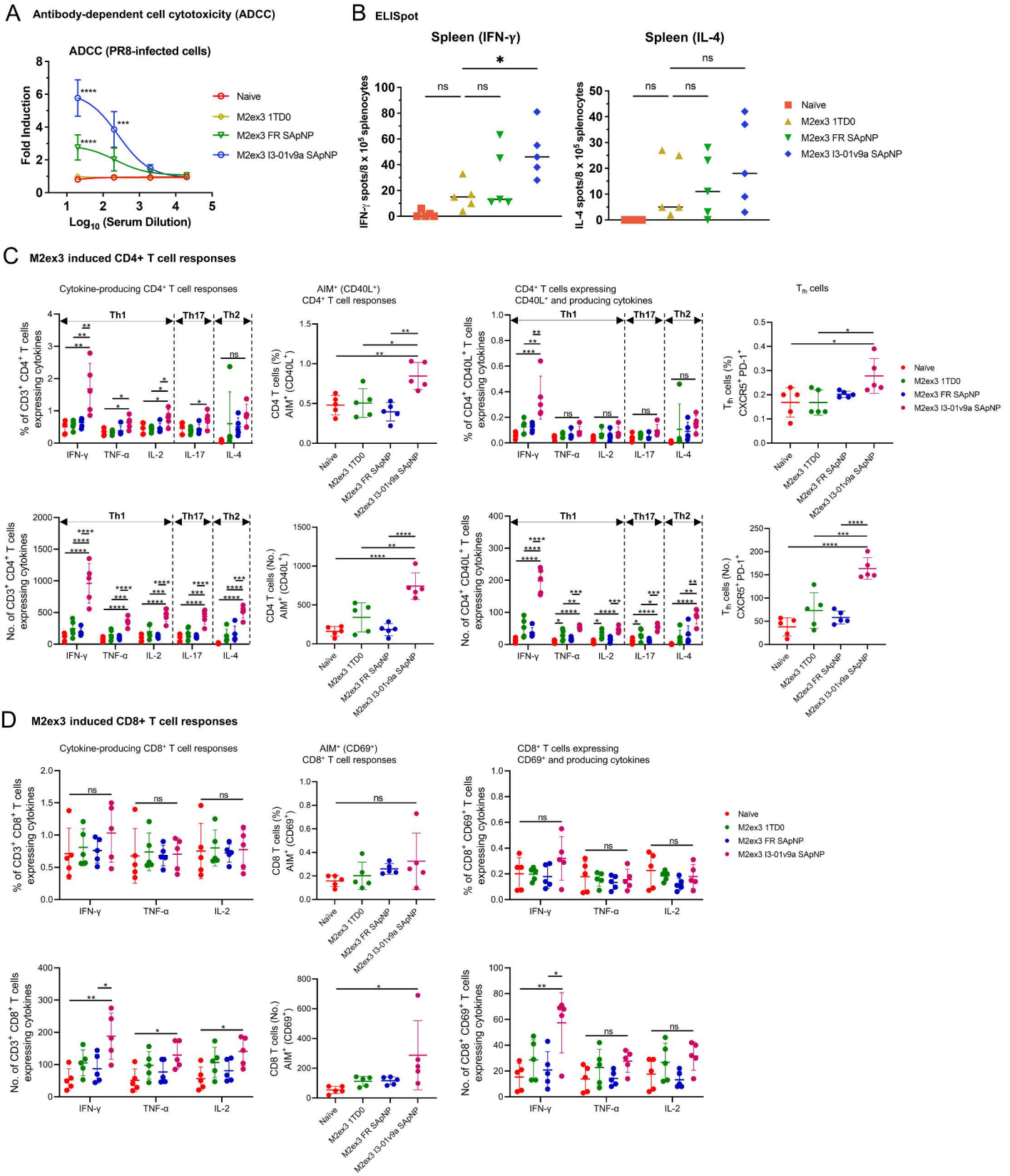
A
Antibody-dependent cell cytotoxicity (ADCC)
ADCC (PR8-infected cells)
Fold Induction
Log10 (Serum Dilution)
Naive
M2ex3 1TD0
M2ex3 FR SApNP
M2ex3 I3-01v9a SApNP
B
ELISpot
Spleen (IFN-γ)
Spleen (IL-4)
IFN-γ spots/8 x 10^5 splenocytes
IL-4 spots/8 x 10^5 splenocytes
ns
*
Naïve
M2ex3 1TD0
M2ex3 FR SApNP
M2ex3 I3-01v9a SApNP
C
M2ex3 induced CD4+ T cell responses
Cytokine-producing CD4+ T cell responses
AIM+ (CD40L+) CD4+ T cell responses
CD4+ T cells expressing CD40L+ and producing cytokines
Tfh cells
Th1
Th17
Th2
% of CD3+ CD4+ T cells expressing cytokines
CD4 T cells (%) AIM+ (CD40L+)
% of CD4+ CD40L+ T cells expressing cytokines
Tfh cells (%) CXCR5+ PD-1+
No. of CD3+ CD4+ T cells expressing cytokines
CD4 T cells (No.) AIM+ (CD40L+)
No. of CD4+ CD40L+ T cells expressing cytokines
Tfh cells (No.) CXCR5+ PD-1+
IFN-γ
TNF-α
IL-2
IL-17
IL-4
Naïve
M2ex3 1TD0
M2ex3 FR SApNP
M2ex3 I3-01v9a SApNP
D
M2ex3 induced CD8+ T cell responses
Cytokine-producing CD8+ T cell responses
AIM+ (CD69+) CD8+ T cell responses
CD8+ T cells expressing CD69+ and producing cytokines
% of CD3+ CD8+ T cells expressing cytokines
CD8 T cells (%) AIM+ (CD69+)
% of CD8+ CD69+ T cells expressing cytokines
No. of CD3+ CD8+ T cells expressing cytokines
CD8 T cells (No.) AIM+ (CD69+)
No. of CD8+ CD69+ T cells expressing cytokines
IFN-γ
TNF-α
IL-2
Naïve
M2ex3 1TD0
M2ex3 FR SApNP
M2ex3 I3-01v9a SApNP

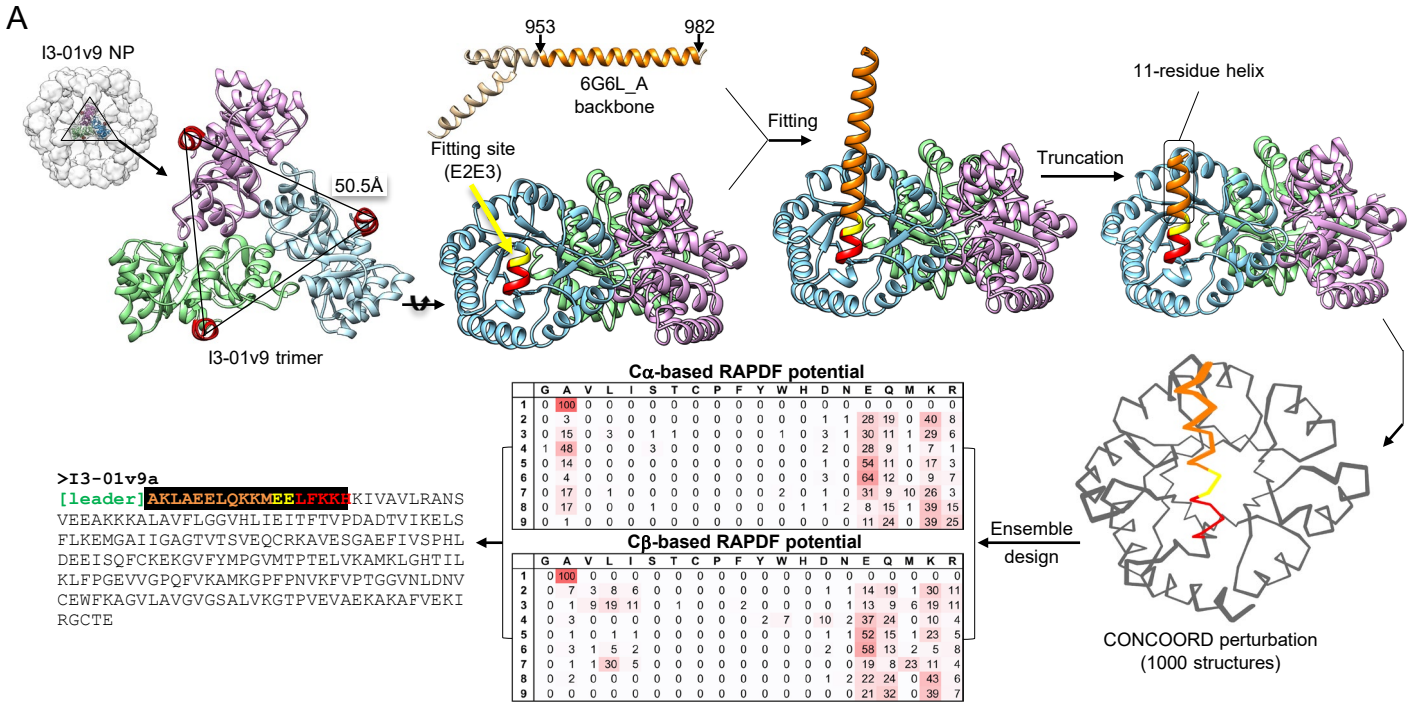

fig. S1. Schematic representation of computational design for I3-01v9a. Top left: The molecular surface model (gray) of I3-01v9 NP and a zoomed-in view of the ribbon model of an I3-01v9 trimer (chains A, B, and C colored in sky blue, plum, and light green, respectively), with the N-termini forming a triangle of 50.5 Å. Also shown is the ribbon model of a c-MYC transcription factor protein (PDB ID: 6G6L), from which the backbone of a helix (residues 953-982, orange) was grafted onto an I3-01v9 subunit by using residues E2 and E3 (yellow) of I3-01v9 for fitting. Top right: A side view of the ribbon model of an I3-01v9 trimer with the fitted full helix backbone (30 residues) and truncated helix backbone (11 residues). Bottom right: 1,000 slightly perturbed backbone conformations of the modified I3-01v9 subunit with an extended N-terminal helix generated using CONCOORD, a protein structure sampling program. Bottom middle: Predicted amino acid (frequency, %) for each position of the first 9 residues using Cα and Cβ-based RAPDF scoring functions. Bottom left: The final sequence design, termed I3-01v9a, with the predicted residues of the N-terminal helical extension colored in orange. The anchoring residues E2 and E3 are colored in yellow, and the last remaining turn of the N-terminal helix is colored in red.

fig. S2

A

```
>hM2e-5GS-1TD0
DAMKRGLCCVLLLCGAVFVSPSQEIHARFRRGARSRSLLTEVETPIRNEWGCRCNDSSDSASGGGGSEVRIFAGNDPAHTATGSSGISSPTPALTPLMLDEATGKLVVWDGQKAGSAVGILVLPLEGTETALTYYKS
GTFATEAIHWPESVDEHKKANAFAGSALSHAA

>hM2e-5GS-FR
DAMKRGLCCVLLLCGAVFVSPSQEIHARFRRGARSRSLLTEVETPIRNEWGCRCNDSSDASGGGGSASGDIIKLLNEQVNKEMQSSNLYMSMSSWCYTHSLDGAGLFLFDHAAEEYEHAKKLIIFLNENNVPVQLTS
ISAPEHKFEGLTQIFQKAYEHEQHISESINNIVDHAIKSKDHATFNFLQWYVAEQHEEEVLFKDILDKIELIGNENHGLYLAD

>hM2e-5GS-E2p-LD4-PADRE(hM2e-E2p-L4P)
DAMKRGLCCVLLLCGAVFVSPSQEIHARFRRGARSRSLLTEVETPIRNEWGCRCNDSSDASGGGGSGAAAKPATTEGEFPETREKMSGIRRAIAKAMVHSKHTAPHVTLMDEADVTKLVAHRKKFKAIAAEKGIKLT
FLPYVVKALVSALREYPVLNTAIDDETEEIIQKHYYNIGIAADTDRGLLVPVIKHADRKPIFALAQEINELAEKARDGKLTPGEMKGASCTITNIGSAGGQWFTPVINHPEVAILGIGRIAEKPIVRDGEIVAAPML
ALSLSFDHRMIDGATAQKALNHIKRLLSDPELLLMGGGGSFSEEQKKALDLAFYFDRRLTPEWRRYLSQRLGLNEEQIERWFRRKEQQIGWSHPQFEKGSAKFVAAWTLKAAA

>hM2e-5GS-I3-01v9a-LD7-PADRE(hM2e-I3-01v9a-L7P)
DAMKRGLCCVLLLCGAVFVSPSQEIHARFRRGARSRSLLTEVETPIRNEWGCRCNDSSDASGGGGSGAKLAEELQKKMEELFKKHKIVAVLRANSVEEAKEKALAVFEGGVHLIEITFTVPDADTVIKELSFLKEKG
AIIGAGTVTSVEQCRKAVESGAEFIVSPHLDAEITVFCLEKGVFYMPGVMTPTELVKAMKLGHNILKLFPGEVVGPQFVKAMKGPFPNVKFVPTGGVNLDNVCEWFKAGVLAVGVGSALVKGTPDEVREKAKAFVEK
IRGCTEGGGGSSPAVDIGDRLDELEKALEALSAEDGHDDVGQRLESLLRRWNSRRADGSAKFVAAWTLKAAA
```

B

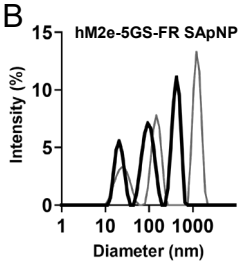

C

mAb65 Binding

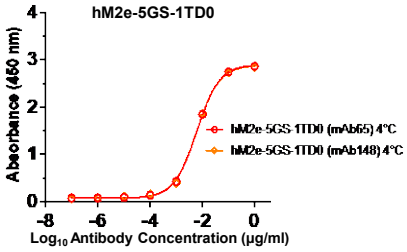

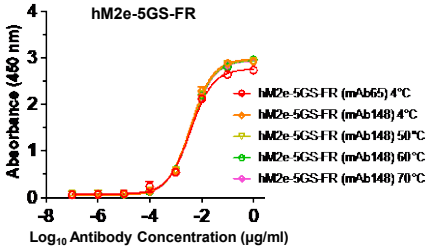

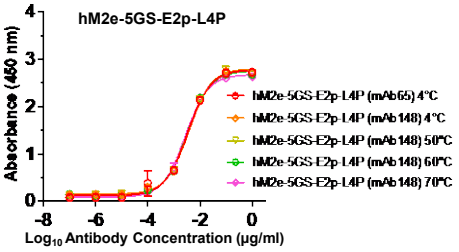

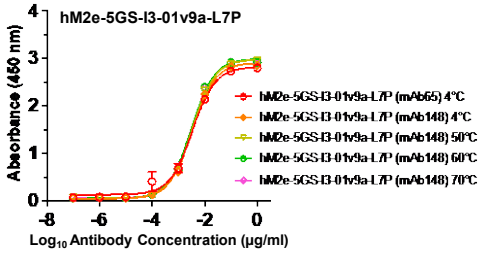

hM2e	Primary Antibody Binding EC_{50} (µg/ml)	
Groups	mAb65	mAb148
hM2e-5GS-1TD0 4°C	0.006025	0.01972
hM2e-5GS-FR 4°C	0.004023	0.01038
hM2e-5GS-FR 50°C	0.003854	0.007114
hM2e-5GS-FR 60°C	0.003853	0.007796
hM2e-5GS-FR 70°C	0.003909	0.007134
hM2e-5GS-E2p-L4P 4°C	0.003703	0.01737
hM2e-5GS-E2p-L4P 50°C	0.003565	0.01721
hM2e-5GS-E2p-L4P 60°C	0.003391	0.01685
hM2e-5GS-E2p-L4P 70°C	0.002789	0.01477
hM2e-5GS-I3-01v9a-L7P 4°C	0.003615	0.01066
hM2e-5GS-I3-01v9a-L7P 50°C	0.003386	0.01315
hM2e-5GS-I3-01v9a-L7P 60°C	0.003107	0.01467
hM2e-5GS-I3-01v9a-L7P 70°C	0.003153	0.0145

mAb148 Binding

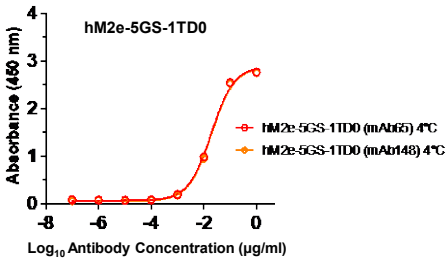

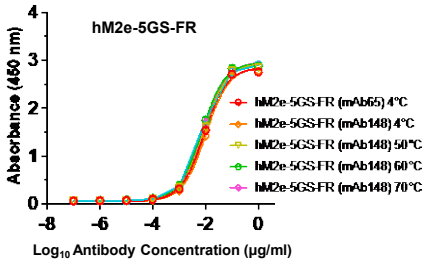

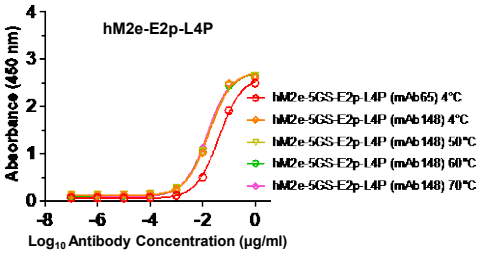

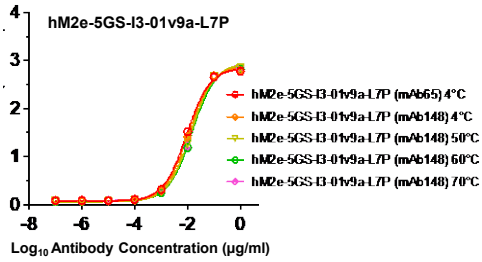

D

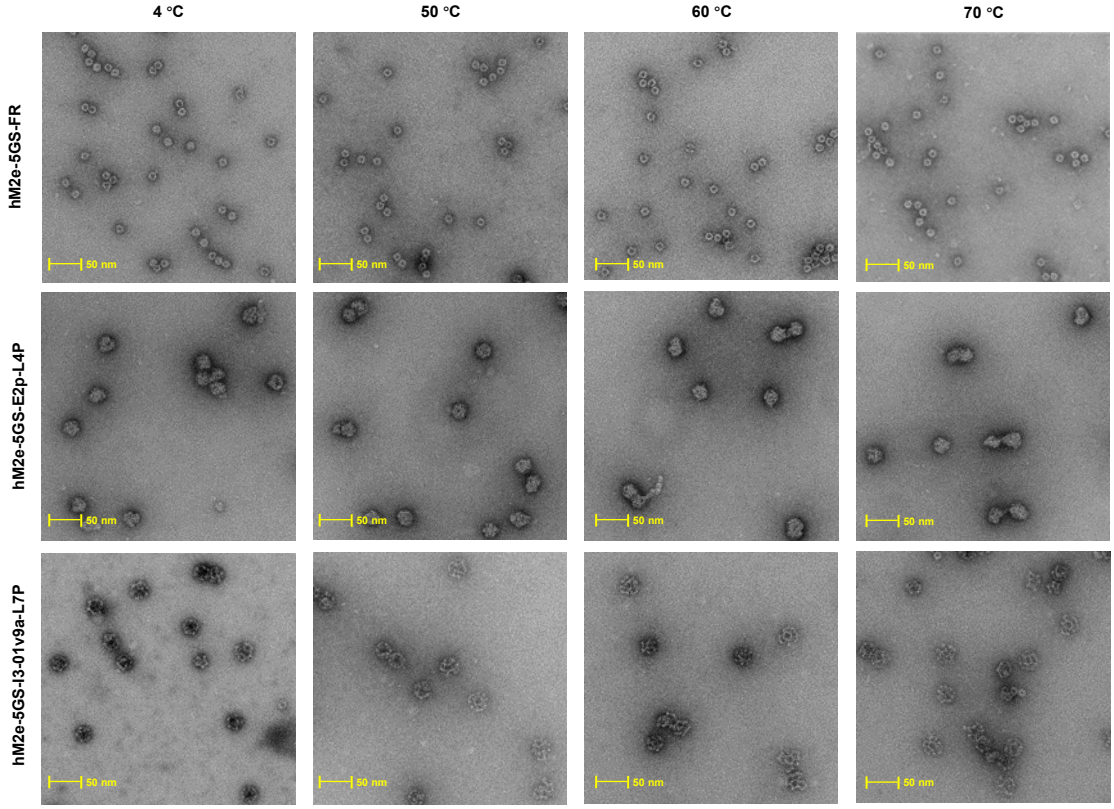

E

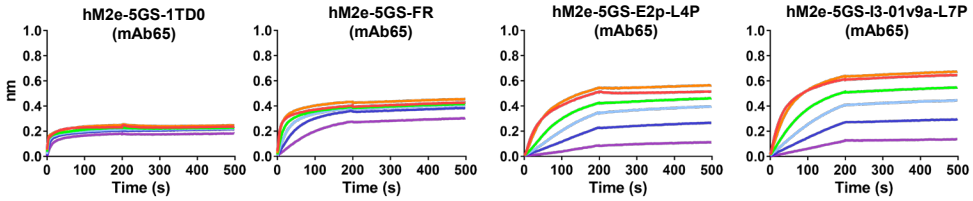

fig. S2. Construct and in vitro characterization of hM2e-presenting trimer and SApNPs. (**A**) Construct sequences of hM2e-presenting FR, E2p-L4P, and I3-01v9-L7P SApNPs, with the gene fragments of leader sequence, restriction site, human Matrix protein 2 extra-virion domain (residue: 2-24), flexible linker, NP-forming subunit, locking domain (LD), and PADRE highlighted in yellow, green, gray, light magenta, cyan, olive green, and red shades, respectively. (**B**) negative stain EM image for hM2e-presenting SApNPs. (**C**) ELISA curves of for hM2e-presenting SApNPs binding to mAb148 and mAb65 antibody. (**D**) Dynamic Light Scatter results for hM2e-FR after SEC purification. (**E**) Antigenic evaluation of hM2e-presenting SApNPs using BLI for mAb65 antibody. A two-fold concentration gradient of antigen, starting at 5.0 uM for hM2e 1TD0 trimer, 80.0 nM for FR-SApNP, and 20.0 nM for E2p and I3-01v9a SApNPs, was used in a titration series of six.

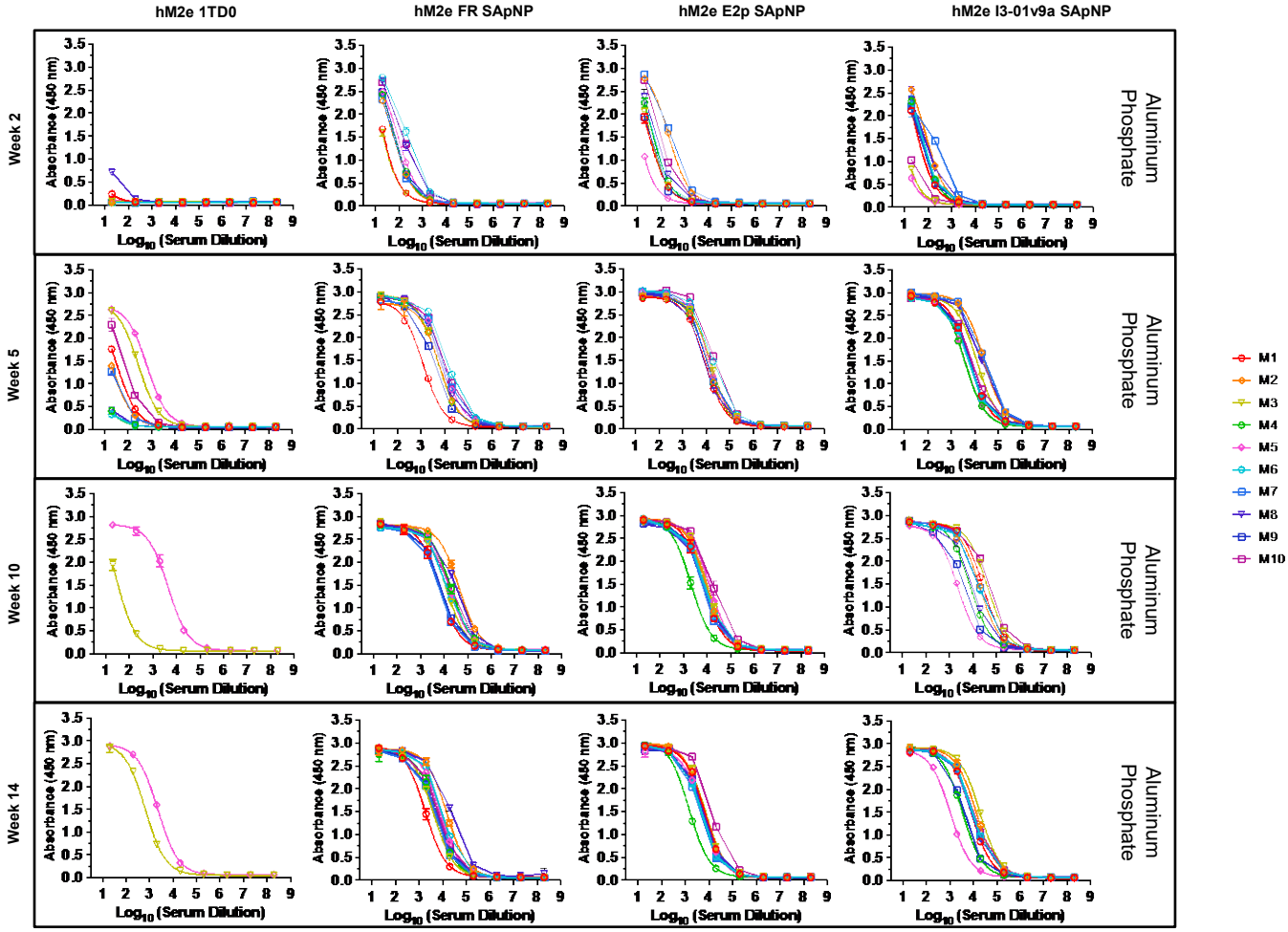

fig. S3. Serum binding of individual mice immunized with hM2e 1TD0 trimer and SApNPs. ELISA curves showing hM2e-immune sera (adjuvanted with aluminum phosphate) binding to the hM2e-5GS-foldon trimer probe and calculated 50% effective concentration (EC_{50}) values for weeks 2 and 5 (N = 10). N = variable at weeks 10 and 14 based on surviving mice/group post-H1N1 and H3N2 challenges at weeks 6 and 10, respectively. Serum was tested was from mice immunized with hM2e 1TD0 trimer, and FR, E2p, and I3-01v9a SApNP at weeks 0 and 3. The assay was performed in duplicate with a starting serum dilution of 20× followed by seven 10-fold titrations.

A

```
>M2ex3-5GS--1TD0
DAMKRGLCCVLLLCGAVFVSPSQEIHARFRRGARSRSLLTEVETPIRNEWGCRCNDSSDGGGGSLLTEVETPTRNGWESKSSDSSDGGGGSLLTEVETPTRSEWESRSSGSSDASGGGGSEVRIFAGNDPAHTATGS
SGISSPTPALTPLMLDEATGKLVVWDGQKAGSAVGILVLPLEGTETALTYYKSGTFATEAIHWPESVDEHKKANAFAGSALSHAA

>M2ex3-5GS-FR
DAMKRGLCCVLLLCGAVFVSPSQEIHARFRRGARSRSLLTEVETPIRNEWGCRCNDSSDGGGGSLLTEVETPTRNGWESKSSDSSDGGGGSLLTEVETPTRSEWESRSSGSSDASGGGGSGDIIKLLNEQVNKEMQS
SNLYMSMSSWCYTHSLDGAGLFLFDHAAEEYEHAKKLIIFLNENNVPVQLTSISAPEHKFEGLTQIFQKAYEHEQHISESINNIVDHAIKSKDHATFNFLQWYVAEQHEEEVLFKDILDKIELIGNENHGLYLAD

>M2ex3-5GS-E2p-LD4-PADRE(M2ex3-E2p-L4P)
DAMKRGLCCVLLLCGAVFVSPSQEIHARFRRGARSRSLLTEVETPIRNEWGCRCNDSSDGGGGSLLTEVETPTRNGWESKSSDSSDGGGGSLLTEVETPTRSEWESRSSGSSDASGGGGSGAAAKPATTEGEFPETR
EKMSGIRRAIAKAMVHSKHTAPHVTLMDEADVTKLVAHRKKFKAIAAEKGIKLTFLPYVVKALVSALREYPVLNTAIDDETEEIIQKHYYNIGIAADTDRGLLVPVIKHADRKPIFALAQEINELAEKARDGKLTPG
EMKGASCTITNIGSAGGQWFTPVINHPEVAILGIGRIAEKPIVRDGEIVAAPMLALSLSFDHRMIDGATAQKALNHIKRLLSDPELLLMGGGGSFSEEQKKALDLAFYFDRRLTPEWRRYLSQRLGLNEEQIERWFR
RKEQQIGWSHPQFEKGSAKFVAAWTLKAAA

>M2ex3-5GS-I3-01v9a-LD7-PADRE(M2ex3-I3-01v9a-L7P)
DAMKRGLCCVLLLCGAVFVSPSQEIHARFRRGARSRSLLTEVETPIRNEWGCRCNDSSDGGGGSLLTEVETPTRNGWESKSSDSSDGGGGSLLTEVETPTRSEWESRSSGSSDASGGGGSAKLAEELQKKMEELFKK
HKIVAVLRANSVEEAKEKALAVFEGGVHLIEITFTVPDADTVIKELSFLKEKGAIIGAGTVTSVEQCRKAVESGAEFIVSPHLDAEITVFCLEKGVFYMPGVMTPTELVKAMKLGHNILKLFPGEVVGPQFVKAMKG
PFPNVKFVPTGGVNLDNVCEWFKAGVLAVGVGSALVKGTPDEVREKAKAFVEKIRGCTEGGGGSSPAVDIGDRLDELEKALEALSAEDGHDDVGQRLESLLRRWNSRRADGSAKFVAAWTLKAAA
```

B

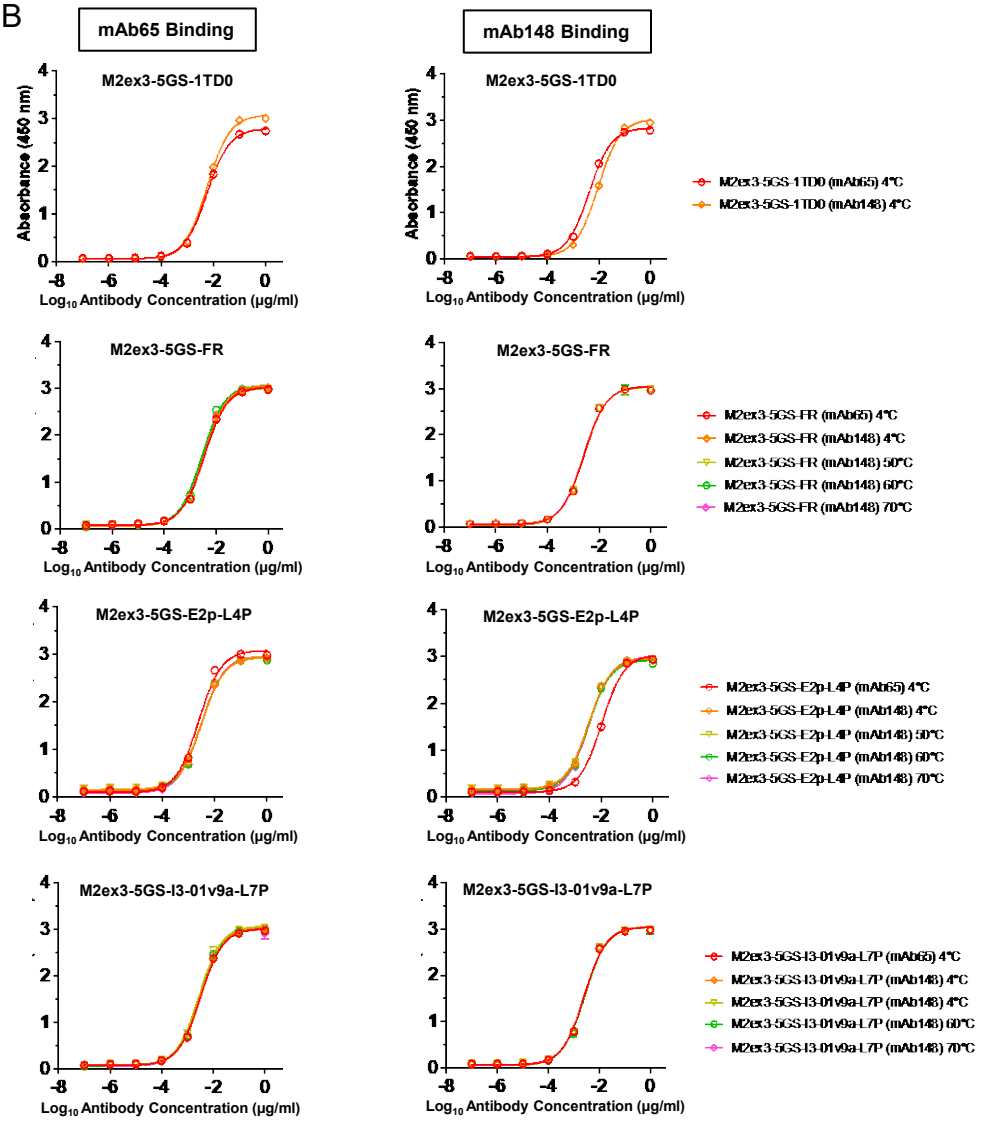

M2ex3	Primary Antibody Binding EC_{50} (µg/ml)	
Groups	mAb65	mAb148
M2ex3-5GS-1TD0 4°C	0.003651	0.009314
M2ex3-5GS-FR 4°C	0.003391	0.002564
M2ex3-5GS-FR 50°C	0.003373	0.00249
M2ex3-5GS-FR 60°C	0.002864	0.002555
M2ex3-5GS-FR 70°C	0.003176	0.002486
M2ex3-5GS-E2p-L4P 4°C	0.003277	0.003288
M2ex3-5GS-E2p-L4P 50°C	0.003149	0.003302
M2ex3-5GS-E2p-L4P 60°C	0.003209	0.003274
M2ex3-5GS-E2p-L4P 70°C	0.003013	0.00337
M2ex3-5GS-I3-01v9a-L7P 4°C	0.003325	0.002538
M2ex3-5GS-I3-01v9a-L7P 50°C	0.002818	0.0026
M2ex3-5GS-I3-01v9a-L7P 60°C	0.003039	0.002729
M2ex3-5GS-I3-01v9a-L7P 70°C	0.002895	0.002561

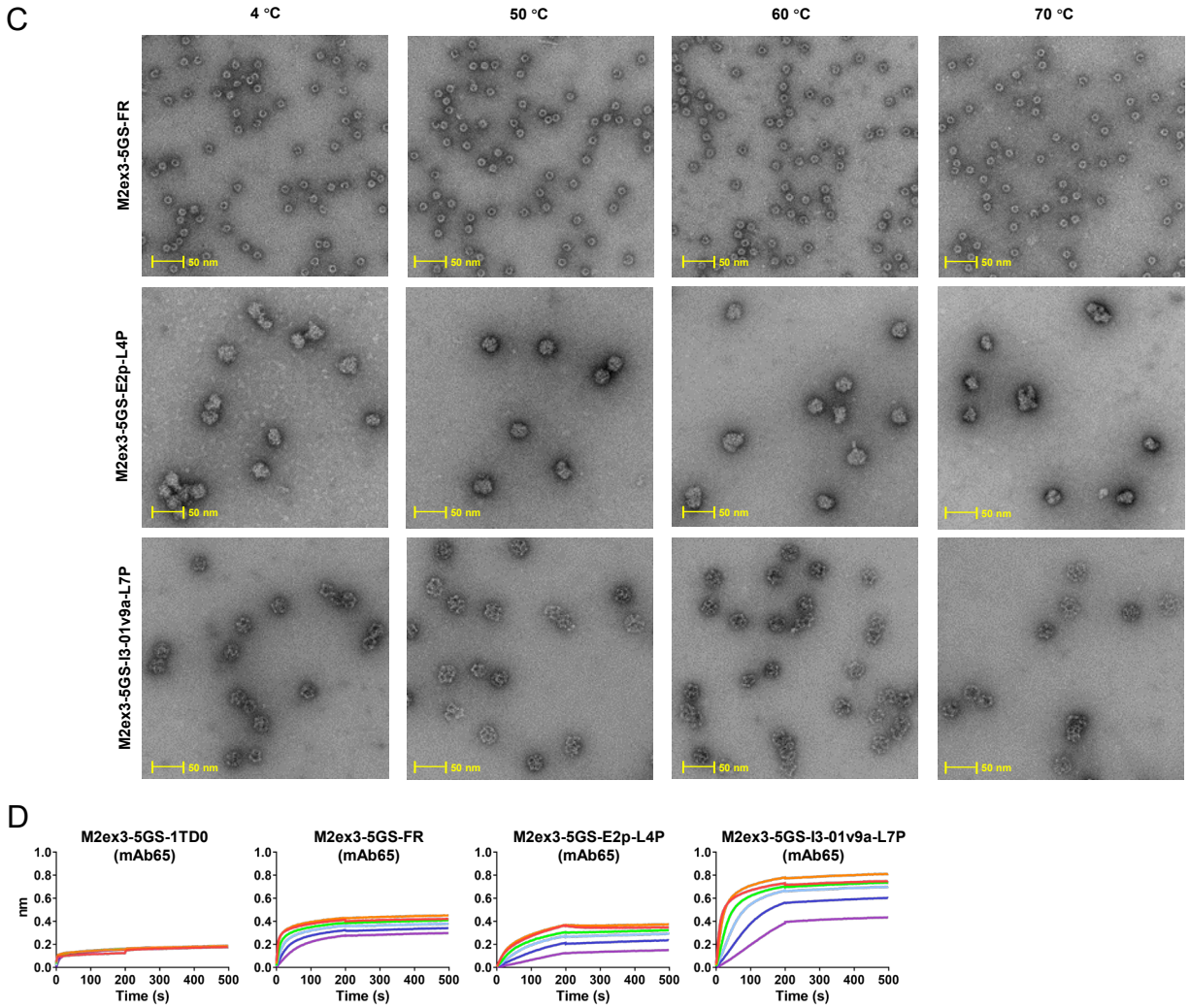

fig. S4. Design and in vitro characterization of M2ex3-presenting SApNPs. (**A**) Construct sequences of tandem M2e-presenting FR, E2p-L4P, and I3-01v9-L7P NPs, with the gene fragments of leader sequence, restriction site, tandem Matrix protein 2 extra-virion domain (including human, avian/swine and human/swine), flexible linker, NP-forming subunit, locking domain (LD), and PADRE highlighted in yellow, green, gray, light magenta, cyan, olive green, and red shades, respectively. (**B**) negative stain EM image for M2ex3-presenting SApNPs. (**C**) ELISA curves of for M2ex3-presenting SApNPs binding to mAb148 and mAb65 antibody. (**D**) Antigenic evaluation of M2eX3-presenting SApNPs using BLI for mAb65 antibody. A two-fold concentration gradient of antigen, starting at 5 uM for M2ex3 1TD0 trimer, 80 nM for FR SApNP, and 20 nM for E2p and I3-01v9a SApNPs, was used in a titration series of six.

fig. S5

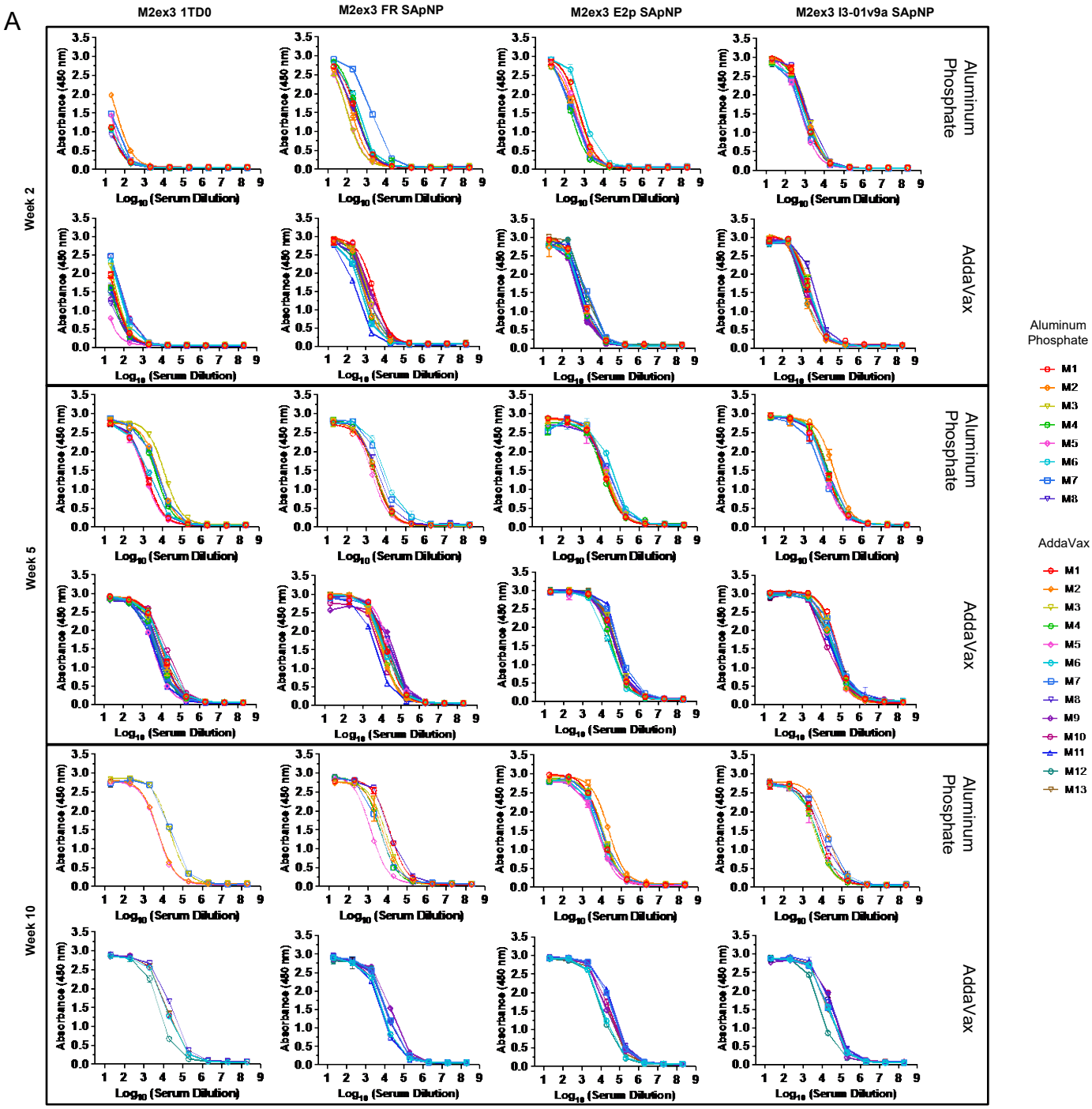
A
M2ex3 1TD0
M2ex3 FR SApNP
M2ex3 E2p SApNP
M2ex3 I3-01v9a SApNP
Week 2
Week 5
Week 10
Aluminum Phosphate
AddaVax
Absorbance (450 nm)
Log10 (Serum Dilution)
Aluminum Phosphate
M1
M2
M3
M4
M5
M6
M7
M8
AddaVax
M1
M2
M3
M4
M5
M6
M7
M8
M9
M10
M11
M12
M13

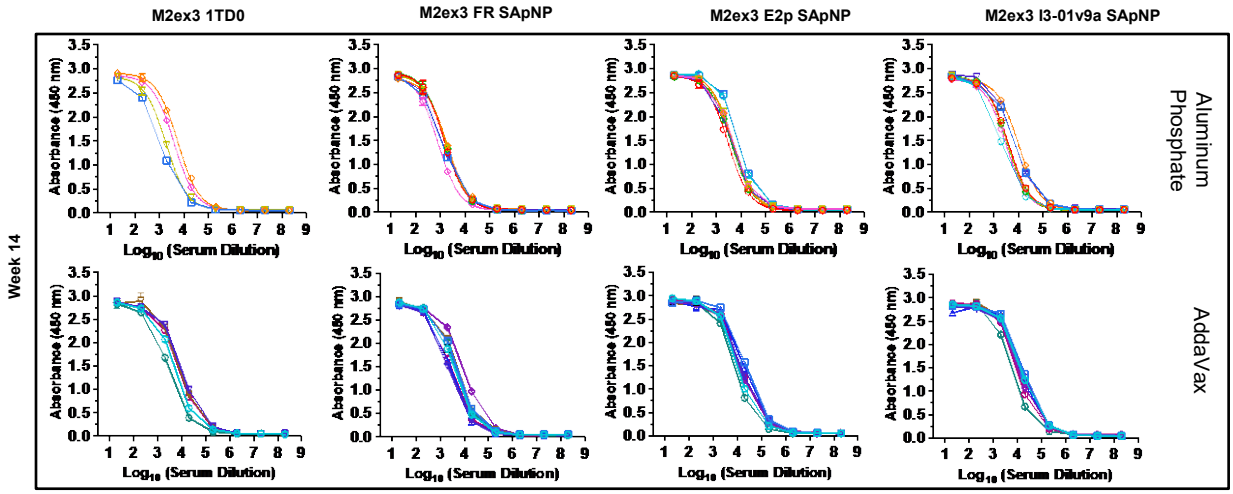

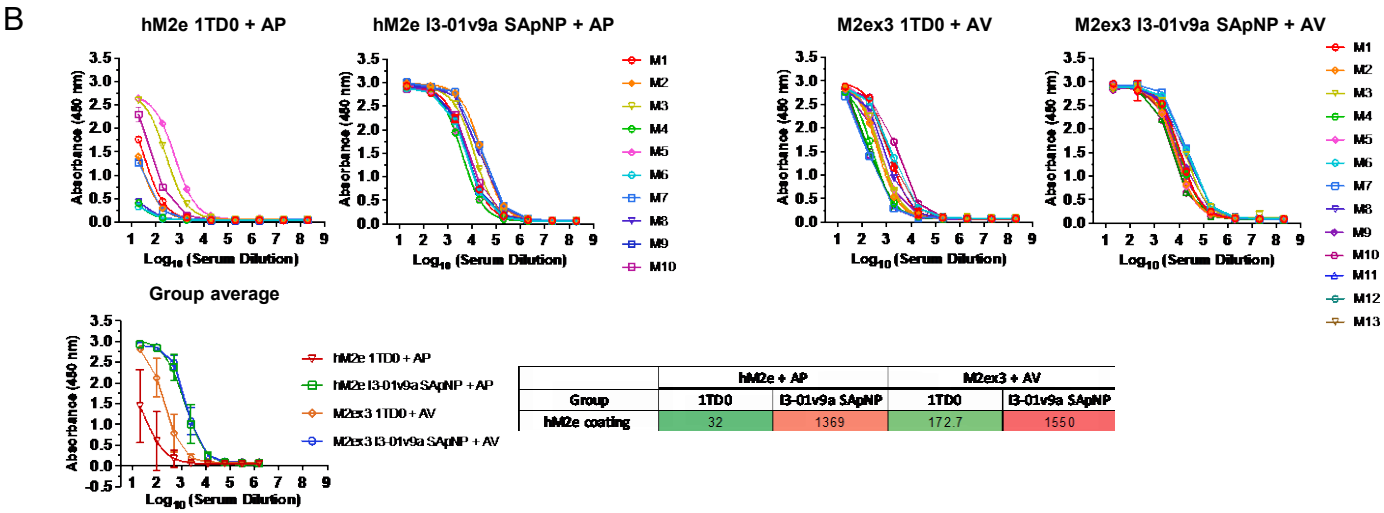

	hM2e + AP		M2ex3 + AV	
Group	1TD0	I3-01v9a SApNP	1TD0	I3-01v9a SApNP
hM2e coating	32	1369	172.7	1550

fig. S5. Serum binding of individual mice immunized with M2ex3 1TD0 trimer and SApNPs. (**A**) ELISA curves showing M2ex3-immune sera (adjuvanted with aluminum phosphate or AddaVax) binding to the M2ex3-5GS-foldon trimer probe and calculated 50% effective concentration (EC_{50}) values for weeks 2, 5, 10, and 14. N = 8 or 13 at weeks 2 and 5. N = variable at weeks 10 and 14 based on surviving mice/group post-H1N1 and H3N2 challenges at weeks 6 and 10, respectively. Serum was tested was from mice immunized with M2ex3 1TD0 trimer, and FR, E2p, and I3-01v9a SApNP at weeks 0 and 3. The assay was performed in duplicate with a starting serum dilution of 20× followed by seven 10-fold titrations. (**B**) ELISA curves showing hM2e (+ AP)- and M2ex3 (+ AV)-immune sera binding to the hM2e-5GS-foldon trimer probe at week 5. N = 10 for hM2e groups. N = 13 for M2ex3 groups. Results indicate that M2ex3-immune sera demonstrates similar or higher binding to hM2e foldon compared to hM2e-immune sera. The assay was performed starting at a serum dilution of 20× followed by seven 10-fold titrations.

fig. S6

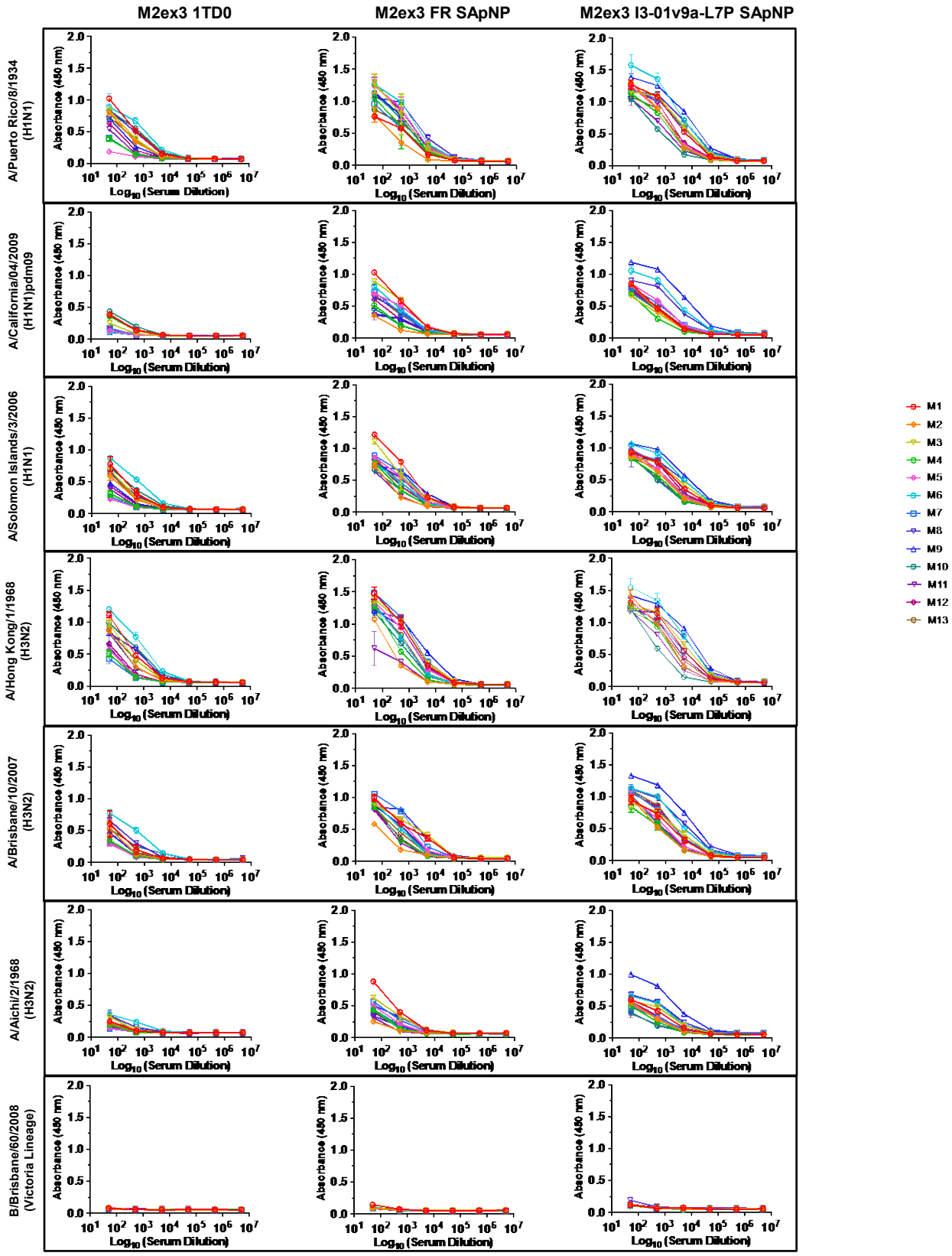
M2ex3 1TD0
M2ex3 FR SApNP
M2ex3 I3-01v9a-L7P SApNP
A/Puerto Rico/8/1934 (H1N1)
A/California/04/2009 (H1N1)pdm09
A/Solomon Islands/3/2006 (H1N1)
A/Hong Kong/1/1968 (H3N2)
A/Brisbane/10/2007 (H3N2)
A/Aichi/2/1968 (H3N2)
B/Brisbane/60/2008 (Victoria Lineage)
Absorbance (450 nm)
Log10 (Serum Dilution)
M1
M2
M3
M4
M5
M6
M7
M8
M9
M10
M11
M12
M13

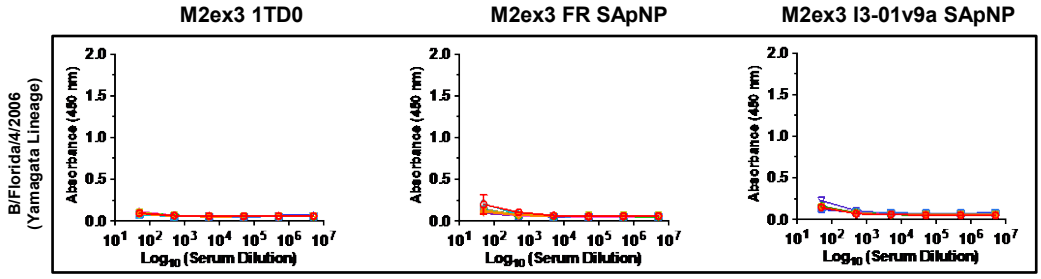

fig. S6. M2ex3 serum binding of individual mice to cell-surface homotetrameric M2e. Week 5 serum from mice immunized with M2ex3 1TD0, FR SApNP, and I3-01v9a SApNPs adjuvanted with AddaVax (n = 13) were tested against homotetrameric M2e on various influenza strains: A/Puerto Rico/8/1934 (H1N1), A/California/04/2009 (H1N1)pdm09, A Solomon Islands/2/2006 (H1N1), A/Hong Kong/1/1968 (H3N2), A/Brisbane/10/2007 (H3N2), A/Aichi/2/1968 (H3N2), B/Brisbane/60/2008 (Flu B, Victoria Lineage), and B/Florida/4/2006 (Flu B, Yamagata Lineage). MAb148 (M2e antibody) was used as a IAV positive control. The assay was performed in duplicate with a starting serum dilution of 50x followed by five 10-fold titrations.

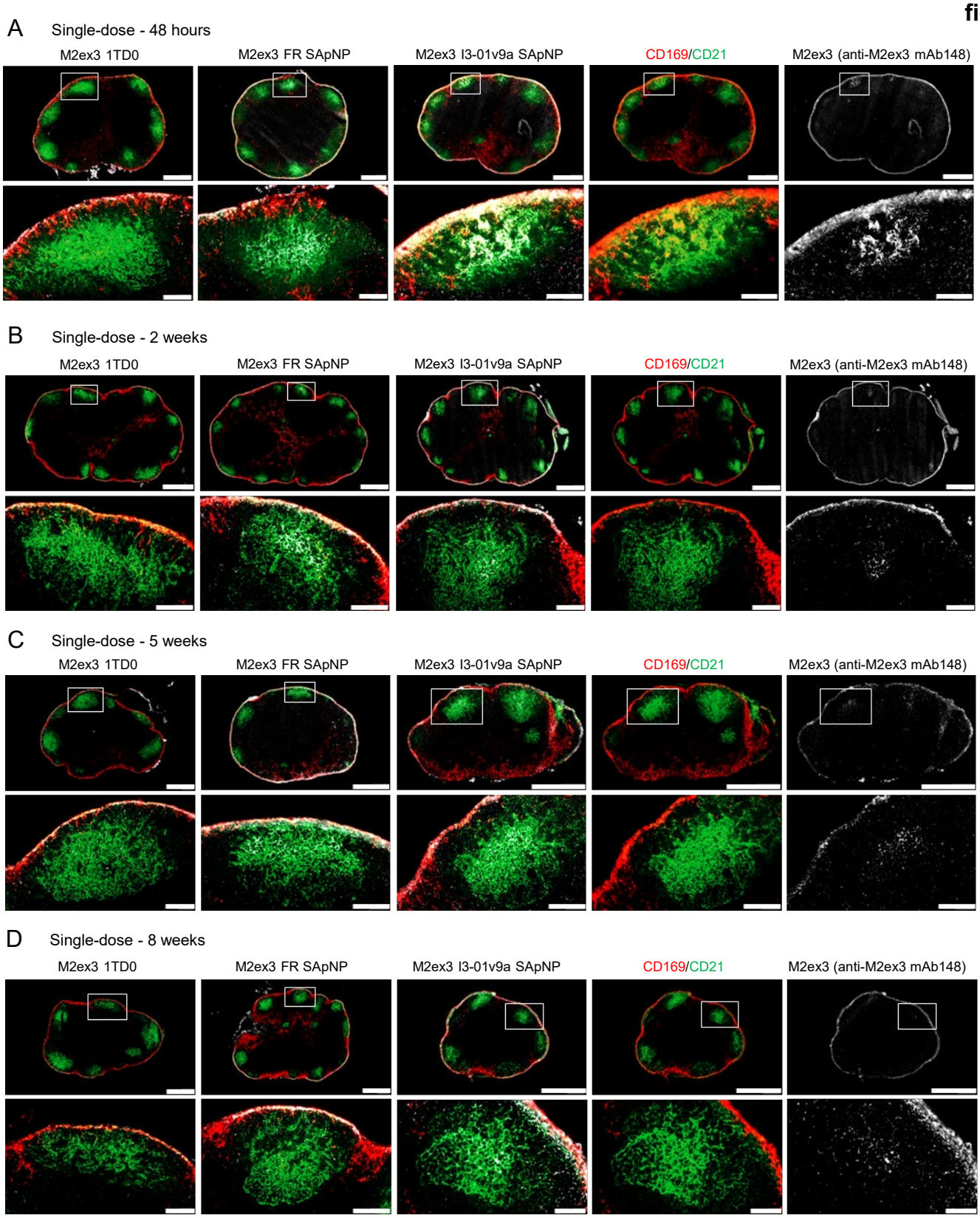

fig. S7. Immunohistological images of M2ex3 1TD0 trimer and SApNPs in lymph nodes. Immunostaining images of M2ex3 1TD0 and M2ex3-presenting FR and I3-01v9a SApNP interaction with FDC networks in lymph node follicles at (**A**) 48 hours, (**B**) 2 weeks, (**C**) 5 weeks, and (**D**) 8 weeks after a single-dose injection (10 μg per injection, totaling 40 μg per mouse). Immunofluorescent images are pseudo color coded (CD21+, green; CD169+, red; anti-M2ex3 mAb148, white). Scale bars = 500 and 100 μm for complete lymph node and enlarged image of a follicle, respectively. Data were collected from more than 10 lymph node follicles (n = 3-5 mice/group).

fig. S8

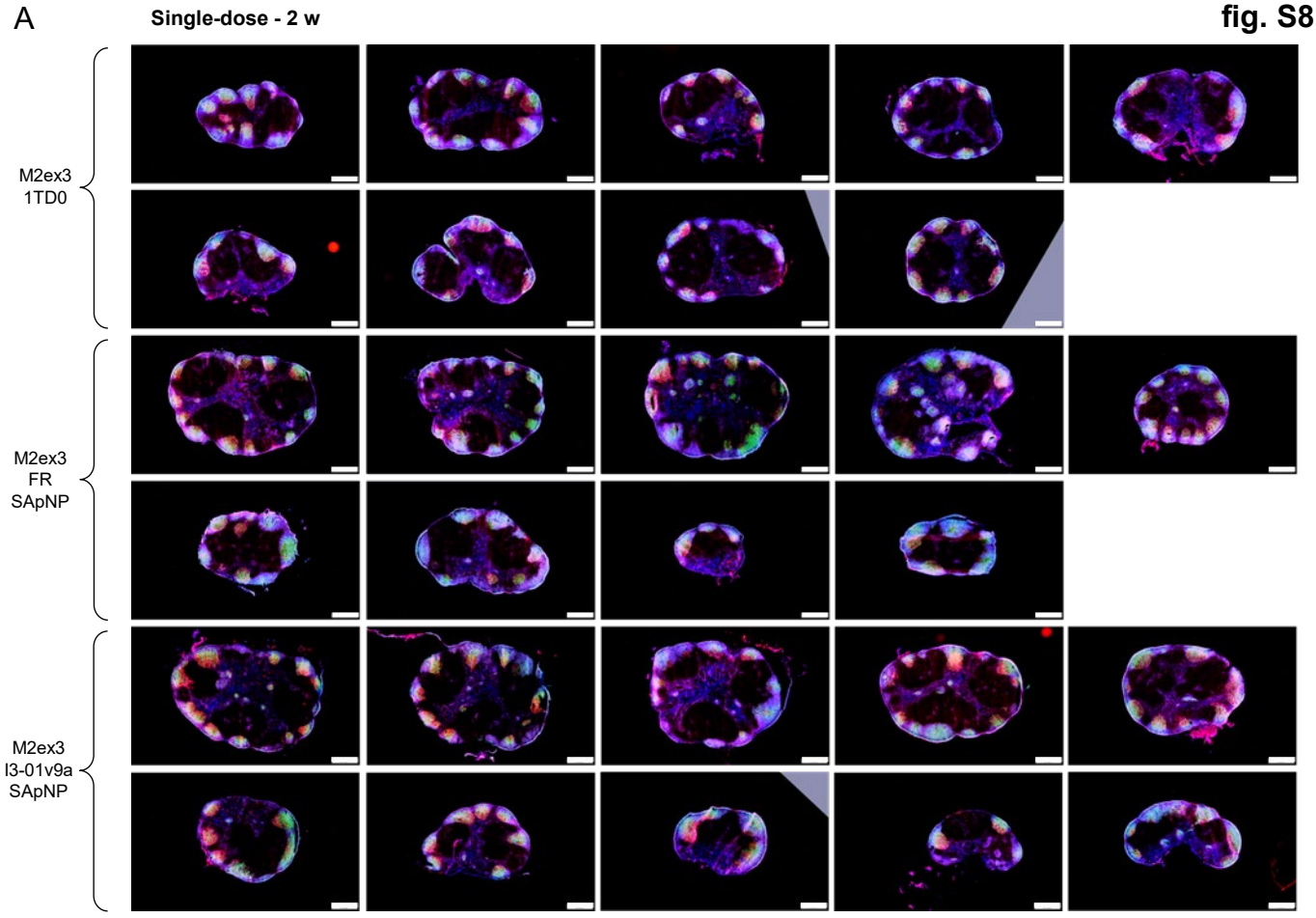
A
Single-dose - 2 w
M2ex3
1TD0
M2ex3
FR
SApNP
M2ex3
I3-01v9a
SApNP

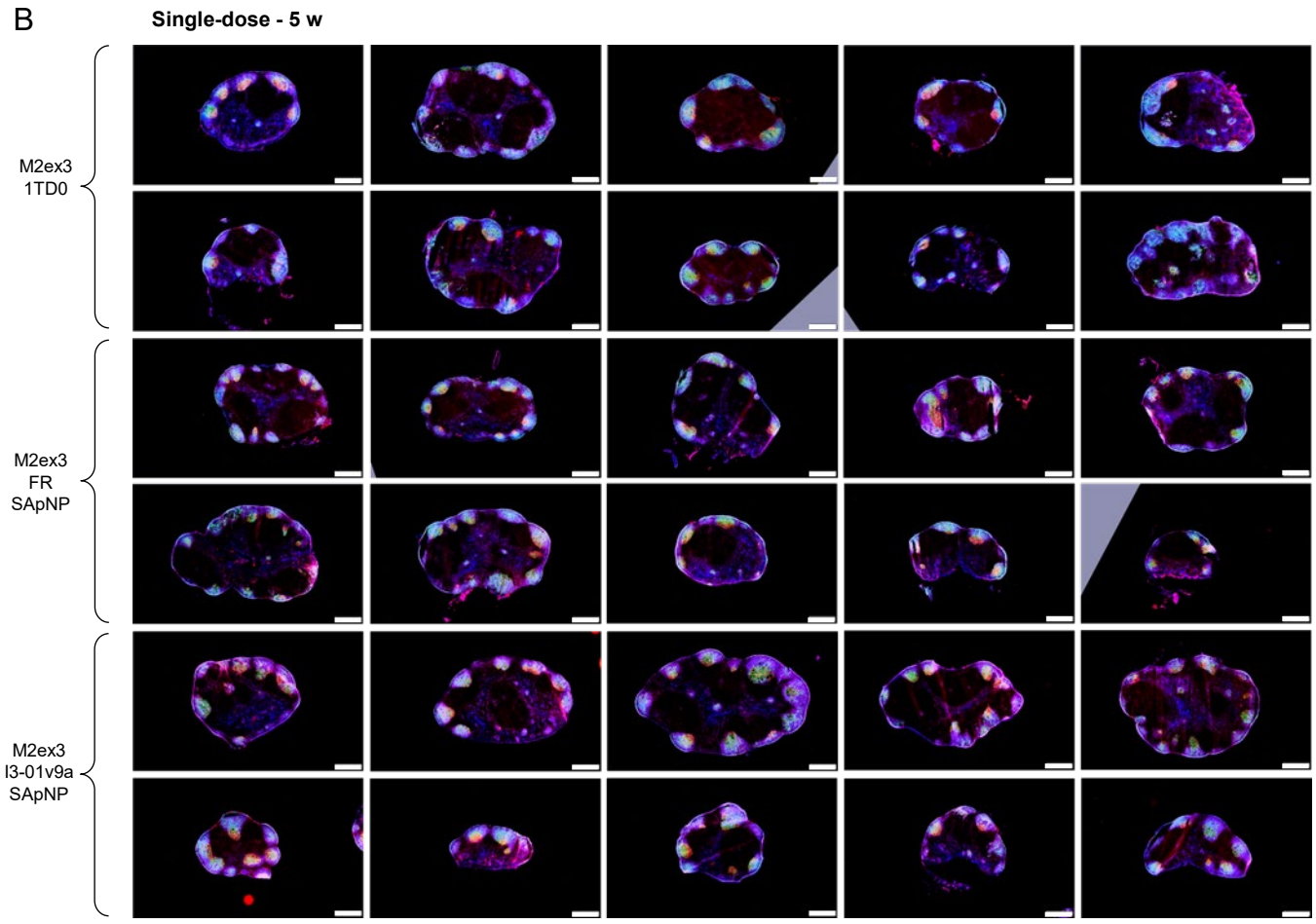
B
Single-dose - 5 w
M2ex3
1TD0
M2ex3
FR
SApNP
M2ex3
I3-01v9a
SApNP

fig. S8

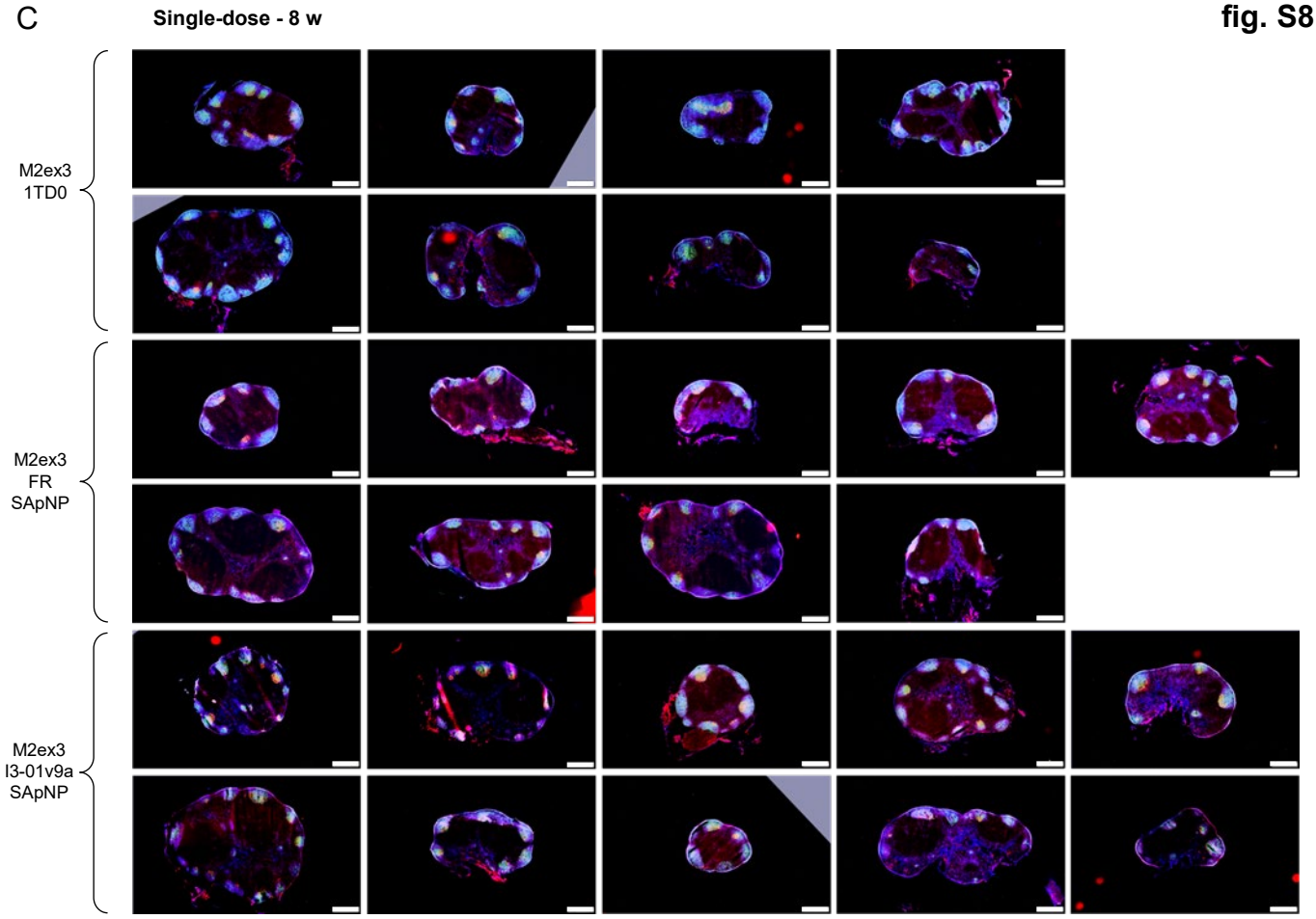
C
Single-dose - 8 w
M2ex3
1TD0
M2ex3
FR
SApNP
M2ex3
I3-01v9a
SApNP

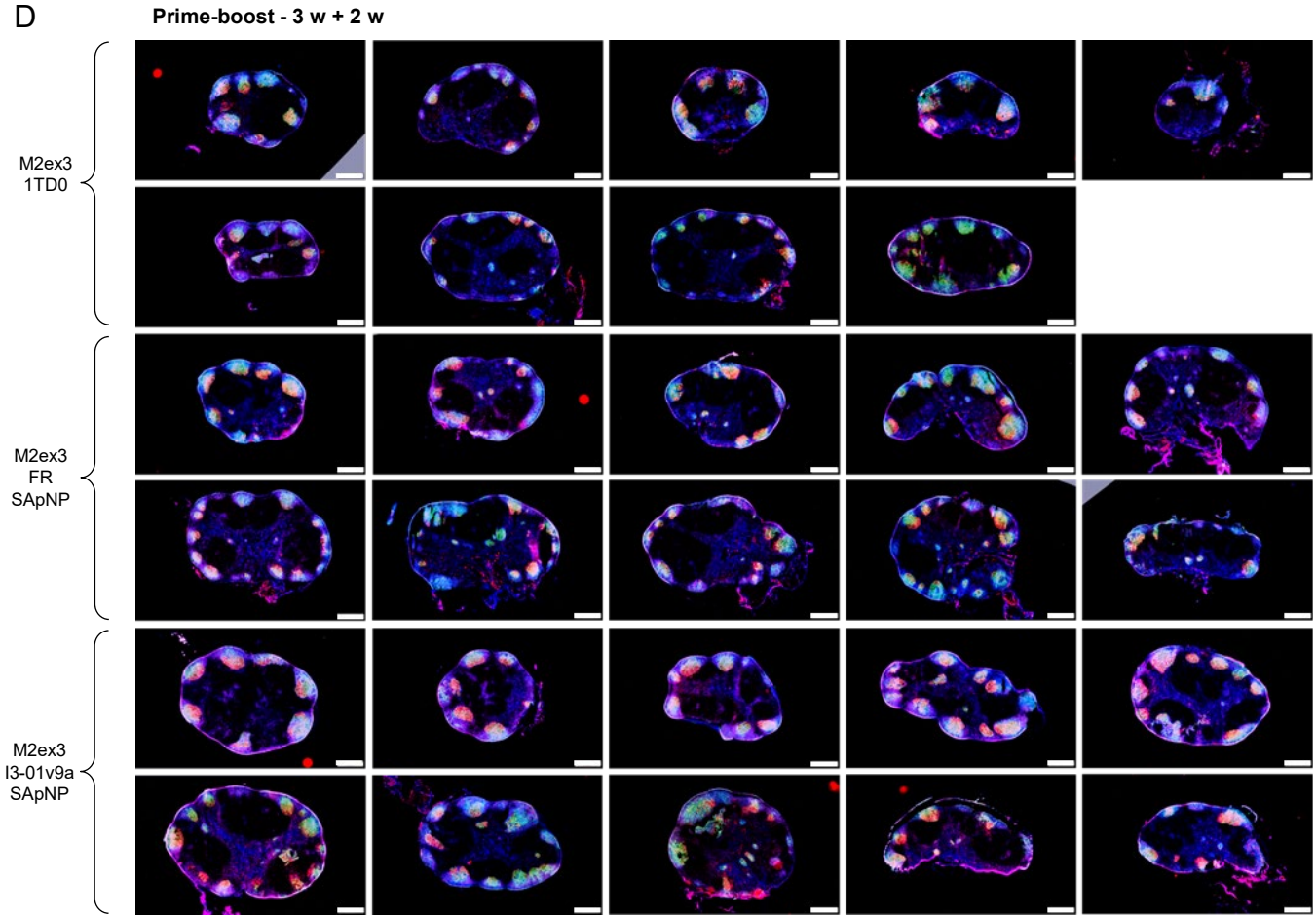
D
Prime-boost - 3 w + 2 w
M2ex3
1TD0
M2ex3
FR
SApNP
M2ex3
I3-01v9a
SApNP

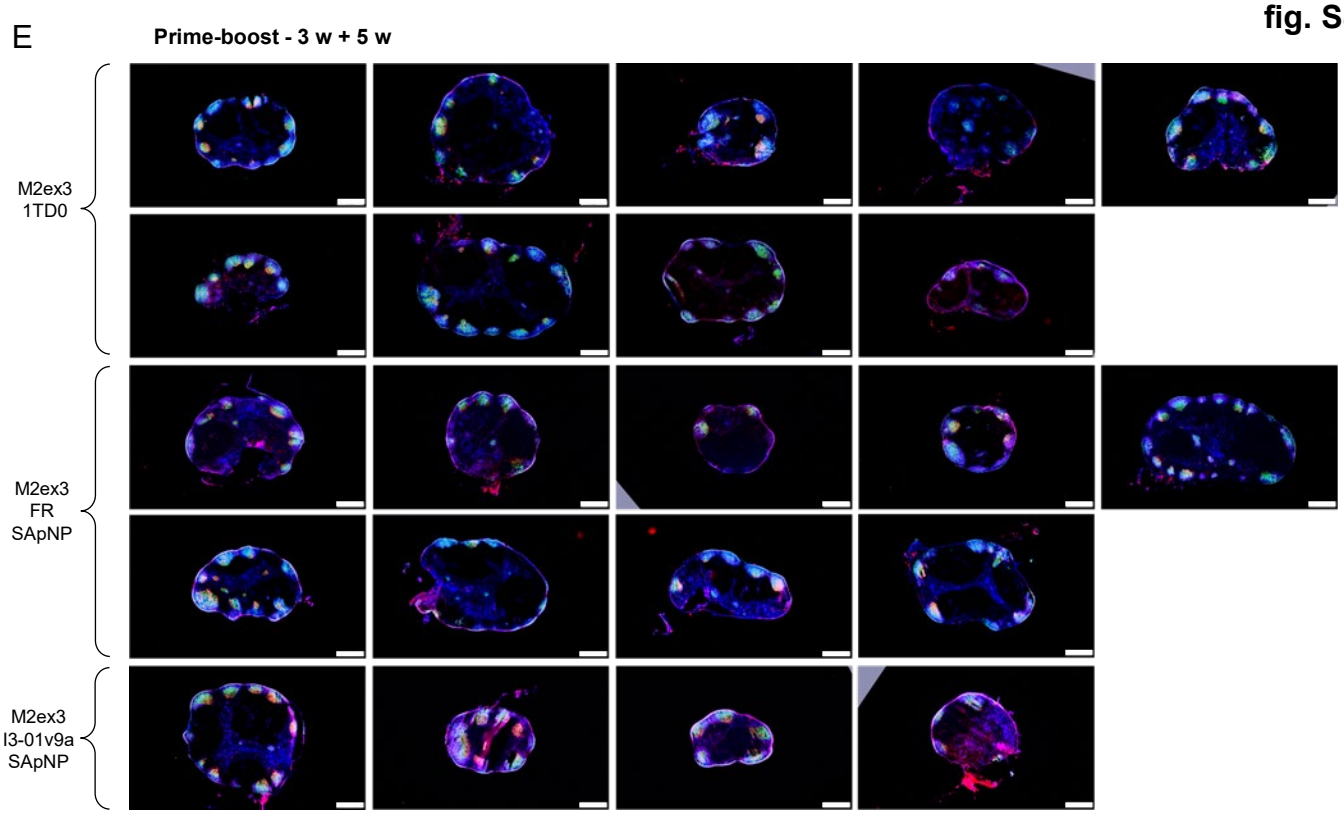

fig. S8. Immunohistological analysis of M2ex3 1TD0 trimer and SApNP-induced GCs. Immunohistological images of GCs at (**A**) 2, (**B**) 5, and (**C**) 8 weeks after a single-dose injection of M2ex3 1TD0 and M2ex3-presenting FR, and I3-01v9a SApNP vaccines (10 μg per injection, totaling 40 μg per mouse), with a scale bar of 500 μm for each image. Images of GCs at (**D**) 2 and (**E**) 5 weeks after the boost, which occurred at 3 weeks after the first dose (n = 5 mice/group).

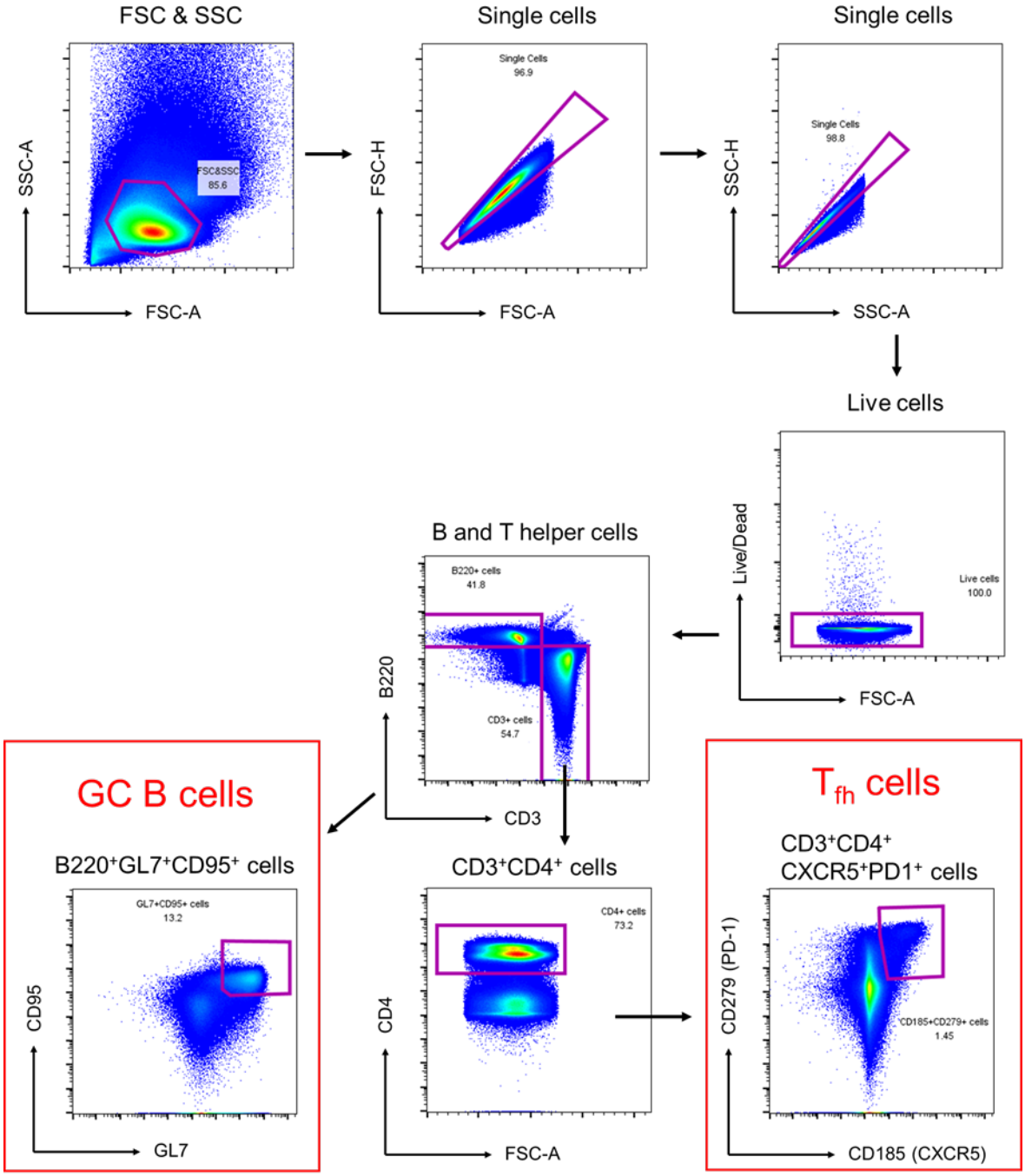

fig. S9. Flow cytometry analysis of M2ex3 1TD0 trimer and SApNP-induced GCs. Gating strategy for analyzing GCs (GC B cells and T follicular helper cells) using flow cytometry (n = 5 mice/group).

fig. S10

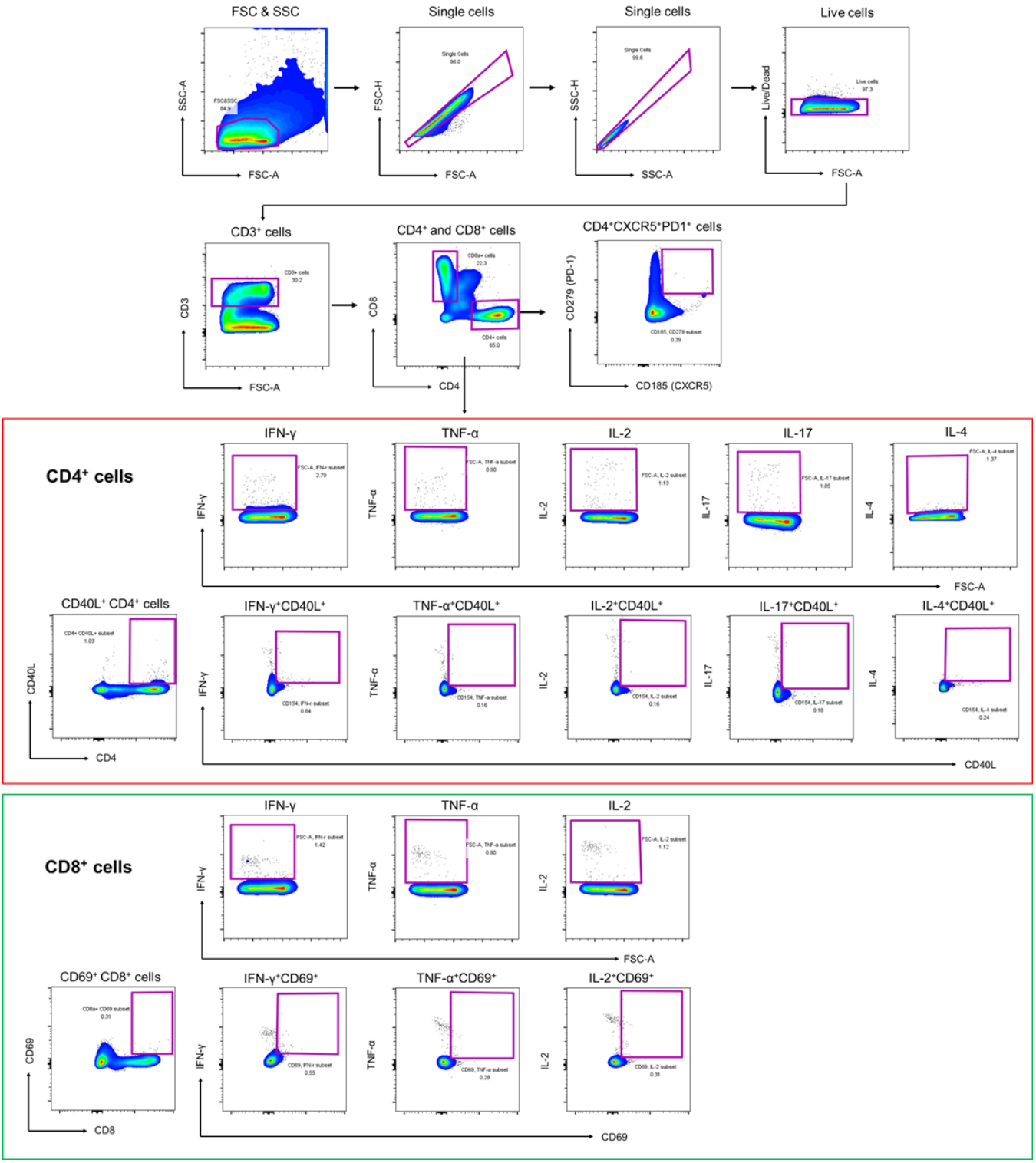

fig. S10. Flow cytometry analysis of M2ex3 1TD0 trimer and SApNP-induced T cell responses. Gating strategy for analyzing CD4+ and CD8+ T cell responses against the M2ex3-5GS-foldon probe using flow cytometry at 5 days after prime-boost immunization and virus challenge (n = 5 mice/group).

Fig. 1

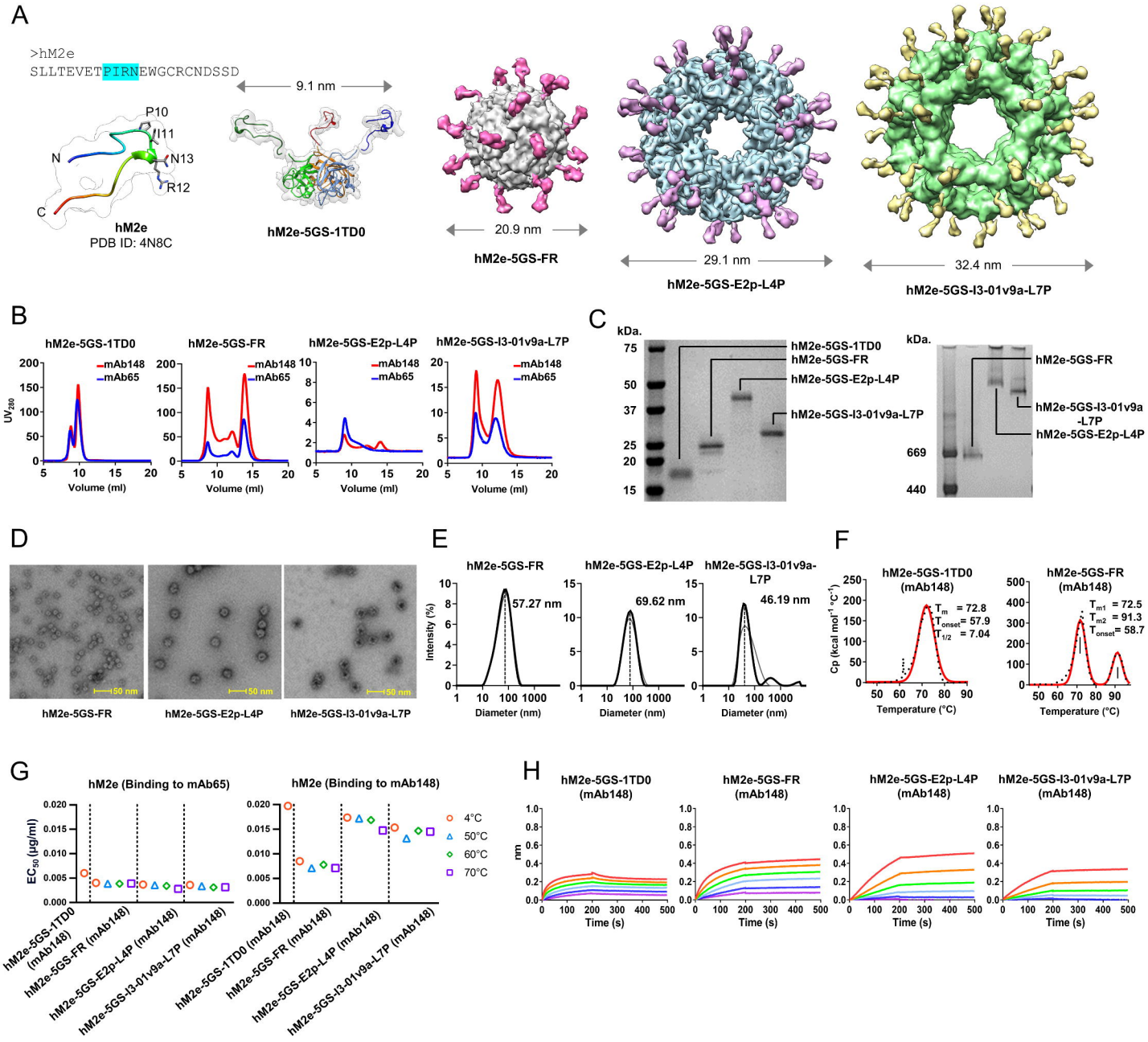
A
>hM2e
SLLTEVETPIRNEWGCRCNDSSD
9.1 nm
P10
I11
N
N13
R12
C
hM2e
PDB ID: 4N8C
hM2e-5GS-1TD0
20.9 nm
hM2e-5GS-FR
29.1 nm
hM2e-5GS-E2p-L4P
32.4 nm
hM2e-5GS-I3-01v9a-L7P
B
hM2e-5GS-1TD0
hM2e-5GS-FR
hM2e-5GS-E2p-L4P
hM2e-5GS-I3-01v9a-L7P
mAb148
mAb65
UV280
Volume (ml)
C
kDa.
75
50
37
25
20
15
hM2e-5GS-1TD0
hM2e-5GS-FR
hM2e-5GS-E2p-L4P
hM2e-5GS-I3-01v9a-L7P
669
440
hM2e-5GS-I3-01v9a -L7P
hM2e-5GS-E2p-L4P
D
50 nm
hM2e-5GS-FR
hM2e-5GS-E2p-L4P
hM2e-5GS-I3-01v9a-L7P
E
57.27 nm
69.62 nm
46.19 nm
Intensity (%)
Diameter (nm)
F
hM2e-5GS-1TD0 (mAb148)
Tm = 72.8
Tonset = 57.9
T1/2 = 7.04
hM2e-5GS-FR (mAb148)
Tm1 = 72.5
Tm2 = 91.3
Tonset = 58.7
Cp (kcal mol-1 °C-1)
Temperature (°C)
G
hM2e (Binding to mAb65)
hM2e (Binding to mAb148)
EC50 (µg/ml)
4°C
50°C
60°C
70°C
hM2e-5GS-1TD0 (mAb148)
hM2e-5GS-FR (mAb148)
hM2e-5GS-E2p-L4P (mAb148)
hM2e-5GS-I3-01v9a-L7P (mAb148)
H
hM2e-5GS-1TD0 (mAb148)
hM2e-5GS-FR (mAb148)
hM2e-5GS-E2p-L4P (mAb148)
hM2e-5GS-I3-01v9a-L7P (mAb148)
nm
Time (s)

Fig. 2

A

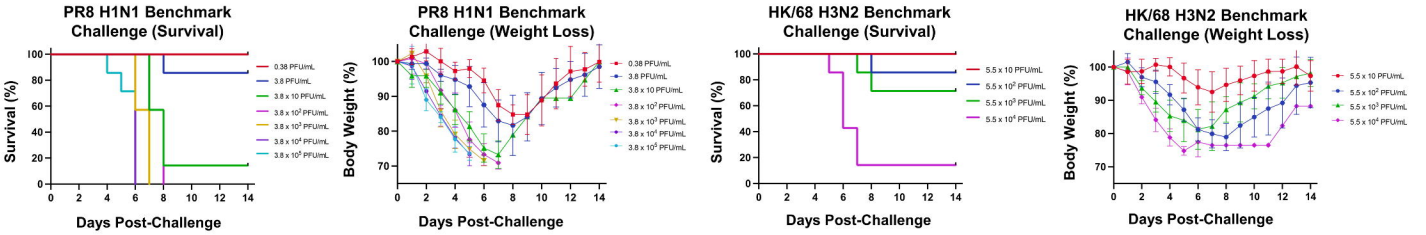

B

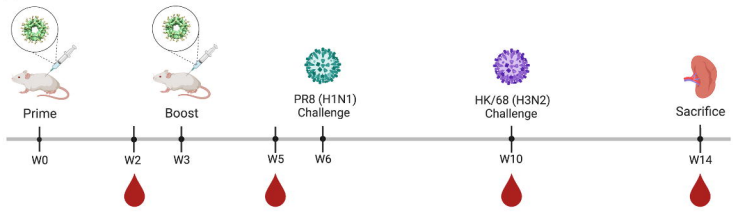

C

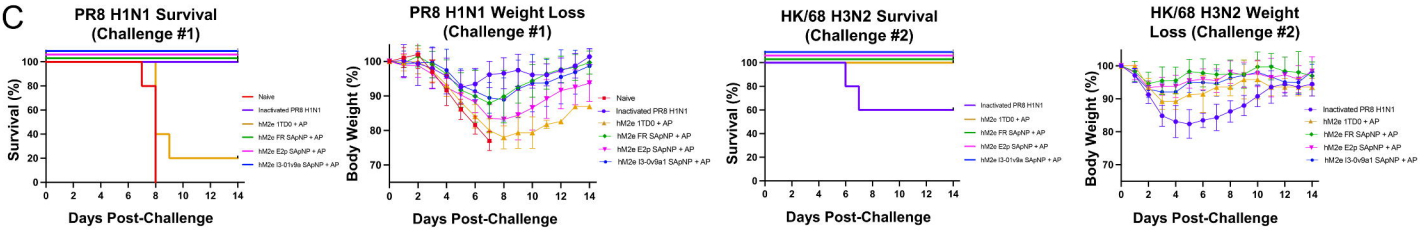

D

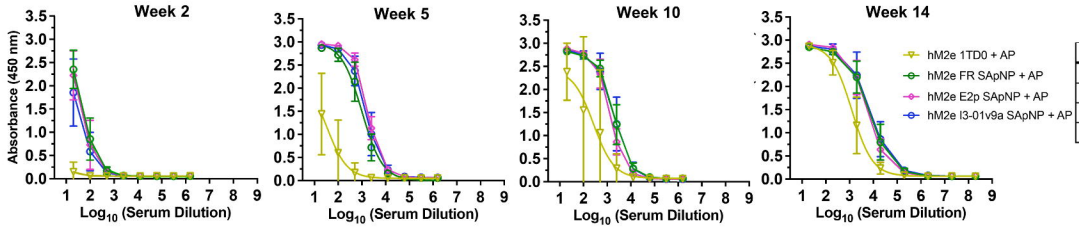

ID_{50} Serum Dilution

hM2e + AP	1TD0	FR	E2p	I3-01v9a
Week 2	N/A	21.82	15.72	13.04
Week 5	31.99	997.2	1678	1369
Week 10	263.4	1925	1249	1878
Week 14	1252	6940	5451	7510

Fig. 3

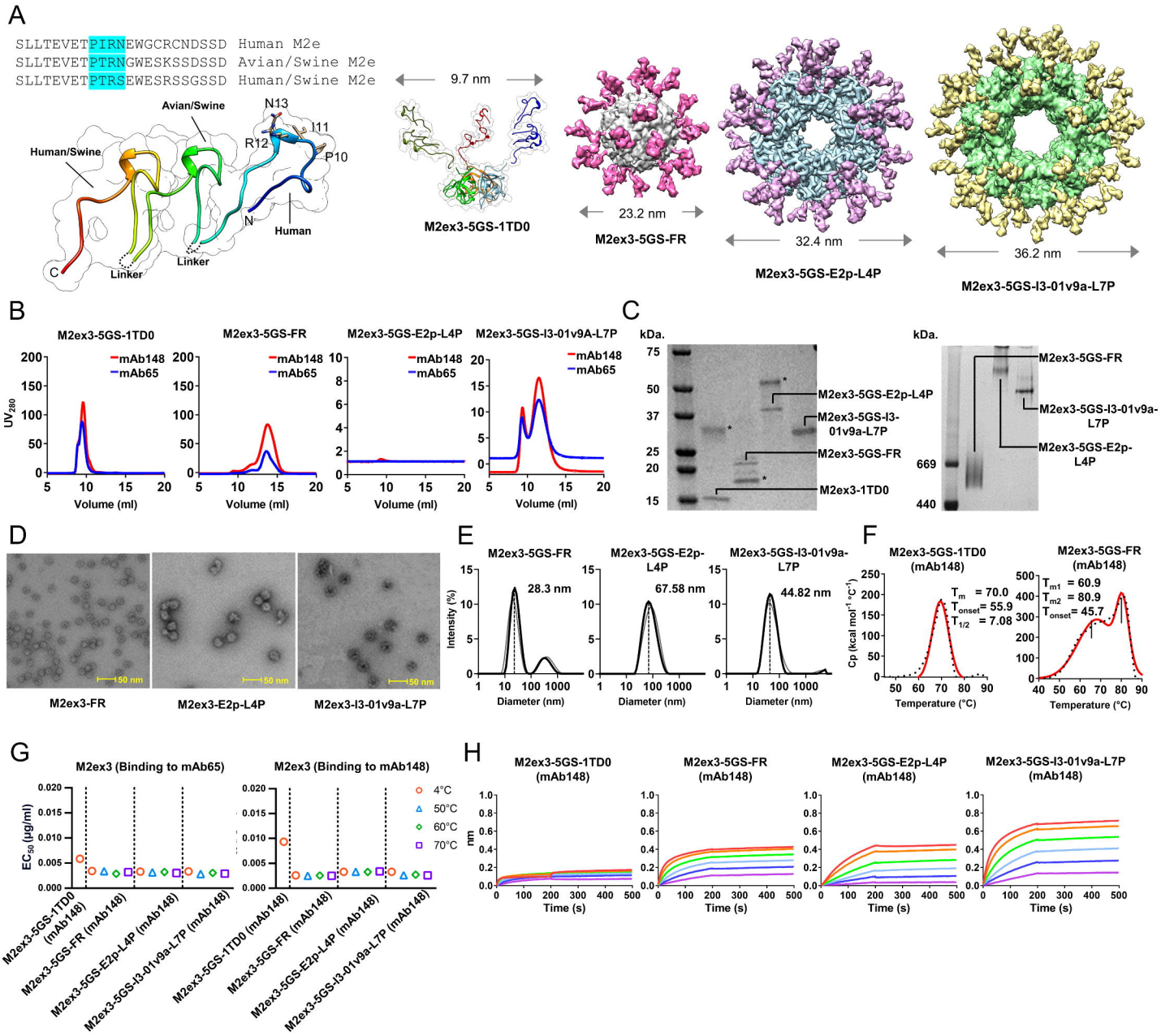
A
SLLTEVETPIRNEWGCRCNDSSD Human M2e
SLLTEVETPTRNGWESKSSDSSD Avian/Swine M2e
SLLTEVETPTRSEWESRSSGSSD Human/Swine M2e
Avian/Swine
N13
I11
R12
P10
Human/Swine
N
Human
C
Linker
Linker
9.7 nm
M2ex3-5GS-1TD0
23.2 nm
M2ex3-5GS-FR
32.4 nm
M2ex3-5GS-E2p-L4P
36.2 nm
M2ex3-5GS-I3-01v9a-L7P
B
M2ex3-5GS-1TD0
M2ex3-5GS-FR
M2ex3-5GS-E2p-L4P
M2ex3-5GS-I3-01v9A-L7P
mAb148
mAb65
UV280
Volume (ml)
C
kDa.
M2ex3-5GS-E2p-L4P
M2ex3-5GS-I3-01v9a-L7P
M2ex3-5GS-FR
M2ex3-1TD0
669
440
D
M2ex3-FR
M2ex3-E2p-L4P
M2ex3-I3-01v9a-L7P
150 nm
E
M2ex3-5GS-FR
28.3 nm
M2ex3-5GS-E2p-L4P
67.58 nm
M2ex3-5GS-I3-01v9a-L7P
44.82 nm
Intensity (%)
Diameter (nm)
F
M2ex3-5GS-1TD0 (mAb148)
Tm = 70.0
Tonset = 55.9
T1/2 = 7.08
M2ex3-5GS-FR (mAb148)
Tm1 = 60.9
Tm2 = 80.9
Tonset = 45.7
Cp (kcal mol-1 °C-1)
Temperature (°C)
G
M2ex3 (Binding to mAb65)
M2ex3 (Binding to mAb148)
EC50 (µg/ml)
4°C
50°C
60°C
70°C
M2ex3-5GS-1TD0 (mAb148)
M2ex3-5GS-FR (mAb148)
M2ex3-5GS-E2p-L4P (mAb148)
M2ex3-5GS-I3-01v9a-L7P (mAb148)
H
M2ex3-5GS-1TD0 (mAb148)
M2ex3-5GS-FR (mAb148)
M2ex3-5GS-E2p-L4P (mAb148)
M2ex3-5GS-I3-01v9a-L7P (mAb148)
nm
Time (s)

Fig. 4

A

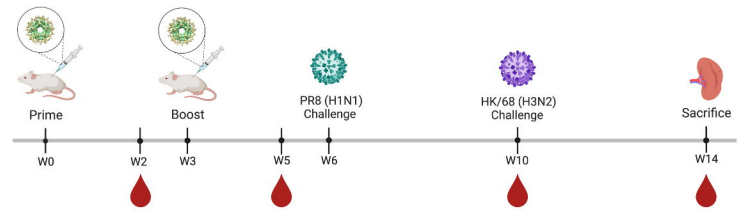

B

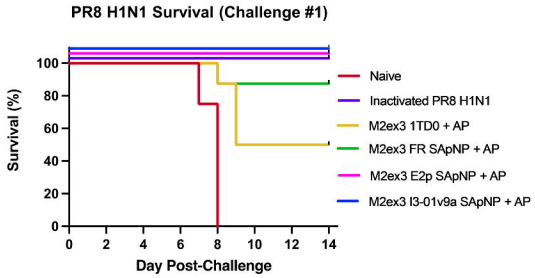

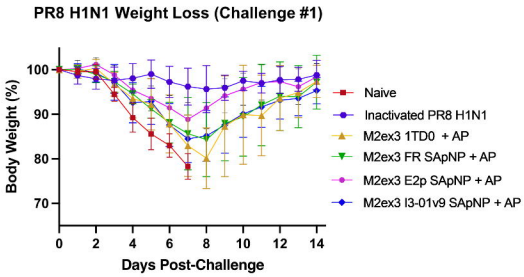

Group (n = 8)	Survival (%)	Peak Weight Loss (%)
Naive	0	21.7 ± 2.9
Inactivated PR8 H1N1	100	4.4 ± 5.3
M2ex3 iTD0	50	19.4 ± 7.3
M2ex3 FR SApNP	88	15.5 ± 8.1
M2ex3 E2p SApNP	100	11.2 ± 3.8
M2ex3 I3-01v9a SApNP	100	15.5 ± 5.3

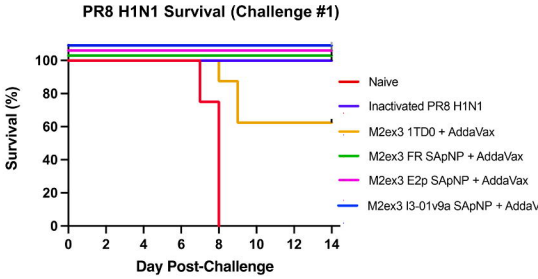

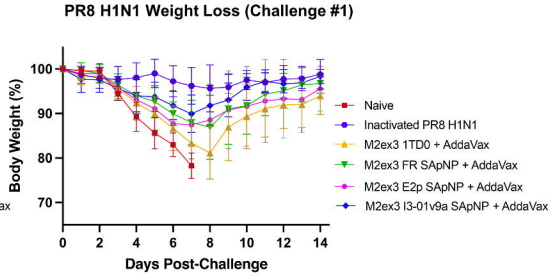

Group (n = 13 up to day 5; n = 8 up to Day 14)	Survival (%)	Peak Weight Loss (%)
Naive	0	21.7 ± 2.9
Inactivated PR8 H1N1	100	4.4 ± 5.3
M2ex3 iTD0	63	18.9 ± 5.9
M2ex3 FR SApNP	100	13.1 ± 7.2
M2ex3 E2p SApNP	100	12.5. ± 7.7
M2ex3 I3-01v9a SApNP	100	10.0 ± 4.2

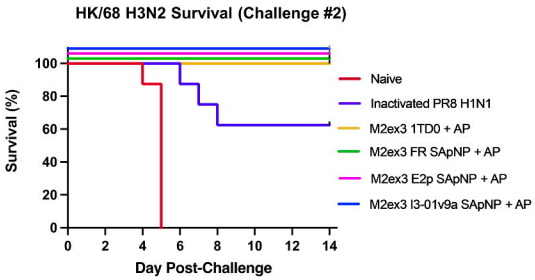

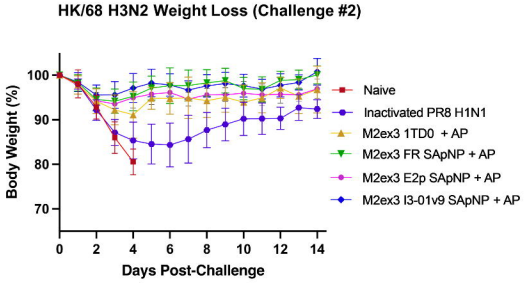

Group	Survival (%)	Peak Weight Loss (%)
Naïve (n = 8)	0	19.5 ± 2.9
Inactivated PR8 H1N1 (n = 8)	63	15.7 ± 4.9
M2e 1TD0 (n = 4)	100	8.9 ± 5.2
M2ex3 FR SApNP (n = 7)	100	4.7 ± 3.22
M2ex3 E2p SApNP (n = 8)	100	6.5 ± 1.9
M2ex3 I3-01v9a SApNP (n = 8)	100	4.4 ± 3.0

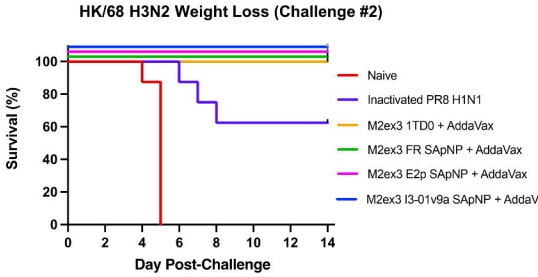

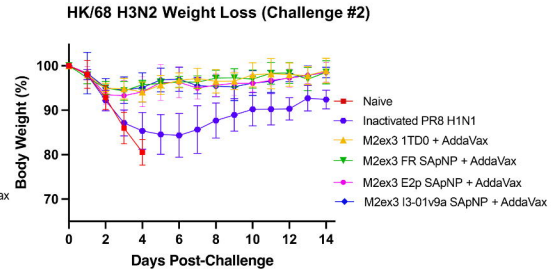

Group	Survival (%)	Peak Weight Loss (%)
Naïve (n = 8)	0	19.5 ± 2.9
Inactivated PR8 H1N1 (n = 8)	63	15.7 ± 4.9
M2ex3 1TD0 (n = 5)	100	4.3 ± 2.1
M2ex3 FR SApNP (n = 8)	100	4.3 ± 1.0
M2ex3 E2p SApNP (n = 8)	100	5.9 ± 3.4
M2ex3 I3-01v9a SApNP (n = 8)	100	4.9 ± 3.3

C

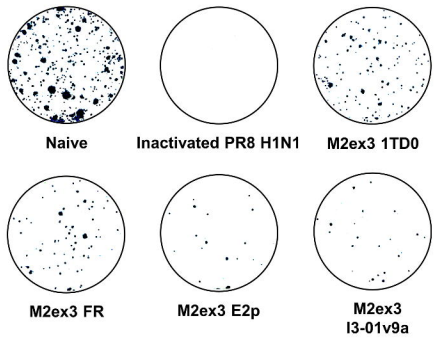

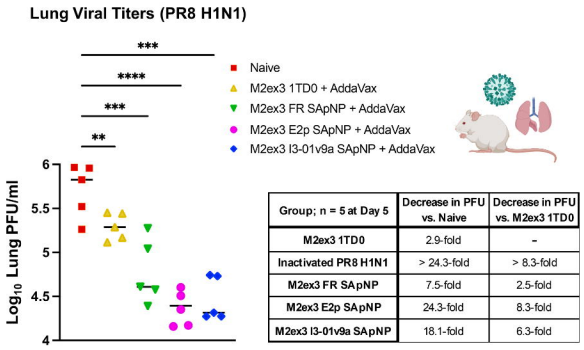

Group; n = 5 at Day 5	Decrease in PFU vs. Naive	Decrease in PFU vs. M2ex3 1TD0
M2ex3 1TD0	2.9-fold	-
Inactivated PR8 H1N1	> 24.3-fold	> 8.3-fold
M2ex3 FR SApNP	7.5-fold	2.5-fold
M2ex3 E2p SApNP	24.3-fold	8.3-fold
M2ex3 I3-01v9a SApNP	18.1-fold	6.3-fold

Fig. 5

A

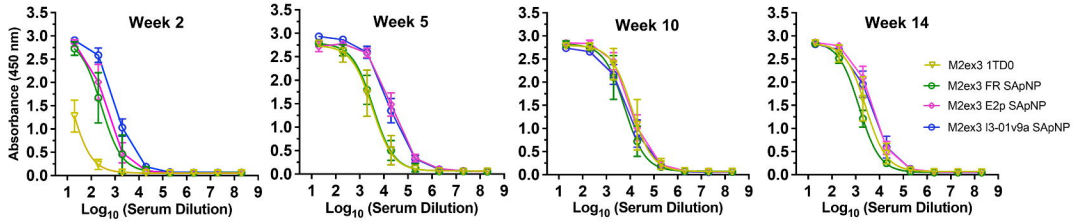

Aluminum Phosphate (AP)

M2ex3 + AP	1TD0	FR	E2p	I3-01v9a
Week 2	12.4	264.4	382.1	1039
Week 5	3340	3564	22383	16448
Week 10	11731	5876	10485	8511
Week 14	2702	1405	4944	4524

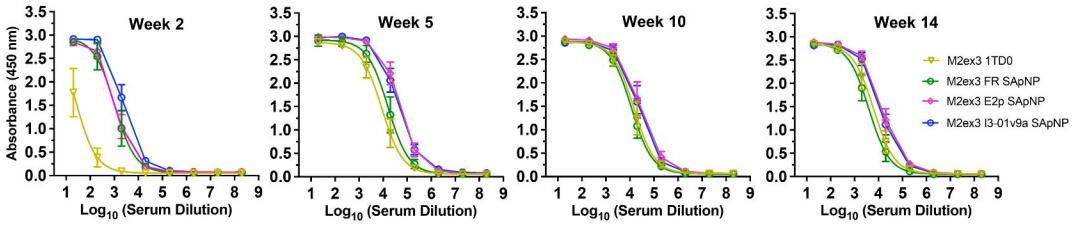

AddaVax (AV)

M2ex3 + AV	1TD0	FR	E2p	I3-01v9a
Week 2	23.19	1026	1104	2375
Week 5	8823	15989	50231	41779
Week 10	14463	11508	25419	23588
Week 14	6239	3947	14225	12500

B

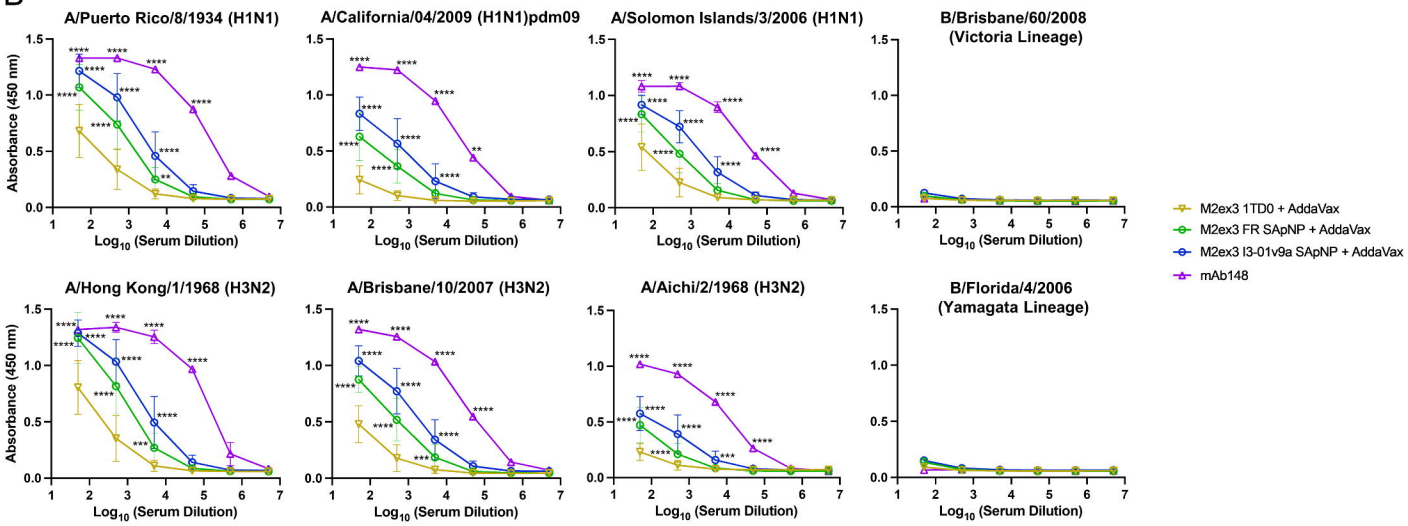

Fig. 6

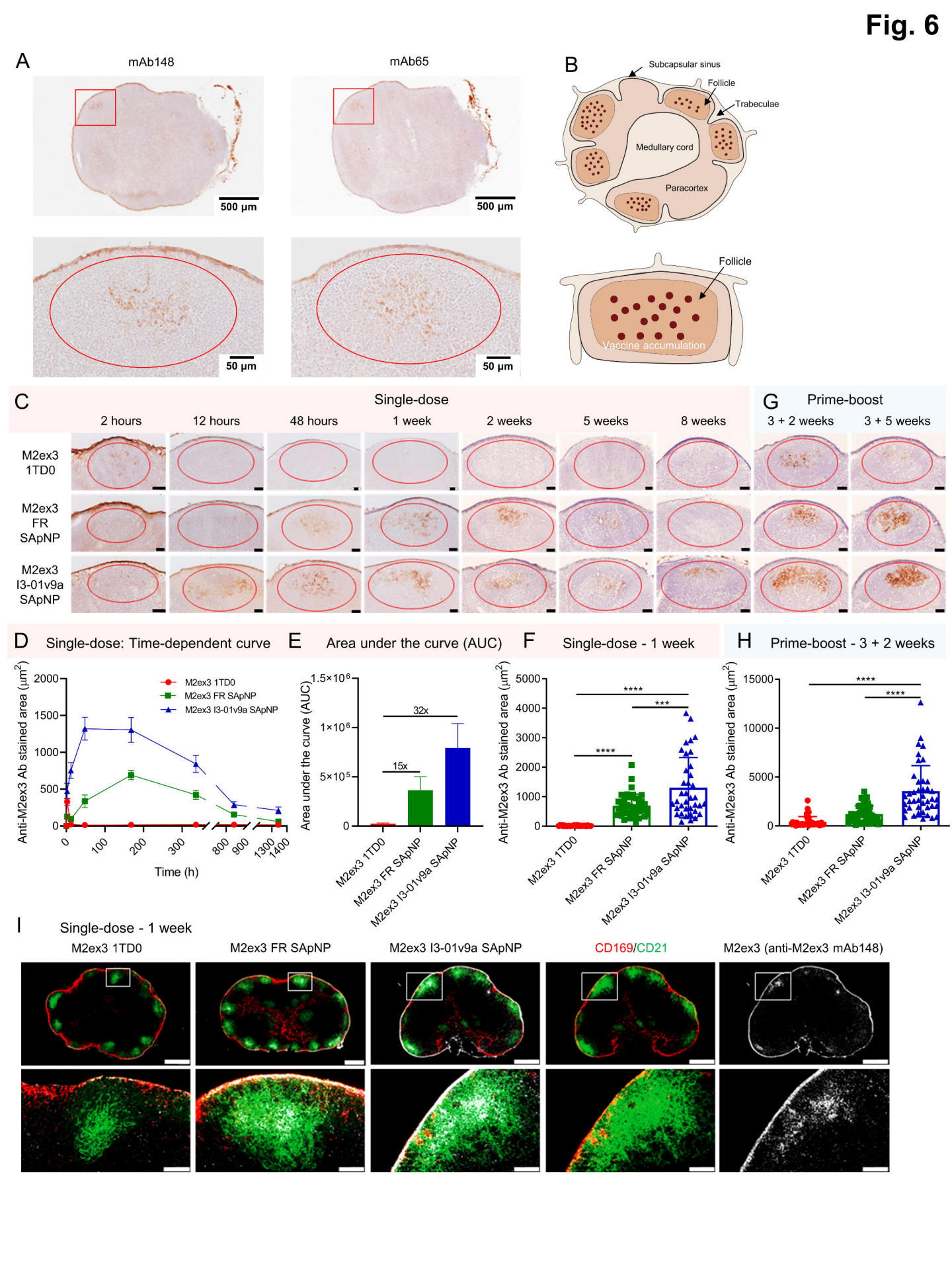
A
mAb148
mAb65
500 µm
50 µm
B
Subcapsular sinus
Follicle
Trabeculae
Medullary cord
Paracortex
Follicle
Vaccine accumulation
C
Single-dose
2 hours
12 hours
48 hours
1 week
2 weeks
5 weeks
8 weeks
G
Prime-boost
3 + 2 weeks
3 + 5 weeks
M2ex3 1TD0
M2ex3 FR SApNP
M2ex3 I3-01v9a SApNP
D
Single-dose: Time-dependent curve
Anti-M2ex3 Ab stained area (µm²)
Time (h)
M2ex3 1TD0
M2ex3 FR SApNP
M2ex3 I3-01v9a SApNP
E
Area under the curve (AUC)
Area under the curve (AUC)
32x
15x
F
Single-dose - 1 week
H
Prime-boost - 3 + 2 weeks
I
Single-dose - 1 week
M2ex3 1TD0
M2ex3 FR SApNP
M2ex3 I3-01v9a SApNP
CD169/CD21
M2ex3 (anti-M2ex3 mAb148)

Fig. 7

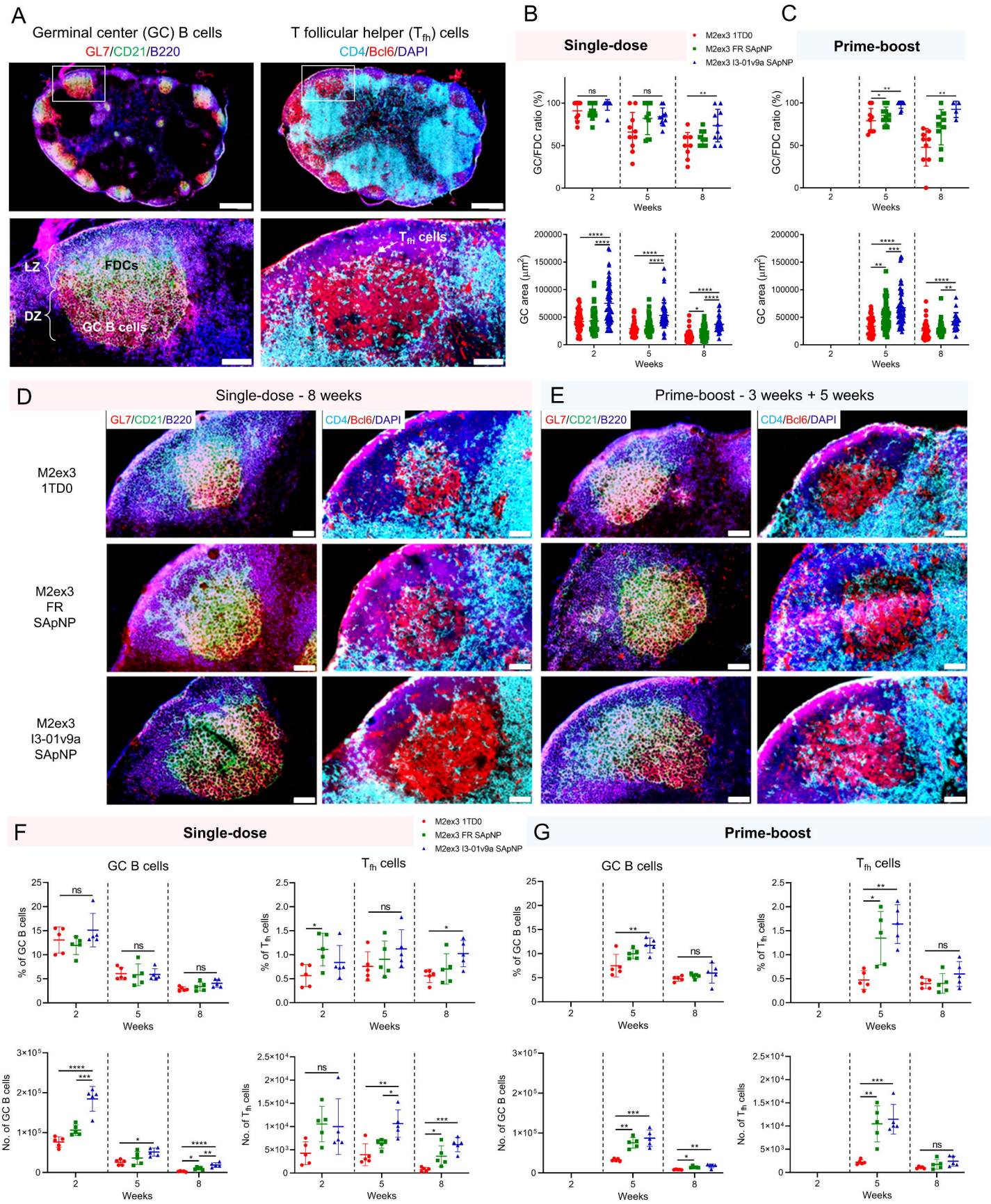
A
Germinal center (GC) B cells
GL7/CD21/B220
T follicular helper (T_{fh}) cells
CD4/Bcl6/DAPI
LZ
FDCs
DZ
GC B cells
T_{fh} cells
B
Single-dose
C
Prime-boost
M2ex3 1TD0
M2ex3 FR SApNP
M2ex3 I3-01v9a SApNP
GC/FDC ratio (%)
GC area (μm²)
Weeks
D
Single-dose - 8 weeks
E
Prime-boost - 3 weeks + 5 weeks
GL7/CD21/B220
CD4/Bcl6/DAPI
M2ex3 1TD0
M2ex3 FR SApNP
M2ex3 I3-01v9a SApNP
F
Single-dose
G
Prime-boost
GC B cells
T_{fh} cells
% of GC B cells
% of T_{fh} cells
No. of GC B cells
No. of T_{fh} cells
Weeks

Fig. 8

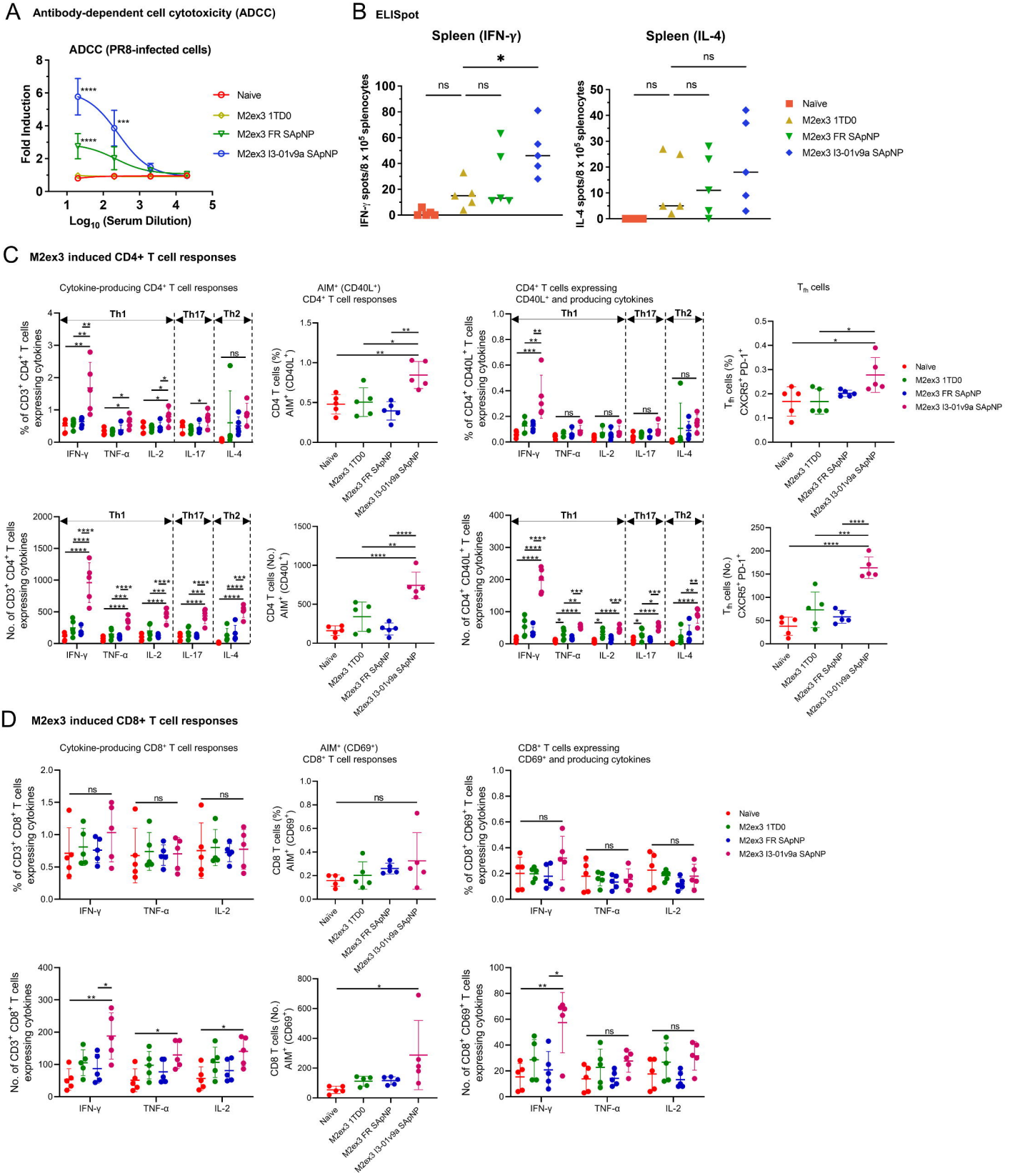
A
Antibody-dependent cell cytotoxicity (ADCC)
ADCC (PR8-infected cells)
Fold Induction
Log10 (Serum Dilution)
Naive
M2ex3 1TD0
M2ex3 FR SApNP
M2ex3 I3-01v9a SApNP
B
ELISpot
Spleen (IFN-γ)
Spleen (IL-4)
IFN-γ spots/8 x 10^5 splenocytes
IL-4 spots/8 x 10^5 splenocytes
C
M2ex3 induced CD4+ T cell responses
Cytokine-producing CD4+ T cell responses
AIM+ (CD40L+) CD4+ T cell responses
CD4+ T cells expressing CD40L+ and producing cytokines
Tfh cells
Th1
Th17
Th2
IFN-γ
TNF-α
IL-2
IL-17
IL-4
Naïve
M2ex3 1TD0
M2ex3 FR SApNP
M2ex3 I3-01v9a SApNP
D
M2ex3 induced CD8+ T cell responses
Cytokine-producing CD8+ T cell responses
AIM+ (CD69+) CD8+ T cell responses
CD8+ T cells expressing CD69+ and producing cytokines